

# **Mesoscale Moisture Fields Retrieved from Satellite Infrared Radiances in Nocturnal Inversion Cases**

by  
Donald W. Hillger

Department of Atmospheric Science  
Colorado State University  
Fort Collins, Colorado

May 1983

**Colorado  
State  
University**

**Department of  
Atmospheric Science**

Paper No. 373

**MESOSCALE MOISTURE FIELDS  
RETRIEVED FROM SATELLITE INFRARED RADIANCES  
IN NOCTURNAL INVERSION CASES**

by

**Donald W. Hillger**

**Department of Atmospheric Science  
Colorado State University  
Fort Collins, CO 80523**

**May 1983**

**Atmospheric Science Paper No. 373**

## ABSTRACT

In this study satellite infrared sounding radiances were used to retrieve lower tropospheric moisture information in addition to surface temperatures and temperature profiles. Polar-orbiting satellite data were obtained for two passes, one at 1000 GMT (local 0400) and the other at 1400 GMT (local 0800) on 30 September 1980, over the central United States. Specifically, infrared radiances from the Tiros Operational Vertical Sounder (TOVS) were used as the satellite input data. The only ancilliary data used were the rawinsondes necessary to generate the initial guess temperature and moisture profiles for the iterative retrieval scheme.

The physical-iterative retrievals require the input of an initial guess profile. The initial guess is then modified through iterations so that upwelling radiances determined by it match radiances measured (observed) by the satellite. However, no other supporting data (such as surface weather observations) were used in the retrievals. Such information was used only for post-retrieval comparisons to the satellite-derived soundings.

Because of the elimination of surface weather data as an input, the satellite window channels alone were used to determine the surface temperature. In addition, because of the nighttime and early morning situations under study, it was necessary to allow the surface temperature to be determined independently (float free) of the temperature profile. This allowed the incorporation of nocturnal

surface temperature inversions into the retrievals. These new aspects of the retrieval method are an advance beyond present day operational satellite retrieval techniques.

The iterative retrievals were performed only in clear situations. Therefore, cloud detection and elimination was necessary. Corrections were also made for reflected solar contamination in the shorter wavelength infrared channels. Another correction for terrain height variations was also necessary for doing retrievals over an area where surface pressures can vary greatly depending on elevation. Iterations were then performed with feedback alternating between the moisture and temperature profiles. Surface temperature feedback was incorporated before feedback to either the moisture or temperature profiles.

Results of the satellite retrievals were compared both quantitatively and qualitatively to conventional meteorological data at two scales. At the synoptic scale (>250 km) the satellite-derived parameters were compared to similar parameters from the 1200 GMT rawinsondes. In the qualitative comparison the same general synoptic features appeared. However, at the surface weather station scale (<250 km) additional moisture features were detected by the satellite which were not seen at the rawinsonde scale. In particular, the satellite-derived total precipitable water was seen to be quite variable. To explore this the satellite-derived values were compared to total water estimated from the surface dew points. The estimated total water was based on a relationship between surface dew point and total water determined by the rawinsondes used to form the initial guess. Comparisons between satellite-derived and surface-estimated total water values showed differences relating to where the atmosphere was dry or

moist aloft. It was determined by this research that the combination of satellite and surface moisture data when analyzed in this particular way gives a better determination of the overall tropospheric moisture structure at the mesoscale than available by either system alone.

Time-difference moisture fields for the four hours between 1000 and 1400 GMT showed similar features at the surface observation scale, in spite of large differences between the individual fields of satellite-derived and surface-estimated total water. This indicates the ability of the satellite data to detect temporal moisture changes within a short time span at least as well as could be estimated from surface weather data alone. As a further check, 700 mb winds were used to confirm that the temporal moisture changes are reasonable when advection of moisture by the mid-level winds is considered.

Finally, a structure analysis of the satellite-derived fields was used to determine inherent noise levels. These satellite data noise levels were much less than the satellite-conventional differences. Signal-to-noise considerations also confirm that there is significant information content in the satellite-derived fields even at the scale of surface weather observations (mesoscale).

## ACKNOWLEDGMENTS

Special thanks go to Dr. C. M. Hayden and others of the NESS group at the University of Wisconsin for providing the calibrated and earth-located TOVS data and also for providing the TOVS transmittance software used in this study. RAOB and surface data were obtained from the NCAR data base through the help of Paul Mulder. Satellite imagery was provided by Judith Bonds of the Bureau of Reclamation offices in Denver and by Dr. Robert Maddox of the NOAA laboratory in Boulder.

The author also recognizes the support and guidance of his advisor, Dr. Thomas H. Vonder Haar and other committee members, Drs. Thomas B. McKee, William R. Cotton, and Frank R. DeMeyer. Constructive review was also provided by Alan Lipton, who was not only involved with related aspects of the same data set, but also relieved the author of some other contract responsibilities, allowing more time for this research.

Computing support at CSU was provided both through contract and graduate accounts by the University Computer Center on the Cyber 171 and 172 computers. Typing of the manuscript was expertly done on a word processor by Andrea Adams and Robin Wilson. Drafting other than computer graphics was performed by Judy Sorbie. Streamlines were drawn by Jim Toth.

Funding for this work was provided initially by NSF Grant ATM-7918513 and later by AFGL Contract AF19628-80-C-0140.

## TABLE OF CONTENTS

<u>Chapter</u>	<u>Page</u>
Abstract. . . . .	ii
Acknowledgements. . . . .	v
List of Tables. . . . .	viii
List of Figures . . . . .	ix
1.0 Introduction. . . . .	1
1.1 Brief History of Satellite Soundings . . . . .	3
1.2 Goals of this Study. . . . .	4
2.0 Satellite Data. . . . .	6
2.1 TOVS System. . . . .	6
2.2 TIROS-N/NOAA-6 Orbits. . . . .	7
2.3 TOVS Data and Availability . . . . .	11
2.4 Satellite Imagery. . . . .	14
3.0 Conventional Data . . . . .	19
3.1 Rawinsondes. . . . .	19
3.2 Surface Observations . . . . .	23
3.3 Meteorological Situation . . . . .	26
3.4 Moisture Estimation from Surface Dew Point . . . . .	30
4.0 Background. . . . .	39
4.1 Other Studies Using TOVS . . . . .	39
4.2 Previous Moisture Retrieval Results. . . . .	40
4.3 Difficulties and Differences . . . . .	41
4.4 Background Work with HIRS-1. . . . .	42
5.0 TOVS Retrieval System . . . . .	45
5.1 HIRS-2 Additional Channels . . . . .	46
5.2 Cloud Detection . . . . .	48
5.3 Reflected Solar Radiation Correction . . . . .	56
5.4 Nocturnal Surface Temperature Inversion Problem. . . . .	63
5.5 Terrain Height Correction. . . . .	65
5.6 Iterative Feedback Mechanisms. . . . .	71
6.0 Retrieval Results	
6.1 Satellite-RAOB Comparisons . . . . .	78
6.2 Satellite-Surface Observation Comparisons. . . . .	78
6.2.1 A Closer Look at 1000 GMT . . . . .	95
6.2.2 A Closer Look at 1400 GMT . . . . .	104
6.2.3 4-Hour Time Differences . . . . .	107
6.3 Structure Analysis of Satellite-Derived Products . . . . .	113

TABLE OF CONTENTS  
(cont.)

<u>Chapter</u>		<u>Page</u>
7.0	Summary and Conclusions . . . . .	117
	7.1 Modifications Necessary for Nocturnal Inversions . . .	119
	7.2 Specific Results . . . . .	120
	7.3 Other Possible Improvements. . . . .	125
	7.4 Concluding Remarks . . . . .	126
	References. . . . .	129
	Appendix A - Terms and Symbols. . . . .	132
	Appendix B - Single Field-of-View Cloud Determination . . .	133
	Appendix C - Numerical Calculation of Moisture Feedback Conversion Factors . . . . .	138

LIST OF TABLES

<u>Table</u>		<u>Page</u>
2.1	Characteristics of TOVS Channels. . . . .	8
2.2	TIROS-N/NOAA A-G Satellite Series . . . . .	10
2.3	TOVS Earth-Located Calibrated Data. . . . .	14
3.1	Synoptic Surface Observations . . . . .	24
5.1	A Comparison of HIRS-2 and HIRS-1 Channels. . . . .	47
5.2	Satellite-Observed Terrestrial and Reflected Solar Radiance Contributions. . . . .	61
6.1	Satellite-RAOB Comparisons. . . . .	79
6.2	Time-Interpolated Surface Observations and Paired Satellite-Surface Observations. . . . .	87
6.3	Satellite-Synoptic Surface Observation Comparisons. . . . .	88
6.4	Synoptic Surface Observation Intercomparisons . . . . .	94
6.5	Structure Analysis of Satellite-Derived Parameters. . . . .	115

## LIST OF FIGURES

<u>Figure</u>	<u>Page</u>
2.1 TOVS weighting functions (normalized) . . . . .	9
2.2a TIROS-N descending orbit (equatorward) for 30 September 1980 at approximately 1000 GMT (0400 LST). HIRS-2 sounding positions are shown . . . . .	12
2.2b NOAA-6 descending orbit (equatorward) for 30 September 1980 at approximately 1400 GMT (0800 LST). HIRS-2 sounding positions are shown . . . . .	13
2.3a GOES visible image for 1430 GMT on 30 September 1980 . . . . .	15
2.3b GOES infrared image for 1400 GMT on 30 September 1980. . . . .	17
2.3c GOES infrared image for 1000 GMT on 30 September 1980. . . . .	18
3.1 Synoptic radiosonde observations (RAOBs) taken at 1200 GMT on 30 September 1980 . . . . .	21
3.2 Mean temperature and moisture profiles composited from the 27 circled RAOBs shown in Figure 3.1. Plotting is done on a USAF skew T-log P thermodynamic diagram. . . . .	22
3.3 Surface observation station identifiers plotted at their respective locations . . . . .	25
3.4a Surface dew point temperatures ( $^{\circ}\text{C}$ ) from RAOBs at 1200 GMT on 30 September 1980 . . . . .	27
3.4b Total precipitable water (mm) from RAOBs at 1200 GMT on 30 September 1980 . . . . .	28
3.4c Ratio of total precipitable water to the surface mixing ratio ( $\text{mm}(\text{g kg}^{-1})^{-1}$ ) from RAOBs at 1200 GMT on 30 September 1980 . . . . .	29
3.5 Plot of total precipitable water versus surface dew point temperature for the 36 RAOBs in Figure 3.1. A linear least-squares regression line has been fit to the points . . . . .	33

LIST OF FIGURES  
(cont.)

<u>Figure</u>	<u>Page</u>
3.6a Estimated precipitable water (mm) at the RAOB positions using the regression line in Figure 3.5 and the RAOB surface dew point temperatures at 1200 GMT on 30 September 1980. The contours are very similar to those for the surface dew point temperatures in Figure 3.4a. . . . .	34
3.6b Precipitable water difference (mm) (measured minus estimated from surface dew point) for RAOBs at 1200 GMT on 30 September 1980. The differences denote areas of dry (-) and moist (+) aloft. . . . .	36
3.7 Exponent for a power-law mixing ratio decrease with pressure as a function of surface dew point temperature. The results are based on Equation 3.6 and precipitable water determined by Equation 3.2 . . . . .	38
5.1a Bi-directional reflectance (%) at 1400 GMT on 30 September 1980 derived from TOVS window channel radiance at 0.69 $\mu$ m divided by its maximum possible value . . . . .	50
5.1b Window brightness temperature difference (K) (3.7-11 $\mu$ m) at 1400 GMT on 30 September 1980. . . . .	51
5.2 Scatter plot of window brightness temperature difference (3.7-11 $\mu$ m) versus bi-directional reflectance for the area from 32-45°N and 87-101°W for the 1400 GMT satellite pass on 30 September 1980. A correlation coefficient of 0.83 is given . . . . .	53
5.3a Window brightness temperature difference (K) (3.7-11 $\mu$ m) at 1000 GMT on 30 September 1980 . . . . .	54
5.3b Infrared minus microwave brightness temperature difference (K) (3.7 $\mu$ m - 50GHz) at 1000 GMT on 30 September 1980 . . . . .	55
5.4 An illustration of the solar and satellite zenith angles which must be taken into account in the reflected radiation correction to the shortwave infrared channels. . . . .	58
5.5 An example of a surface temperature inversion being added to the initial guess temperature profile by using the maximum window channel brightness temperature as a floating surface or interface temperature. . . . .	66

LIST OF FIGURES  
(cont.)

<u>Figure</u>	<u>Page</u>
5.6 An example of numerical integration of the radiative transfer equation when an elevated surface ( $p_{sfc} < 1000\text{mb}$ ) is encountered . . . . .	70
5.7 Simulated brightness temperature response as a function of the total atmospheric precipitable water and surface temperature deviation from a given temperature profile .	74
6.1a Satellite-derived total precipitable water (mm) at RAOB scale for 1000 GMT on 30 September 1980. . . . .	82
6.1b Satellite-derived total precipitable water (mm) at RAOB scale for 1400 GMT on 30 September 1980. . . . .	83
6.1c Satellite-derived total precipitable water (mm) at RAOB scale interpolated to 1200 GMT on 30 September 1980. . .	84
6.1d Satellite-derived minus RAOB total precipitable water (mm) at RAOB scale for 1200 GMT on 30 September 1980. . . . .	86
6.2a Satellite-derived versus synoptic (time-interpolated) surface temperatures at both 1000 and 1400 GMT on 30 September 1980 . . . . .	91
6.2b Satellite-derived versus synoptic (time-interpolated) surface dew point temperatures at both 1000 and 1400 GMT on 30 September 1980 . . . . .	92
6.2c Satellite-derived versus synoptic (time-interpolated) surface-estimated total precipitable water at both 1000 and 1400 GMT on 30 September 1980. . . . .	93
6.3a Satellite-derived total precipitable water (mm) at surface observation resolution for 1000 GMT on 30 September 1980 . . . . .	96
6.3b Total precipitable water (mm) estimated from time-interpolated surface observations at 1000 GMT on 30 September 1980 by using Equation 3.2 . . . . .	98
6.3c Difference between satellite-derived and surface-estimated total precipitable water (mm) at 1000 GMT on 30 September 1980 . . . . .	99

LIST OF FIGURES  
(cont.)

<u>Figure</u>	<u>Page</u>
6.4a Topeka, Kansas RAOB at 1200 GMT on 30 September 1980 showing a shallow moist layer near the surface. The dotted line is a power law moisture profile based on the RAOB surface dew point temperature. (See text for more explanation.) Also plotted is the nearest satellite sounding at 1000 GMT which does not contain the vertical detail of the RAOB but which better approximates the dry-over-moist situation. . . . .	101
6.4b Peoria, Illinois RAOB at 1200 GMT on 30 September 1980 with a deep moist layer near the surface. The dotted line is a power law moisture profile based on the RAOB surface dew point temperature. (See text for more explanation.) Also plotted is the nearest satellite sounding at 1000 GMT with its better reconstruction of the low-level moisture. . . . .	103
6.5a Satellite-derived total precipitable water (mm) at surface observation resolution for 1400 GMT on 30 September 1980 . . . . .	105
6.5b Total precipitable water (mm) estimated from time-interpolated surface observations at 1400 GMT on 30 September 1980 by using Equation 3.2 . . . . .	106
6.5c Difference between satellite-derived and surface-estimated total precipitable water (mm) at 1400 GMT on 30 September 1980 . . . . .	108
6.6a 4-hour time difference between satellite-derived total precipitable water (mm) at surface observation scale at 1000 and 1400 GMT on 30 September 1980. . . . .	109
6.6b 4-hour time difference between surface-estimated total precipitable water (mm) at 1000 and 1400 GMT on 30 September 1980 . . . . .	110
6.7 Winds (m/s) and streamlines at 70 kPa (700 mb) from 1200 GMT RAOBs on 30 September 1980. . . . .	112
6.8 Structure as a function of separation distance for satellite-derived 85 kPa (850 mb) dew point temperatures at 1400 GMT on 30 september 1980. A third-degree polynomial with zero slope at $x=0$ is fitted to the first four points. . . . .	114

## 1.0 INTRODUCTION

Satellite or other remote sounding systems used to obtain meteorological parameters were at one time thought to be able to replace conventional (balloon and other ground based) measurement systems. This, however, has never come true other than over the oceans or in other data sparse regions where conventional soundings are few. Satellites do have the ability to gather large amounts of data at high space and time resolutions and to cover virtually all of the earth with such measurements within a short period of time. This capability alone has probably been the main reason for the continued use of satellites, and not the quality of the satellite-derived products.

Satellite and conventional measurement systems are inherently different in that one is remote and the other is basically in-situ. For this reason the two systems are not redundant and they can be complementary. This contrast also causes problems when trying to measure one system against the other. If the inherent differences and limitations of each system are considered, satellite measurement systems can be used along with the conventional measurement systems which have already found their place in meteorological history.

The main reason for measuring atmospheric parameters eventually boils down to the ability to better forecast the weather. In the process of trying to provide better forecasts, the need for better analyses is vital. Better analyses come in one sense from larger numbers of measurements over a large area. The satellite alone has the

ultimate capability in this respect, being able to sample the whole earth, or parts thereof, with high-density measurements. These high-density measurements include both space and time sampling.

More recently the need for high-density measurements for numerical model input has reconfirmed the need for the satellite platform. Satellite measurements, however, can generally be more useful if they are interpreted as meteorological variables rather than radiances or brightness temperatures. The satellite-derived values may not be the same meteorological variables measured by conventional systems, but they must relate to important atmospheric quantities, such as temperature and moisture. The closer the satellite-derived values come to conventional measurements, the more it would please most users. However, it is not always entirely possible or desirable to duplicate conventional measurements. The challenge of this new data set is then twofold: 1) to be able to derive useable meteorological parameters from satellite data, and 2) to use those measurements effectively.

Being able to derive useful meteorological parameters is the immediate goal, since unless proven to be able to reproduce certain basic atmospheric variables, the satellite platform may not continue as a desirable expenditure of time and effort. This study shows that satellite-derived parameters are able to reproduce details at the resolution of synoptic surface observations (at much higher resolution than the rawinsonde network), that they can add limited vertical resolution to conventional surface measurements, and that they can provide temporal information over a relatively short time span.

### 1.1 Brief History of Satellite Soundings

The retrieval of atmospheric parameters from satellite radiances has a relatively short history. The first meteorological satellite was launched in 1959. At that time the idea of using remote sounding to derive meteorological variables, such as temperature and moisture, from satellite measurements was also new. Kaplan (1959), Wark (1961), and King (1963) devised methodology for satellite soundings, if only on paper. Such satellite sounding techniques, however, were first tested in 1969 with the launch of the SIRS (Satellite Infrared Spectrometer) and IRIS (Infrared Interferometer Spectrometer) instruments on board the Nimbus series of experimental satellites. These early instruments were followed by the VTPR (Vertical Temperature Profile Radiometer) instruments on the NOAA operational satellite series. An article published by the author was among the first to give results of using VTPR infrared radiances to derive high-resolution temperature and moisture fields over land areas (Hillger and Vonder Haar, 1977).

Further refinements in satellite soundings were incorporated into the experimental HIRS (High-resolution Infrared Radiation Sounder) on board Nimbus-6 which was launched in 1975. This again in 1978 lead into the operational version, HIRS-2, on board the continuing NOAA satellite series. These all, however, were polar-orbiting satellites. Most recently remote sounders have been placed on satellites in geosynchronous orbit to take advantage of a stationary vantage point from which to view time-changing meteorological variables (Smith et al., 1981). So, in a short span of a little over 20 years satellite soundings have gone from theory to operational use. This operational use, however, is limited to the synoptic scale and to twice-a-day

soundings from any one polar-orbiting satellite. Only relatively recently have satellite soundings been applied to the mesoscale (below 250 km) and at more frequent time intervals. This study is one of those attempts at obtaining high spatial and time resolution satellite soundings using HIRS-2 data. Retrieval techniques such as this may some day be put into operational use. The time resolution of HIRS-2 is limited by the polar-orbiting satellite platform, but it gives a hint at the capabilities which will be utilized for satellite soundings from geosynchronous orbit (Chesters et al., 1982).

### 1.2 Goals of this Study

In contrast to most previous work with satellite soundings by those with expertise in this area, several differences make this work unique. The retrieval process for obtaining meteorological variables has been constantly modified to incorporate the minimum input of conventional data to produce the most useful output of satellite-derived information. This statement is explained more thoroughly in the following goals or conditions set upon this study:

- a) The minimum ingest of conventional data is realized by use of balloon soundings only to produce the initial guess sounding. This single initial guess is used for the entire set of satellite-derived mesoscale soundings. By using only one initial guess sounding, any features resolvable in the high-resolution satellite-derived products are a result of changes in the satellite input and are not due to any changes forced upon the satellite input by a varying initial guess profile. In certain situations the initial guess profile may even be obtained from climatology, or a forecast profile may be used, making the satellite sounding products even more independent of contemporary balloon soundings. Also, synoptic surface observations are used only for verification purposes. This completely independent data set therefore provides a good basis for comparison.
- b) The physical, iterative retrieval process uses the radiative transfer equation explicitly to best utilize the strengths of each of the various satellite channels or measurements. This

also allows incorporation of local modifications necessary to correct for reflected solar radiation and varying terrain height. A major modification is also necessary due to the existence of nocturnal temperature inversions during the nighttime and early morning situations under study. The incorporation of a surface temperature which floats independently of the temperature profile allows the addition of surface temperature inversions and increases the vertical resolution of the retrieved soundings near the surface. These corrections are necessary in the use of real data, as contrasted with simulated or controlled sounding experiments where the complexity of the problem is greatly reduced. The use of a physical retrieval algorithm also eliminates the need for a statistical data base upon which regression techniques rely.

- c) This study was also devised to determine mainly lower tropospheric temperature and moisture parameters from the satellite radiances. Both quantitative and qualitative comparisons are made at both the rawinsonde and surface observation scales. A concentration on satellite-derived total precipitable water is made in the qualitative comparisons. Also, by contrasting the satellite-derived values at the two scales, features become apparent at the higher resolution of the surface observations which were undetected at the rawinsonde scale. Information on vertical moisture extent is also obtained by comparing the satellite-derived to the surface-estimated total water. Finally, time difference fields are computed to show that the satellite is capable of detecting moisture changes at both high space and time resolutions. This has potential for application to geosynchronous sounding data now available over the western hemisphere.

## 2.0 SATELLITE DATA

The satellite data used in this study are measurements obtained from the infrared sounding channels on the TIROS-N polar-orbiting satellite series. These far-infrared channels are designed to probe the vertical mass and moisture structure of the atmosphere by employing frequencies which vary greatly in their atmospheric absorption. One inherent drawback of infrared measurements is their inability to sound below clouds. In this study no satellite retrievals were produced in cloudy situations, although an attempt was made in which cloudy situations were only treated by the very simplest of means. The complete TIROS-N sounding system is described below.

Besides the infrared sounding channels, much higher resolution visible (1 km) and infrared (8 km) imagery from geosynchronous orbit were used to help determine when clouds were contaminating any of the satellite soundings. These images also give a good indication of the meteorological situation under study as will be described in a following section.

### 2.1 TOVS System

The TIROS Operational Vertical Sounder System (Schwalb, 1978; Werbowetzki, 1981) consists of three instruments. These three instruments are: 1) the High-resolution Infrared Radiation Sounder (HIRS); 2) the Stratospheric Sounding Unit (SSU); and 3) the Microwave Sounding Unit (MSU). Only the HIRS-2 or infrared data were used in this

study, except for a microwave window channel used to help detect clouds. This instrument is an adaptation of the HIRS-1 instrument first flown on the Nimbus-6 satellite (Smith et al., 1975). Two major changes were made in the instrument design from the first to the second version of HIRS. One change was the addition of three new infrared channels at  $9.71 \mu\text{m}$  ( $\text{O}_3$ ),  $7.32 \mu\text{m}$  ( $\text{H}_2\text{O}$ ), and  $3.98 \mu\text{m}$  (window). The HIRS-2 channels are listed in Table 2.1 (Smith et al., 1979b). Along with the wavelengths and wavenumbers, the principal absorbing constituents and the level at which the peak energy contribution arises (for a standard atmosphere) are listed. The weighting functions for all TOVS channels are shown in Figure 2.1.

The second major change from HIRS-1 to HIRS-2 instruments was the increased horizontal resolution (decreased spot size) at the surface. This increased resolution is accompanied by an increased number of scan positions along the scan track. HIRS-2 scans in 56 steps (28 on each side of nadir) compared to 42 (21 on each side of nadir) for HIRS-1. The sub-satellite spot diameter is  $17.4 \text{ km}$  (a function of the satellite altitude), but the closest possible pair of measurements along any scan is  $26 \text{ km}$ . This distance is considered the maximum ground resolution, but the separation distance and the spot size or field-of-view increase as the satellite scans away from nadir. The distance between scan lines which is  $42 \text{ km}$  is timed so as not to allow any overlap between individual spots at large scan angles.

## 2.2 TIROS-N/NOAA-6 Orbits

TIROS-N and NOAA-6, both of which carry the TOVS instrument, are polar-orbiting satellites with sun-synchronous orbits. In other words, they view any particular non-polar region of the earth twice a day (12

**Table 2.1**  
**Characteristics of TOVS Channels (after Smith et al., 1979b).**

HIRS Channel number	Channel central wavenumber	Central wavelength ( $\mu\text{m}$ )	Principal absorbing constituents	Level of peak energy contribution	Purpose of the radiance observation
1	668	15.00	CO <sub>2</sub>	30 mb	<i>Temperature sounding.</i> The 15- $\mu\text{m}$ band channels provide better sensitivity to the temperature of relatively cold regions of the atmosphere than can be achieved with the 4.3- $\mu\text{m}$ band channels. Radiances in Channels 5, 6, and 7 are also used to calculate the heights and amounts of cloud within the HIRS field of view.
2	679	14.70	CO <sub>2</sub>	60 mb	
3	691	14.50	CO <sub>2</sub>	100 mb	
4	704	14.20	CO <sub>2</sub>	400 mb	
5	716	14.00	CO <sub>2</sub>	600 mb	
6	732	13.70	CO <sub>2</sub> /H <sub>2</sub> O	800 mb	
7	748	13.40	CO <sub>2</sub> /H <sub>2</sub> O	900 mb	
8	898	11.10	Window	Surface	<i>Surface temperature</i> and cloud detection.
9	1 028	9.70	O <sub>3</sub>	25 mb	<i>Total ozone</i> concentration.
10	1 217	8.30	H <sub>2</sub> O	900 mb	<i>Water vapor sounding.</i> Provides water vapor corrections for CO <sub>2</sub> and window channels. The 6.7- $\mu\text{m}$ channel is also used to detect thin cirrus cloud.
11	1 364	7.30	H <sub>2</sub> O	700 mb	
12	1 484	6.70	H <sub>2</sub> O	500 mb	
13	2 190	4.57	N <sub>2</sub> O	1 000 mb	<i>Temperature sounding.</i> The 4.3- $\mu\text{m}$ band channels provide better sensitivity to the temperature of relatively warm regions of the atmosphere than can be achieved with the 15- $\mu\text{m}$ band channels. Also, the short-wavelength radiances are less sensitive to clouds than those for the 15- $\mu\text{m}$ region.
14	2 213	4.52	N <sub>2</sub> O	950 mb	
15	2 240	4.46	CO <sub>2</sub> /N <sub>2</sub> O	700 mb	
16	2 276	4.40	CO <sub>2</sub> /N <sub>2</sub> O	400 mb	
17	2 361	4.24	CO <sub>2</sub>	5 mb	
18	2 512	4.00	Window	Surface	<i>Surface temperature.</i> Much less sensitive to clouds and H <sub>2</sub> O than the 11- $\mu\text{m}$ window. Used with 11- $\mu\text{m}$ channel to detect cloud contamination and derive surface temperature under partly cloudy sky conditions. Simultaneous 3.7- and 4.0- $\mu\text{m}$ data enable reflected solar contribution to be eliminated from observations.
19	2 671	3.70	Window	Surface	
20	14 367	0.70	Window	Cloud	<i>Cloud detection.</i> Used during the day with 4.0- and 11- $\mu\text{m}$ window channels to define clear fields of view.

MSU	Frequency (GHz)	Principal absorbing constituents	Level of peak energy contribution	Purpose of the radiance observation
1	50.31	Window	Surface	<i>Surface emissivity</i> and cloud attenuation determination.
2	53.73	O <sub>3</sub>	700 mb	<i>Temperature sounding.</i> The microwave channels probe through clouds and can be used to alleviate the influence of clouds on the 4.3- and 15- $\mu\text{m}$ sounding channels.
3	54.96	O <sub>3</sub>	300 mb	
4	57.95	O <sub>3</sub>	90 mb	

SSU	Wavelength ( $\mu\text{m}$ )	Principal absorbing constituents	Level of peak energy contribution	Purpose of the radiance observation
1	15.0	CO <sub>2</sub>	15.0 mb	<i>Temperature sounding.</i> Using CO <sub>2</sub> gas cells and pressure modulation, the SSU observes thermal emissions from the stratosphere.
2	15.0	CO <sub>2</sub>	4.0 mb	
3	15.0	CO <sub>2</sub>	1.5 mb	

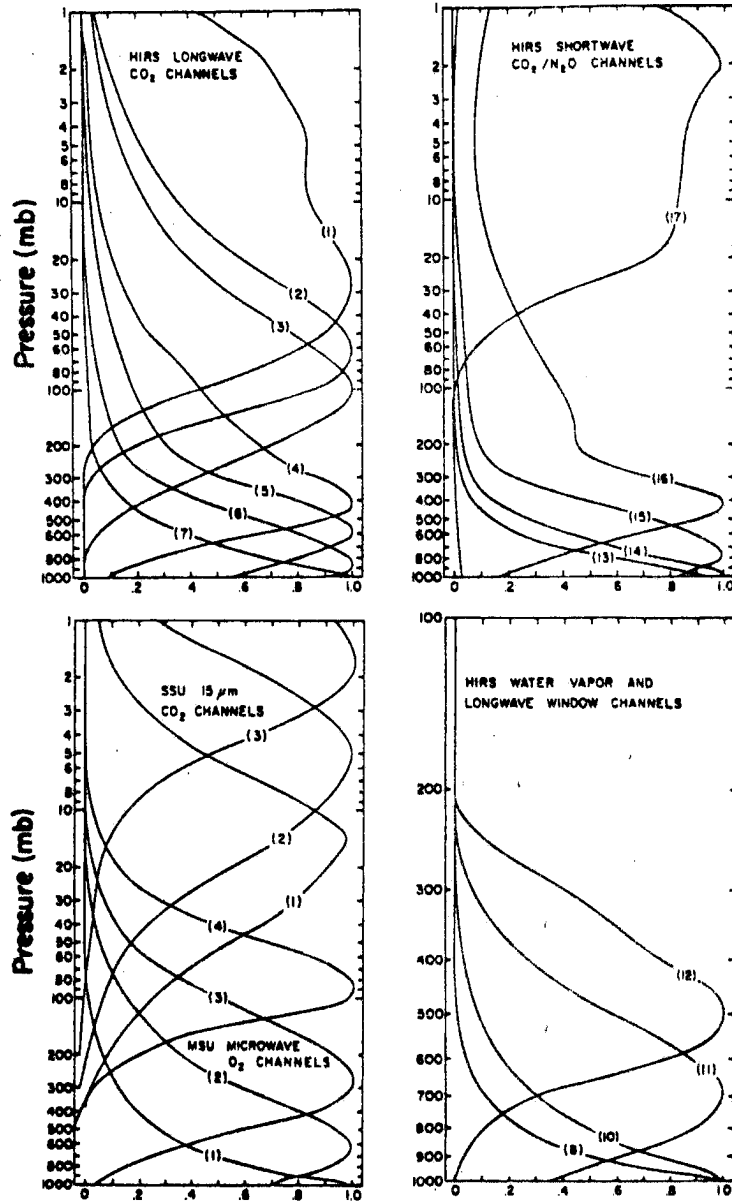


Figure 2.1 TOVS (normalized) weighting functions (after Smith et al., 1979b).

hours apart) at approximately the same local time each day. The TIROS-N series of satellites orbit at about 850 km altitude with an orbital inclination of about 99 degrees retrograde. Table 2.2 gives the satellite launch and end-of-operation dates and the satellite local equator-crossing times. The first two satellites were able to collect data in unison from June 1979, when NOAA-6 was launched, until January 1981 when TIROS-N ceased operation. As of June 1981 NOAA-7 took over as the operational satellite for the local 3 a.m.- 3 p.m. time slot.

Table 2.2

## TIROS-N/NOAA A-G Satellite Series

<u>Satellite</u>	<u>Launched</u>	<u>Ended Operation</u>	<u>Local Equator-Crossing Time</u>
TIROS-N	Oct. 1978	Jan. 1981	4 a.m.-4 p.m.
NOAA-6	June 1979	---	8 a.m.-8 p.m.
NOAA-7	June 1981	---	3 a.m.-3 p.m.

During the period when both TIROS-N and NOAA-6 were operational data for any non-polar region could be obtained at both local 0400 and 0800 with a time separation of 4 hours. The satellite orbits, however, were designed to oscillate about any particular equator crossing. This is a result of the satellite orbit period not being equally divisible into one day (i.e., approximately 14.2 orbits per day). So, although each satellite views the same non-polar region of the earth twice a day, sometimes the orbit tracks lie to the east or west of that location and only occasionally directly overhead. Also, because both satellites display this behavior but with different periods they have a beat frequency or a certain period at which they cover almost exactly the same regions of the earth. For TIROS-N and NOAA-6 with orbital periods

of about 101.9 and 101.1 minutes, respectively, the beat frequency is 9.28 days. So approximately every 9 days the two satellites view nearly the same regions of the earth. This large beat period limits the number of times when the two satellites are in synchronization and are able to simulate the higher time resolutions only possible from geosynchronous orbit.

### 2.3 TOVS Data and Availability

One of the periods when both TIROS-N and NOAA-6 were in synchronization occurred on 30 September 1980. TIROS-N viewed the earth on a descending node (towards the equator) at approximately 1000 GMT (0400 LST) as shown in Figure 2.2a and NOAA-6 viewed almost the same region at approximately 1400 GMT (0800 LST) as shown in Figure 2.2b. These two orbits are separated by about 4 hours. This 4-hour difference will allow an examination of changes in the satellite-derived meteorological variables, especially moisture, during a small time span and at high spatial resolution. Data coverage was continuous along the satellite sub-track except for a calibration period every 40 scan lines (approximately every 1600 km along the sub-orbital track on the surface of the earth). The calibration sequence lasts the time equivalent to three scan lines, thereby skipping a swath about 120 km wide. A special objective analysis procedure has been developed elsewhere to interpolate into such calibration gaps when a continuous field is desired or is necessary (Lipton and Hillger, 1982).

The calibrated earth-located TOVS data obtained from the NESS group at the University of Wisconsin consists of 30 parameters as listed in Table 2.3. Of the available parameters only selected HIRS-2 (infrared) channels are used. NESS personnel also provided the atmospheric

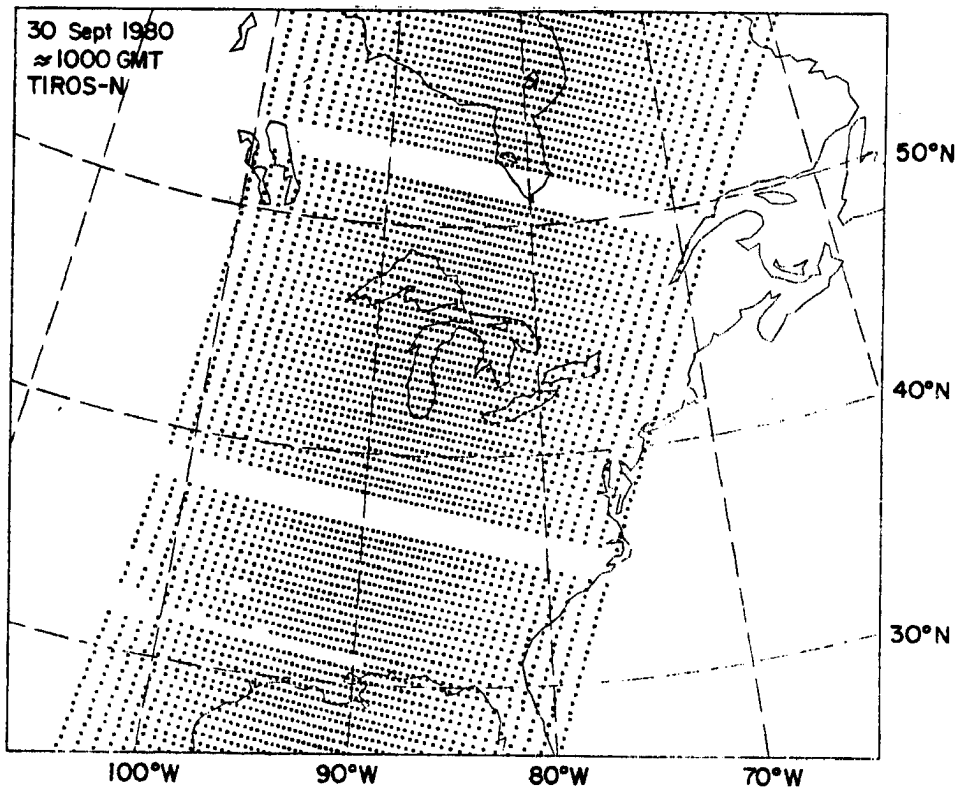


**Figure 2.2a** TIROS-N descending orbit (equatorward) for 30 September 1980 at approximately 1000 GMT (0400 LST). HIRS-2 sounding locations are shown.

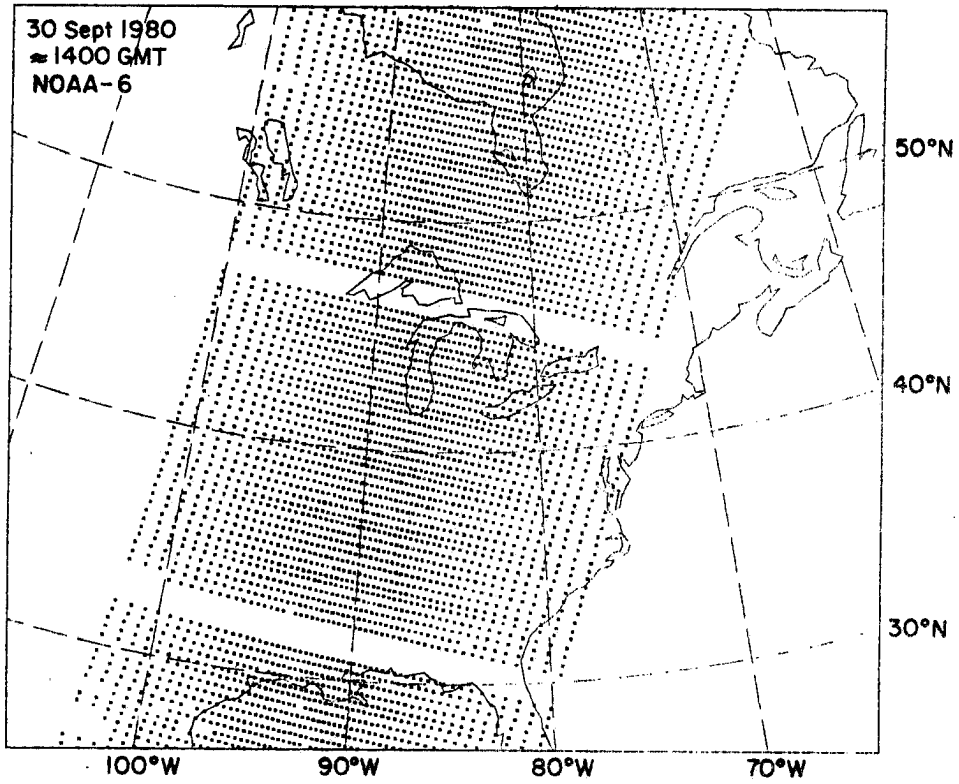


**Figure 2.2b NOAA-6 descending orbit (equatorward) for 30 September 1980 at approximately 1400 GMT (0800 LST). HIRS-2 sounding locations are shown.**

transmittance software appropriate for HIRS-2 (Weinreb et al., 1981).

Table 2.3

## TOVS Earth-located Calibrated Data

<u>Parameter</u>	<u>Description</u>	<u>Units</u>
1	Latitude	Degrees North
2	Longitude	Degrees West
3	Solar Zenith Angle	Degrees from Nadir (night = 90°)
4	HIRS Ch1	Brightness Temperature (K)
5	' Ch2	' ' '
6	' Ch3	' ' '
7	' Ch4	' ' '
8	' Ch5	' ' '
9	' Ch6	' ' '
10	' Ch7	' ' '
11	' Ch8	' ' '
12	' Ch9	' ' '
13	' Ch10	' ' '
14	' Ch11	' ' '
15	' Ch12	' ' '
16	' Ch13	' ' '
17	' Ch14	' ' '
18	' Ch15	' ' '
19	' Ch16	' ' '
20	' Ch17	' ' '
21	' Ch18	' ' '
22	' Ch19	' ' '
23	MSU Ch1	' ' '
24	' Ch1	' ' '
	(sfc and liquid water removed)	
25	' Ch2	' ' '
26	' Ch3	' ' '
27	' Ch4	' ' '
28	Total Outgoing Longwave Flux	(Watts/m <sup>2</sup> )
29	Bidirectional Reflectance	(percent of maximum possible)
30	HIRS Ch18	Brightness Temperature (K)
	(corrected for reflected sunlight)	

#### 2.4 Satellite Imagery

The GOES infrared imagery for the times of the TOVS soundings best serve to illustrate the cloud situation. Figure 2.3a shows the visible image at 1430 GMT on 30 September 1980, which is one half hour past the 1400 GMT NOAA-6 pass. The central U.S. from Minnesota down into Oklahoma is partly covered by a layer of fog. The fact that this is fog

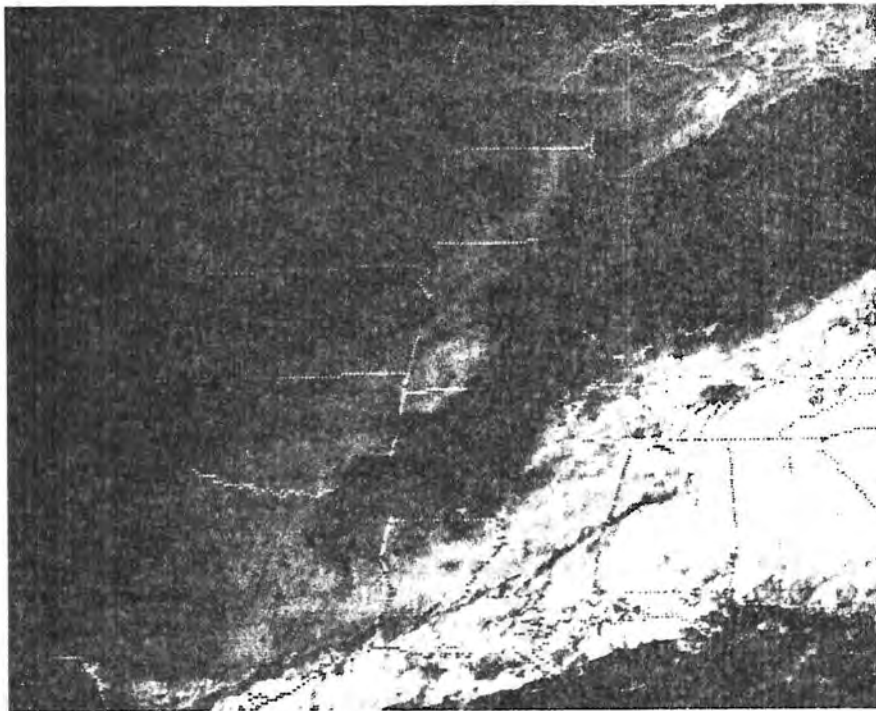


Figure 2.3a GOES visible image for 1430 GMT on 30 September 1980.

is best illustrated by the infrared (thermal) image at 1400 GMT in Figure 2.3b. In this image the fog, being only slightly cooler than the surrounding surface, is barely discernable. The temperature change is only on the order of 10 K.

The GOES infrared image for the TIROS-N pass at 1000 GMT is given in Figure 2.3c. This is a nighttime infrared image (no visible possible). Here portions of the region that later turn foggy appear warmer (darker) than the surrounding clear areas. The fact that the areas which produce fog appear warmer is indicative of low-level moisture. One explanation for this warm appearance relative to surrounding areas is that the surrounding areas are drier and are not as radiatively insulated, thereby allowing a stronger nocturnal cooling to take place (Parmenter, 1976). These dry areas cooled more rapidly during the night and show strong thermal inversions as the 1200 GMT RAOBs indicate. The foggy area, however, appears cooler than the surroundings if we go ahead to 1400 GMT (back to Figure 2.3b). By this time the solar heating has increased the surrounding surface temperatures above that of the top of the fog.

The clues to the cloud situation help us interpret the TOVS satellite soundings. The transition period from nighttime to daytime is a period of strong thermal change. This will be an especially tough situation in which to produce time continuity in the satellite products.

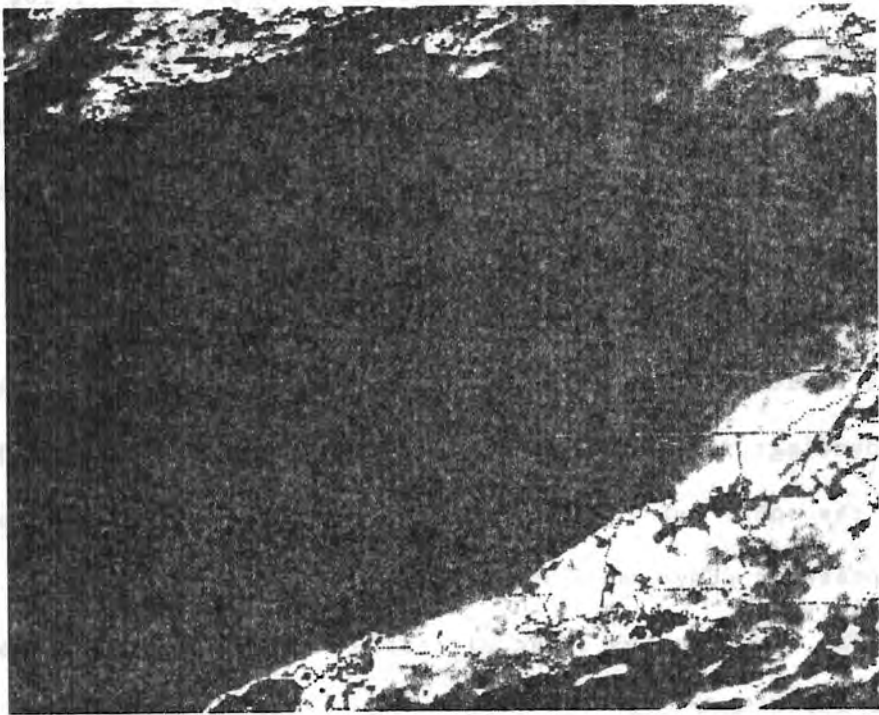


Figure 2.3b GOES infrared image for 1400 GMT on 30 September 1980.

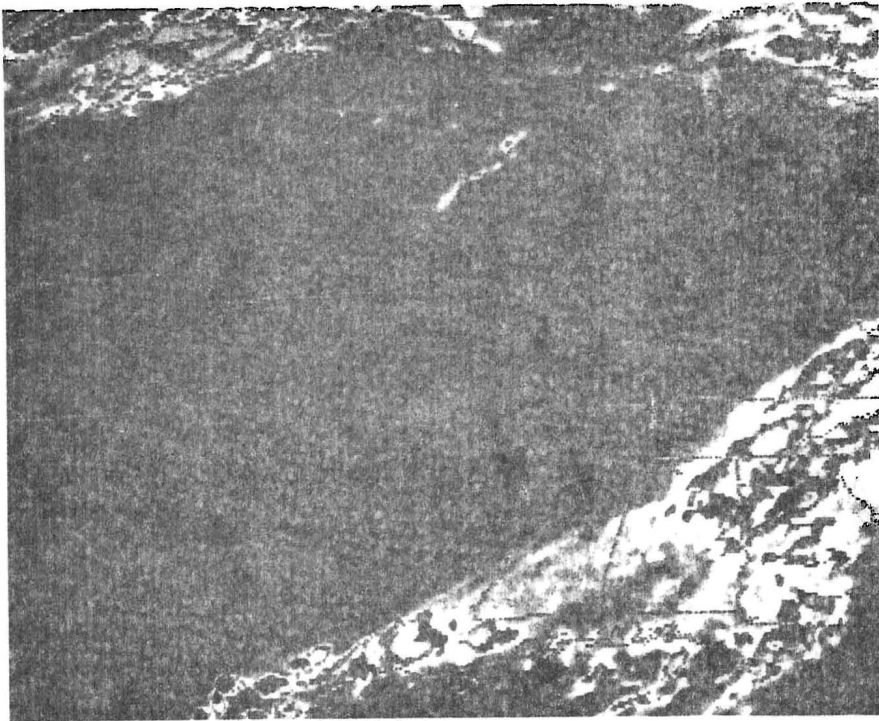


Figure 2.3c GOES infrared image for 1000 GMT on 30 September 1980.

### 3.0 CONVENTIONAL DATA

Two sources of conventional data were used: 1) rawinsonde (balloon) soundings, and 2) surface weather observations. The rawinsondes were used mainly to provide the initial guess temperature and moisture profiles for the iterative satellite retrieval system. Because the rawinsondes were the only source of conventional upper-air data, they were also used for comparison to the satellite-derived upper-air parameters at the synoptic scale.

The surface weather observations, being spatially more dense than the balloon soundings, were used only for verification of the satellite-derived meteorological parameters at the surface observation scale. However, some small differences between the fields of measurements are expected to appear because of the inherent differences between the satellite and conventional measuring systems. The resultant similarities and differences between the conventional and satellite-derived products are important and will be examined.

#### 3.1 Rawinsondes

The only conventional upper-air measurements taken for the time period under consideration were the 1200 GMT rawinsonde observations (RAOBs). The 1200 GMT synoptic time was midway between the two satellite sounding times of 1000 and 1400 GMT. This places the RAOBs within 2 hours of the satellite measurements. The only other conventional soundings were taken 10 hours before and after the first and second satellite passes, respectively (both at 0000 GMT).

Therefore, this set of 1200 GMT RAOBs included all the conventional soundings used in this study.

The RAOBs were used mainly to provide the starting temperature and moisture profiles for the iterative retrieval process. To generate this initial guess profile the RAOBs were composited for the region extending from 31 to 49 degrees north latitude and from 83 to 105 degrees west longitude, as outlined by the solid box in Figure 3.1. (The dashed box is the area where the higher-density satellite retrievals were later performed.) Of the 27 RAOBs which went into the composited initial guess, all but one are part of the NWS sounding network which are typically spaced at least 250 km apart. The remaining sounding was launched at Fort Sill, Oklahoma (FSI) which is approximately 100 km from Oklahoma City (OKC).

The temperature and moisture profiles created by compositing the 1200 GMT RAOBs are shown in Figure 3.2. There were some large differences among the individual soundings which went into this composited mean profile, especially with regards to the moisture and temperature structure near the surface. If the moisture profiles can be categorized into three regimes, they would be characterized by 1) deep moisture, 2) a shallow moist layer near the surface with overlying dry air, and 3) relatively dry throughout the troposphere. Green Bay (GRB) and Salem (SLO), with deep moist layers from the surface to as high as 75 kPa (750 mb), are the moist extreme, whereas Topeka (TOP) and Fort Sill (FSI) typify the dry over moist situation with shallow moist layers of less than 10 kPa (100 mb) thickness (TOP sounding shown later). At the dry extreme are Omaha (3NO) and Amarillo (AMA). Other soundings displayed intermediate degrees of each of these three broad regimes.



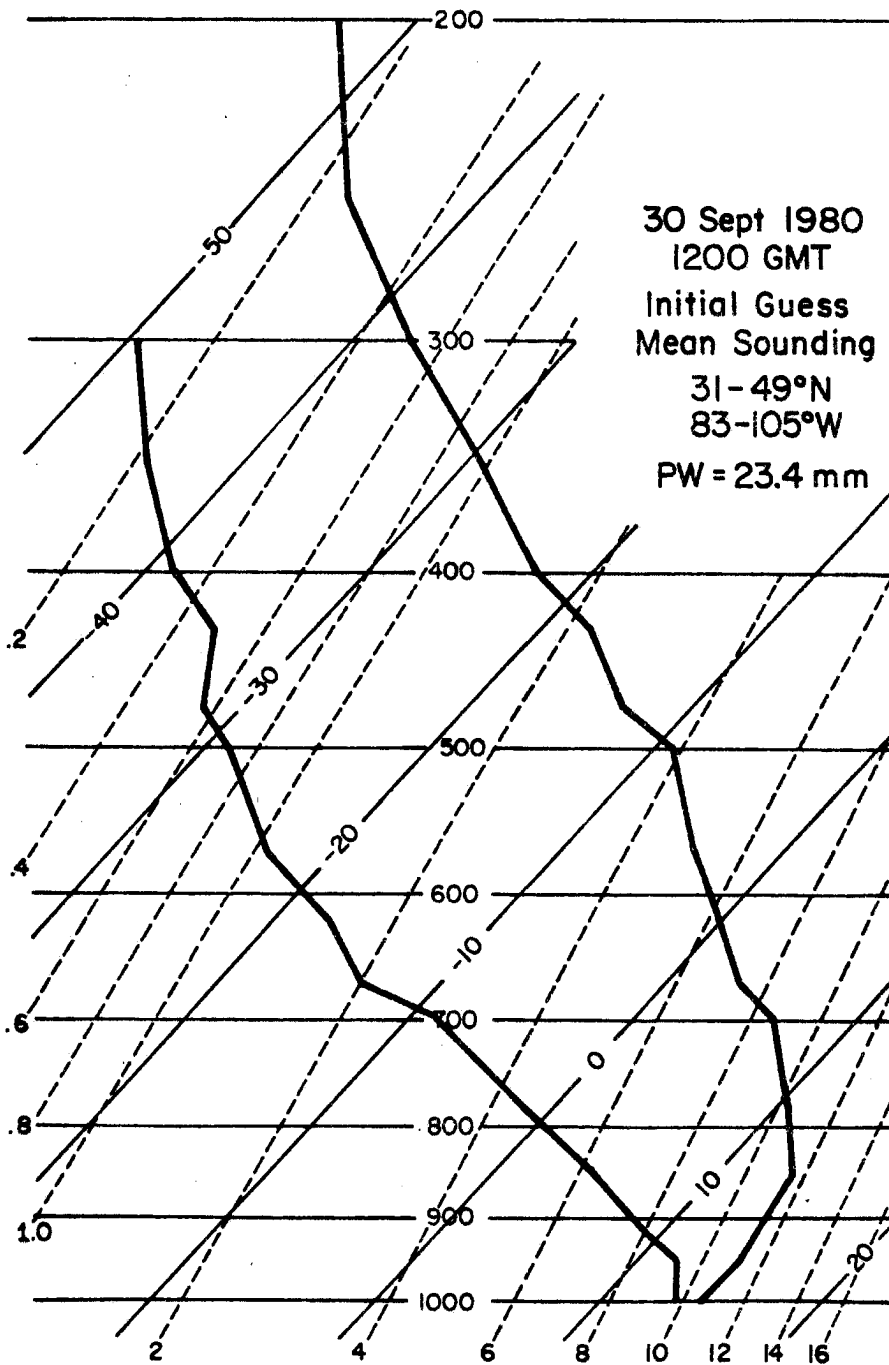


Figure 3.2 Mean temperature and moisture profiles composited from the 27 circled RAOBs shown in Figure 3.1. Plotting is done on a USAF skew T-log P thermodynamic diagram.

The RAOB temperature profiles were generally less variable than the moisture profiles except near the surface where many soundings contained shallow temperature inversions with temperature increases with height of around 10 K within the lowest 2 kPa (20 mb). Soundings typical of these large temperature inversions occurred at North Platte (LBF) and Omaha (3NO). These inversions, however, were removed from the soundings when creating the composite temperature profile. The reason for this is due to the special problems caused by nocturnal temperature inversions in the retrieval of satellite soundings as will be explained in a later section.

A second use of the RAOBs was as a source of conventional upper-air data for comparison to the satellite soundings. These RAOBs were the only conventional data set which contained vertical structure in the meteorological parameters, unlike the surface observations which contained no vertical information. By comparing and contrasting the conventional measurements with the satellite-derived values, some important differences may be noted which relate to the measuring systems involved.

### 3.2 Surface Observations

The surface observations were obtained from two sources. One was the synoptic surface weather charts generated by the National Weather Service (NWS) every 3 hours. The synoptic reporting times surrounding the TIROS-N and NOAA-6 satellite passes were 0900, 1200, and 1500 GMT. The analyzed synoptic charts, however, many times do not include all the surface observations which were taken at a particular time. Both space and time limitations in creating the plotted charts can prevent all the measurements from appearing. To alleviate this problem, a second source

of synoptic surface observations was tapped. This was the National Meteorological Center (NMC) data base as archived at the National Center for Atmospheric Research (NCAR). This data base included as many additional surface observations as were plotted on the NWS surface charts. The higher data density of this more complete set of surface observations provided a data set more readily comparable to the potentially higher-density satellite observations.

A plot of all surface observation stations reporting at either 0900, 1200, or 1500 GMT for the smaller area under consideration is given in Figure 3.3. Not all stations reported at each synoptic time. Table 3.1 gives the number of reporting stations at each of the three synoptic times and the total number of observing stations.

Table 3.1

Synoptic Surface Observations  
(32-45°N 87-101°W)

<u>Time</u>	<u>Number of Observations</u>
0900 GMT	101
1200 GMT	123
1500 GMT	126
all stations	137

The meteorological variables which were extracted from each of the synoptic surface stations were the temperature, dew point temperature and relative humidity. Since these three surface parameters are the variables which were obtained at a density approaching that of the satellite data, they alone formed the basis for our satellite-conventional data comparisons.

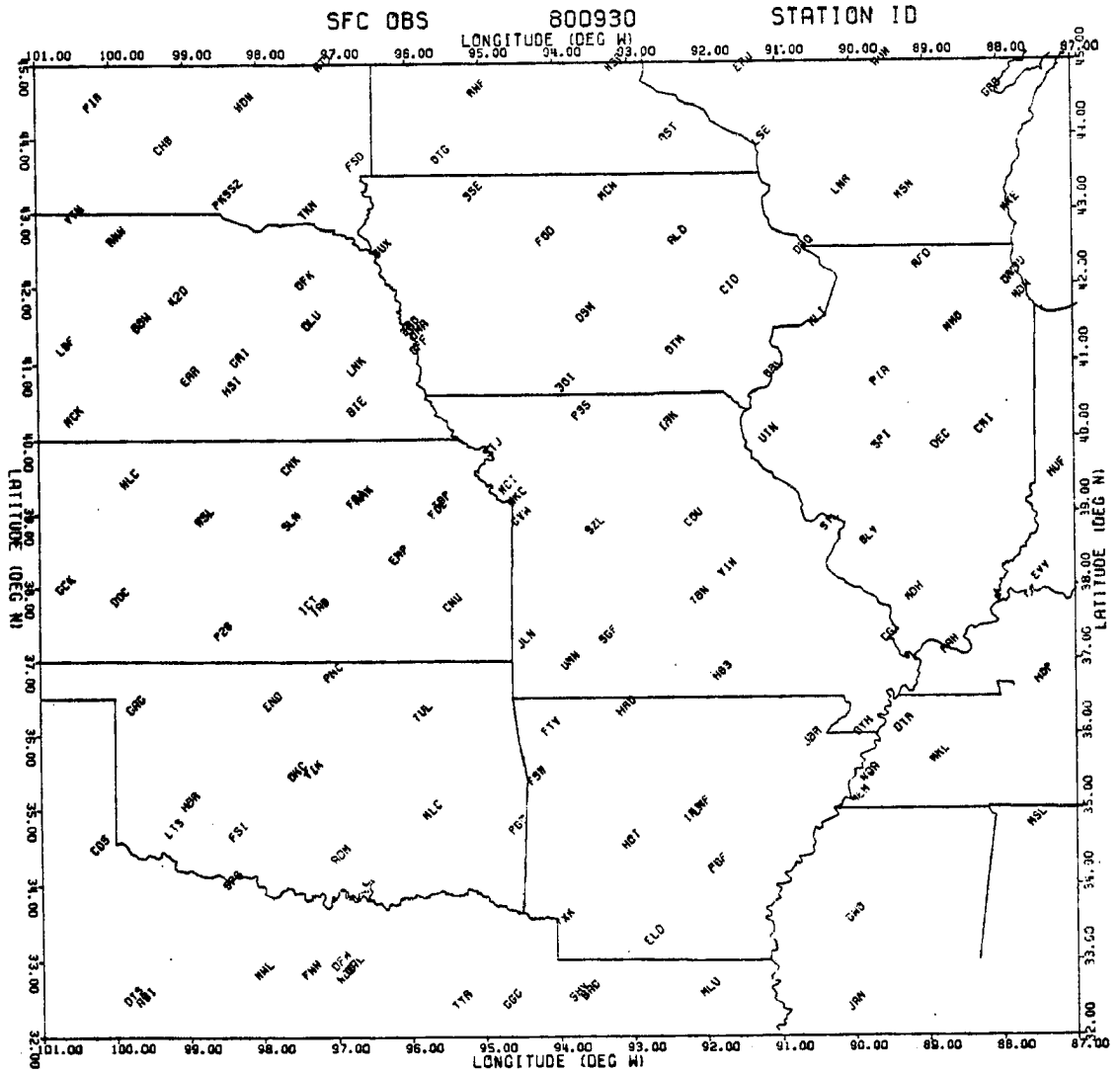


Figure 3.3 Surface observation station identifiers plotted at their respective locations.

### 3.3 Meteorological Situation

The moisture situation at 1200 GMT on 30 September 1980 can be summarized by synoptic-scale plots of some of the RAOB moisture parameters. Specifically, the RAOB surface dew point temperature, the RAOB total precipitable water and the ratio of the total precipitable water to the surface mixing ratio are plotted in Figures 3.4a, b, and c. The outlined area in these figures is approximately the area over which the RAOBs were composited for the initial guess sounding.

Figure 3.4a shows the surface dew point temperatures which range from less than  $0^{\circ}\text{C}$  in western South Dakota and Colorado to over  $20^{\circ}\text{C}$  in the southern parts of Texas and Louisiana. A dry slot at the surface exists through the central states from Nebraska to Ohio. As shown in the satellite images earlier, the moist regions to the north and south are linked to cloudy areas associated with weak low pressure systems.

Figure 3.4b shows the total precipitable water for the same area. The pattern here differs from the surface moisture field in Figure 3.4a. A much stronger moisture gradient exists from the southeast to the northwest. However, a similar dry tongue extends from Nebraska into Illinois with a local minimum at Omaha (3NO).

By using the surface mixing ratio rather than the surface dew point the ratio of the total moisture to the surface moisture can be formed. (The mixing ratio is used rather than dew point temperature to avoid division by values at or near zero.) This ratio is plotted in Figure 3.4c. Low values of the ratio signify dry or dry-over-moist situations and large values signify deep moist situations. The dry or dry-over-moist area extends from Texas up into Minnesota. This covers the area where the fog formed at 1400 GMT. Radiation fog is most likely

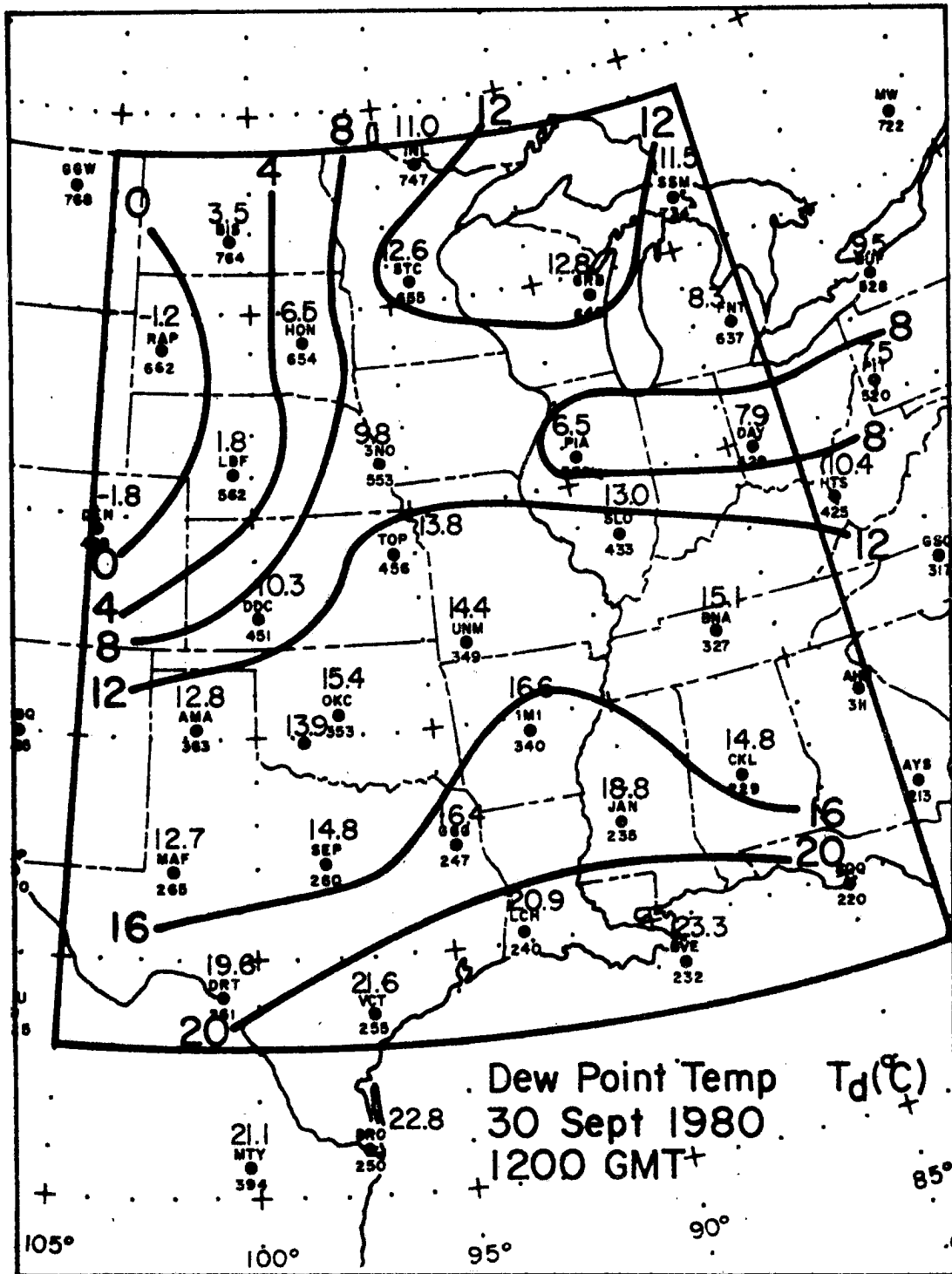


Figure 3.4a Surface dew point temperatures ( $^{\circ}\text{C}$ ) from RAOBs at 1200 GMT on 30 September 1980.



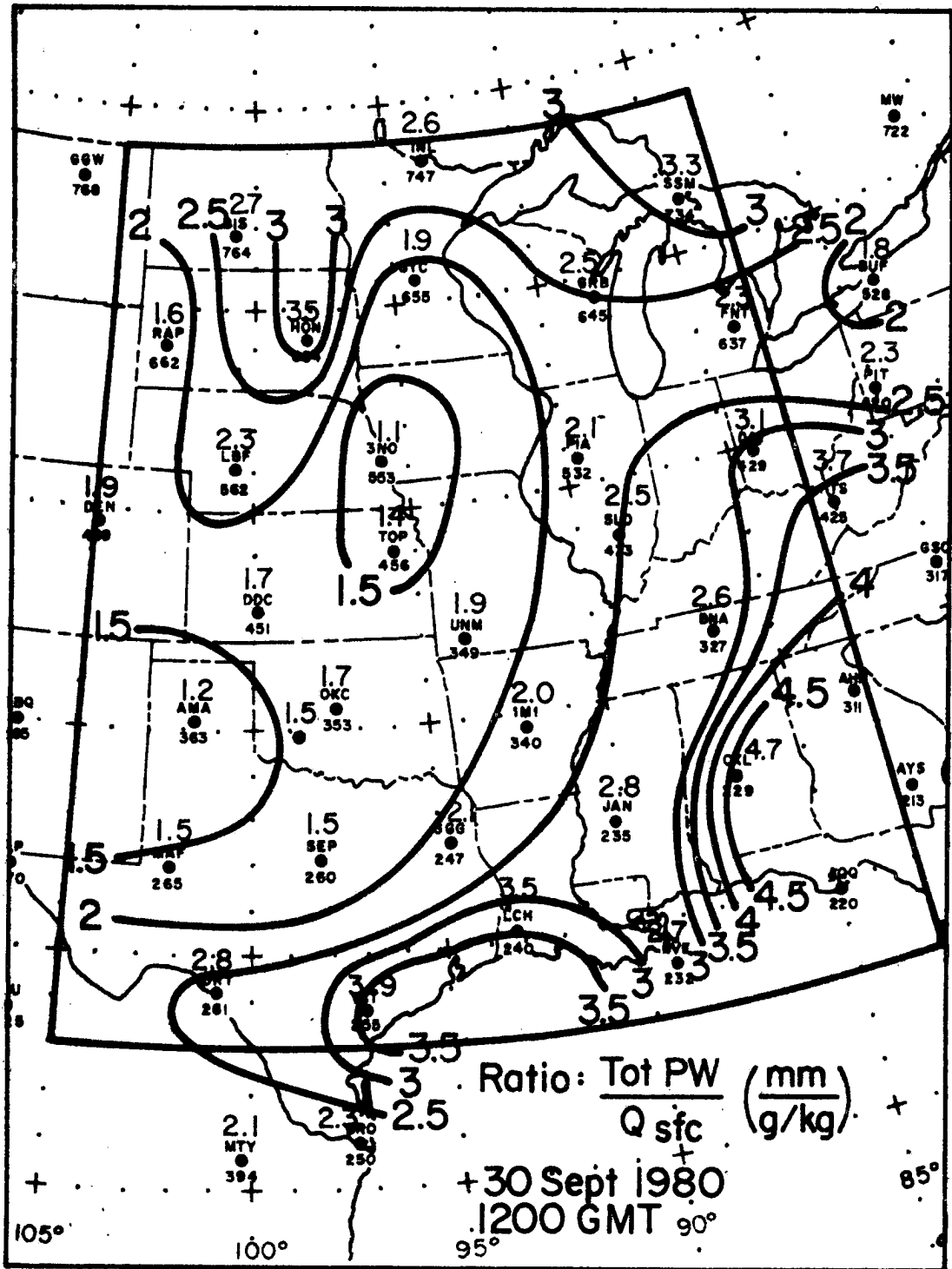


Figure 3.4c Ratio of total precipitable water to the surface mixing ratio ( $\text{mm}(\text{g kg}^{-1})^{-1}$ ) from RAOBs at 1200 GMT on 30 September 1980.

to form in a situation where enough low-level moisture exists, but where the upper levels are dry enough to allow sufficient radiative cooling at the surface. The fog seemed to form in a narrow band on the eastern side of this region of low ratios. From a radiative point of view areas farther to the west were too dry at the surface to produce fog, and areas farther to the east were too moist aloft to allow sufficient radiative cooling even though the low levels were moist.

#### 3.4 Moisture Estimation from Surface Dew Point

In recent meteorological history there have been many attempts to use surface moisture measurements to estimate the total atmospheric water content. Reitan (1963) rekindled an interest in the surface dew point to precipitable water relationship by using mean monthly values of both parameters to determine the relationship

$$\ln PW = a + b \cdot T_d \quad (3.1)$$

where PW is the precipitable water (in millimeters) and  $T_d$  is the surface dew point (in degrees Celsius). His mean monthly values for 15 U.S. RAOB stations gave a correlation coefficient of 0.98 for a total of 540 observations. His 'a' and 'b' coefficients turned out to be  $a = 2.413$  and  $b = 0.061 \text{ (}^\circ\text{C)}^{-1}$ . This relationship covers three years of mean monthly values.

Bolsenga (1965) using the same relationship derived coefficients of  $a = 2.420$  and  $b = 0.077 \text{ (}^\circ\text{C)}^{-1}$  for 72 mean daily values with a correlation coefficient of 0.85, and  $a = 2.243$  and  $b = 0.069 \text{ (}^\circ\text{C)}^{-1}$  for 97 hourly values with a correlation coefficient of 0.80.

Smith (1966), realizing that the 'a' coefficient depends on the vertical distribution of moisture, suggested a latitudinal and seasonal dependence when relating surface dew point to total water vapor content. This was in an effort to reduce errors that may result from using a relationship derived for mean monthly values. Smith also concluded that 'the longer the time period over which the mean values of water vapor content and surface dew point are formed, the more unique the relation is between these two variables'.

In later work Reber and Swope (1972), also using mean monthly values, derived correlation coefficients ranging from -0.29 to 0.83, indicating 'that a direct but widely variable relationship exists between the total precipitable water and surface absolute humidity'. They also concluded that estimates of total precipitable water from surface humidity measurements are not valid. Their results were for three stations in California and were later contested by Glahn (1973). Especially under attack was the statement 'that estimates of precipitable water from surface measurements, on an individual measurement basis, are not sufficiently reliable to justify making surface measurements to infer existing precipitable water'.

Finally in our historical review, Benwell (1965) in studying the temporal and spatial variability of precipitable water found 'that the observed value of precipitable water is not normally a good estimate of the value at that place 12 hours later'. His study included five months of data at three Atlantic ocean weather stations. The interest was in obtaining estimates of precipitable water based on higher-density surface observations over the ocean. He also concluded that the correlation coefficients between surface moisture and total water 'are

considerably higher than the autocorrelation coefficients over periods of 12 hours or more and seem likely to be higher than the autocorrelation for periods as short as six hours'. In other words, it is better to estimate the precipitable water from surface moisture than to assume persistence for periods much longer than six hours.

Along the lines of Benwell, it was thought to be possible to use the surface dew point measurements in this study to estimate the total precipitable water at a higher density than that of the synoptic RAOBs. First, the relationship of total water to surface dew point was established for the 1200 GMT RAOBs as shown in Figure 3.5. Points are plotted for 36 RAOBs as well as a least squares line fit to those points. The 36 RAOBs include the 27 RAOBs which went into the initial guess profile as well as nine other RAOBs outlined by squares in Figure 3.1. The extra RAOBs to the south were especially helpful in establishing the regression line by supplying a set of more moist soundings in the upper right corner of Figure 3.5.

The equation for the regression line is given as

$$\ln PW = 2.093 + .074 T_d. \quad (3.2)$$

The a and b coefficients are specific to this one date and time but are only slightly different than those given earlier. The correlation coefficient between the variables is 0.81 (66% explained variance). By eliminating a few outlying points the correlation can be increased, but the equation for the line remains almost unchanged.

To see how well this relationship works, Figure 3.6a is a plot of the estimated total precipitable water using the RAOB surface dew point values. The contours are very similar to those for the dew points in

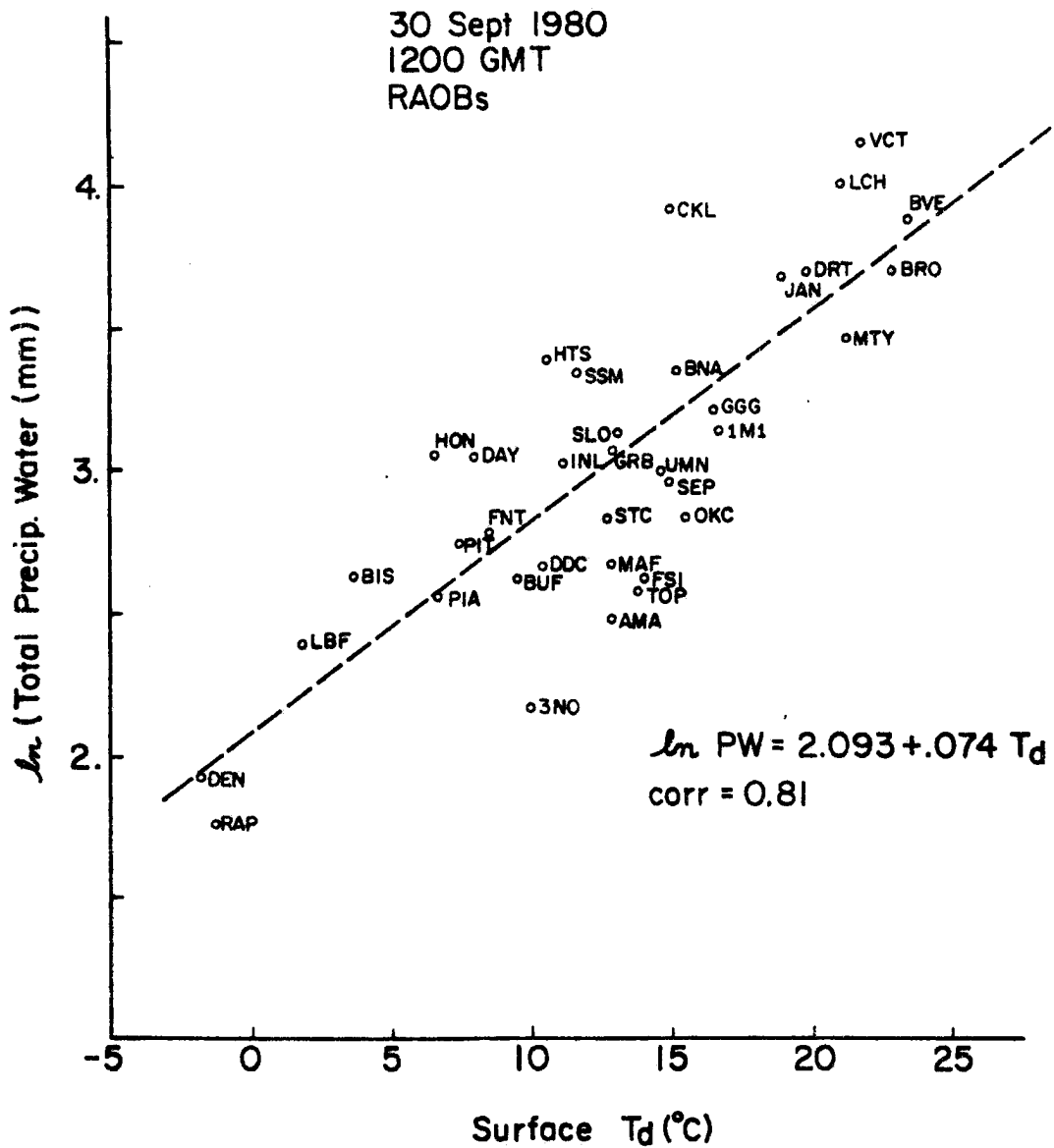


Figure 3.5 Plot of total precipitable water versus surface dew point temperature for the 36 RAOBs in Figure 3.1. A linear least-squares regression line has been fit to the points.

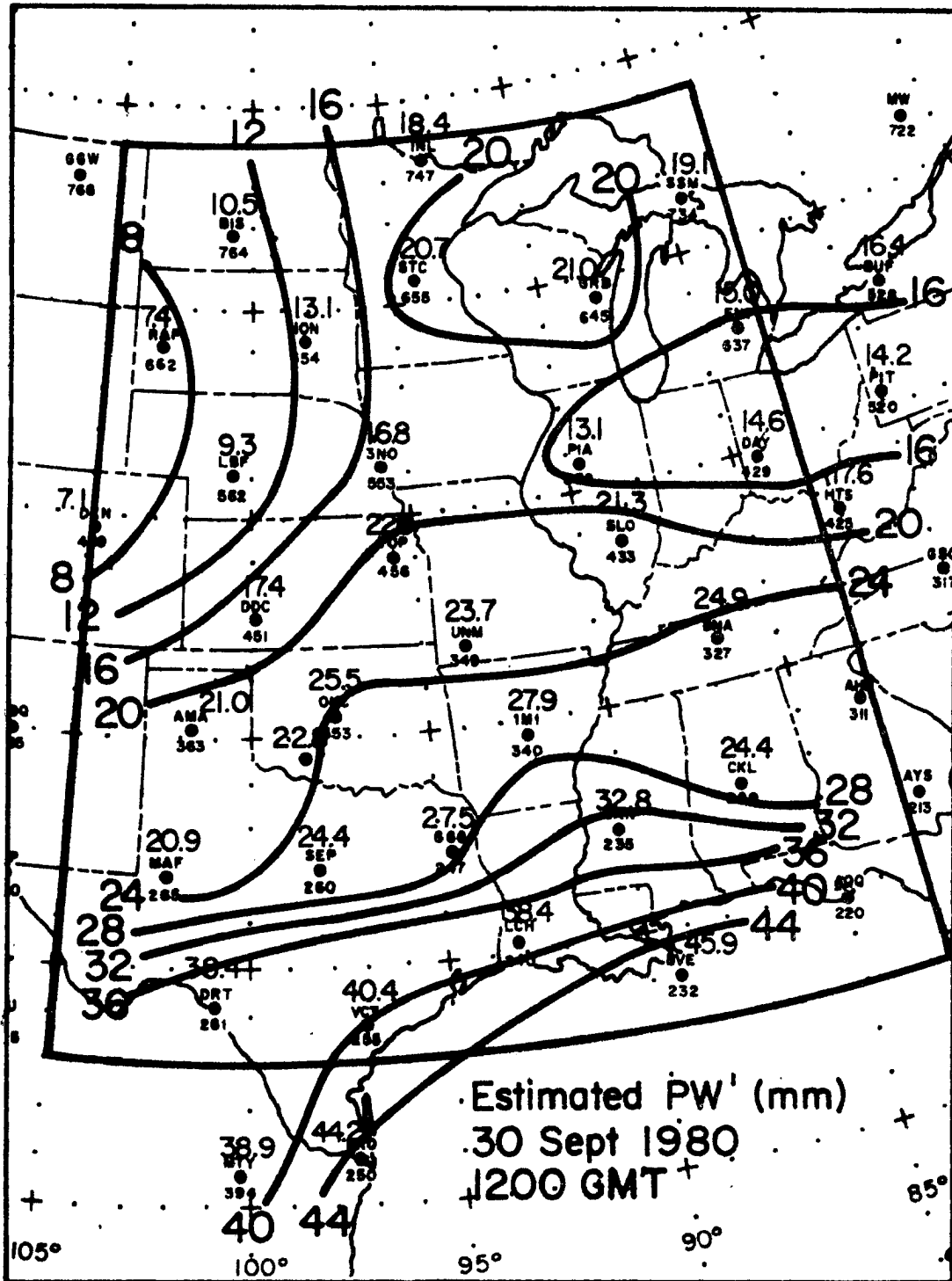


Figure 3.6a Estimated precipitable water (mm) at the RAOB positions using the regression line in Figure 3.5 and the RAOB surface dew point temperatures at 1200 GMT on 30 September 1980. The contours are very similar to those for the surface dew point temperatures in Figure 3.4a.

Figure 3.4a, but the values and gradient are changed. By differencing the actual precipitable water and the estimated value the plot in Figure 3.6b is formed. Here it is shown that large differences do occur.

Generally, the RAOBs above the regression line in Figure 3.5 contain more moisture than would be estimated from the surface and give positive differences. On the other hand, the RAOBs below the regression line have less total water than estimated from the surface and give negative differences.

The contours in Figure 3.6b show that the negative values extend from Texas up into Minnesota, similar to the low values of the ratio of total water to surface mixing ratio as was shown in Figure 3.4c. These are the dry over moist situations where the estimated total water values are greater than the actual values. This is also approximately the region where the fog forms. Likewise, the positive values show where the troposphere is moist through a large depth. These differences, therefore, give an indication of regions where the atmosphere is dry (-) and moist (+) aloft.

This type of estimated total water analysis will later be extended to the surface observations and then compared to the satellite-derived total moisture. Because of the lack of upper-air measurements of higher density than the RAOBs, the estimated total water at the surface stations will be used to compare and contrast with the satellite-derived total water. Differences again will be related to areas where the troposphere is dry or moist aloft.

To understand the type of moisture profile represented when only a surface dew point is given, a power-law decrease in mixing ratio with pressure

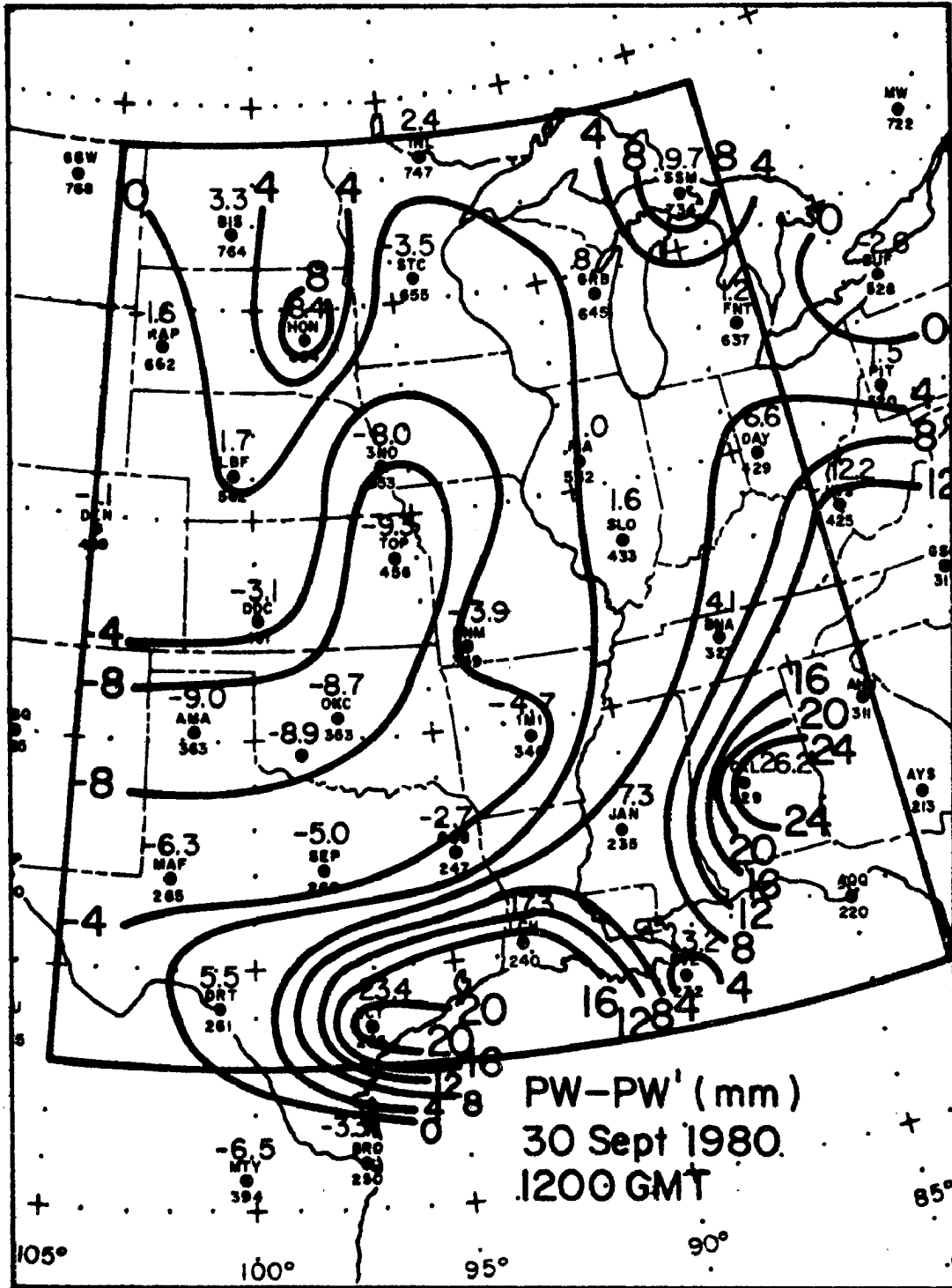


Figure 3.6b Precipitable water difference (mm) (measured minus estimated from surface dew point) for RAOBs at 1200 GMT on 30 September 1980. The differences denote areas of dry (-) and moist (+) aloft.

$$Q(p) = Q_{\max} \left( \frac{p}{p_{\max}} \right)^{\gamma} \quad (3.3)$$

was used in the Smith (1966) theoretical development, where  $Q_{\max}$  is the surface or maximum mixing ratio at  $p = p_{\max}$ . When inserted into the precipitable water integral

$$U = g^{-1} \int_0^{p_{\max}} Q(p) \cdot dp \quad (3.4)$$

where  $U$  is the precipitable water the result is

$$U = \frac{Q_{\max} \cdot p_{\max}}{g \cdot (\gamma+1)} \quad (3.5)$$

Inverting Equation 3.5 results in

$$\gamma = \frac{Q_{\max} \cdot p_{\max}}{g \cdot U} - 1. \quad (3.6)$$

The exponent  $\gamma$  can then be found as a function of dew point temperature, which determines uniquely the surface mixing ratio. The total water  $U$  is also determined uniquely by the surface dew point by using a relationship of the form of Equation 3.1.

For the surface dew point to precipitable water relationship found for the 1200 GMT RAOBs in Equation 3.2 the exponent  $\gamma$  varies slightly with dew point as shown in Figure 3.7. A mean value for  $\gamma$  of approximately 3.5 would represent most situations. This value can be used to construct an estimated moisture profile given only a surface dew point temperature. This technique will be used later for comparisons with satellite-derived moisture profiles.

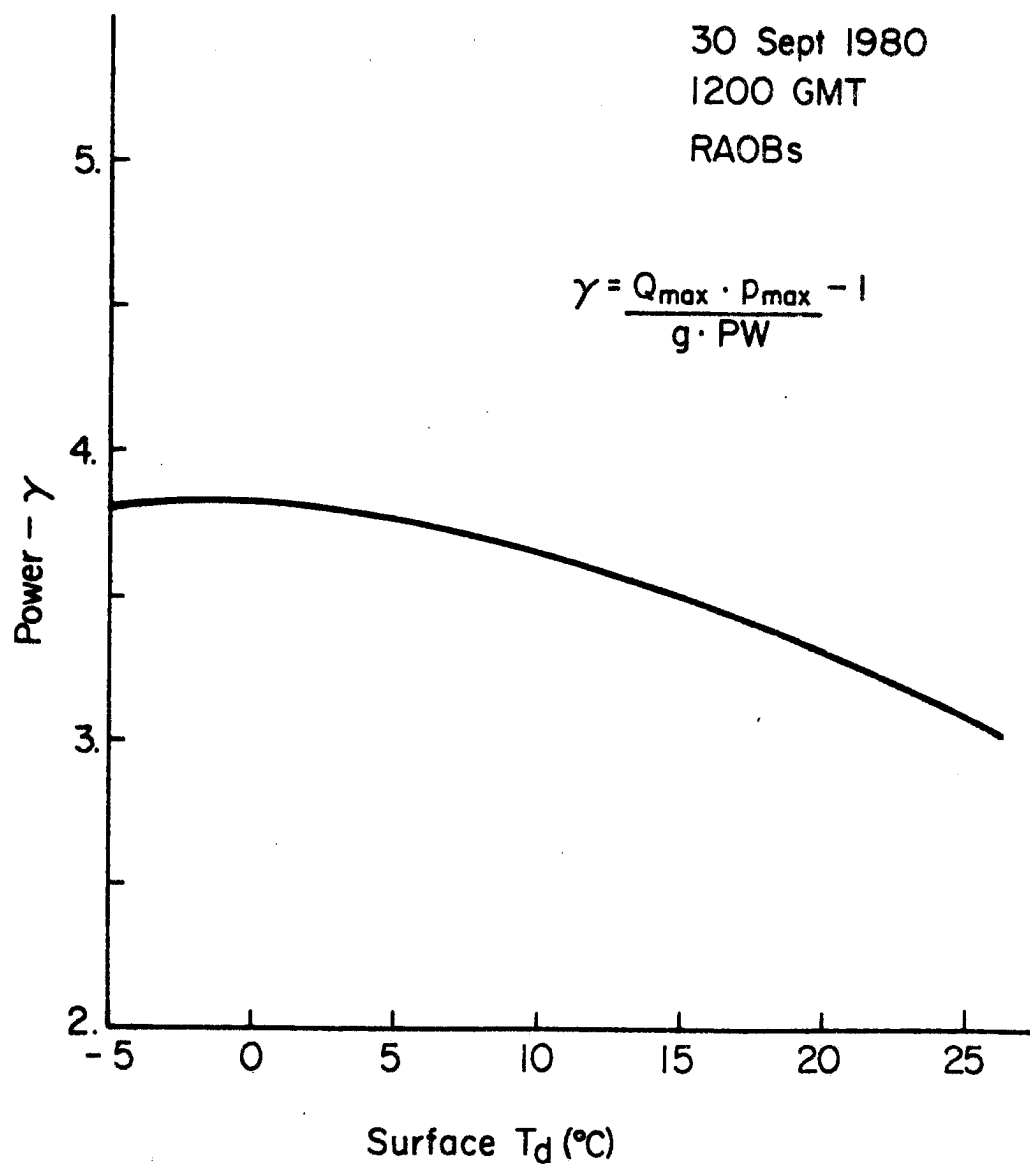


**Figure 3.7** Exponent for a power-law mixing ratio decrease with pressure as a function of surface dew point temperature. The results are based on Equation 3.6 and precipitable water determined by Equation 3.2.

#### 4.0 BACKGROUND

The retrieval of meteorological parameters from HIRS-2 measurements has been accomplished by other groups and has been documented in the published literature. However, most of these studies have dealt mainly with satellite temperature retrieval capability. The main emphasis of this work is the moisture retrievals, on which the published results are fewer. Important differences in the retrieval scheme also exist. One major difference is the use of only a single set of satellite measurements, from a single field-of-view, to retrieve meteorological parameters. This single field-of-view retrieval scheme is based on previous work with HIRS-1 satellite measurement in which moisture parameters in particular were successfully retrieved in a summertime pre-convective situation.

#### 4.1 Other Studies Using TOVS

Several studies have been made to determine the accuracy of meteorological parameters derived from the TOVS instrument. Many of these studies compared satellite-derived parameters to the same parameters measured by conventional rawinsonde (RAOB) soundings. Only a relative accuracy of the satellite-derived parameters can be determined by this method because the conventional data are not error free. Therefore the term 'error' in the strict sense must not be used.

Typically, most satellite-RAOB comparisons have produced similar results. As far as temperature comparisons are concerned, Phillips et al. (1979) gave a temperature difference for clear and partly cloudy

cases of typically less than 2 K rms with a bias of generally less than 1 K except near the surface. This was for a relatively small number of comparisons over the ocean for a period of two months in 1979.

Schlatter (1981) did an independent comparison for a 2 week period in 1979 using over 1500 clear and cloudy TIROS-N soundings. His results gave rms differences varying from 1.5 to 2 K except near the tropopause and surface where the differences were larger.

These temperature comparison results have been typically unchanged throughout the history of satellite soundings with possibly only slight improvements. The predecessor to the HIRS-2, the HIRS-1 instrument on board Nimbus-6, produced similar results. Moyer et al. (1978) gave a 2.1 K rms discrepancy for all levels and stations for a single satellite pass. Another study by Schlatter and Branstator (1979) for an 8-day series in August 1975 using approximately 1000 satellite-RAOB comparisons gave an rms error of from 1 to 2.9 K with the maximum error at the tropopause.

#### 4.2 Previous Moisture Retrieval Results

Besides the temperature comparison results which were summarized above, a few studies have dealt with satellite-derived moisture parameters. Gruber and Watkins (1979) determined that total column precipitable water was 'reasonably well represented' by the TOVS retrievals. Their results included a rms precipitable water difference (compared to RAOBs) of 6 mm or about 27% of a mean value of 23 mm. They pointed out, however, that moisture data at individual levels was at best marginal. This result is due to both the layered structure of the atmosphere and the inherently low vertical resolution of the satellite sounder. Another study by Hayden et al. (1981) showed that strong

horizontal moisture gradients can be clearly defined which are consistent with conventional observations. This, however, was only a qualitative comparison. Going back to the study of Moyer et al. (1978), using HIRS-1 data, they achieved an rms dew point temperature difference (compared to RAOBs) of 7.3 K for all levels and stations for a single pass of HIRS retrievals. This is a large difference for retrieved moisture at any single level, but when the moisture is analyzed in terms of integrated precipitable water the discrepancy was 2.6 mm of H<sub>2</sub>O which represented only 20% of the total precipitable water.

#### 4.3 Difficulties and Differences

To retrieve moisture parameters from satellite measurements is generally more difficult than to retrieve temperature parameters. This is true because moisture is a highly variable absorbing and emitting constituent which causes strong changes in the H<sub>2</sub>O weighting functions. In the case of temperature retrievals the absorbing constituent, CO<sub>2</sub>, has a relatively constant mixing ratio throughout the atmosphere. The temperature is merely a characteristic of the absorber, so temperature changes leave the weighting functions largely unchanged. However, the effect which moisture has on the weighting functions must be considered in every step in the retrieval process in which the moisture changes.

Another degree of difficulty in retrieving moisture information from satellite measurements arises because the moisture lies largely near the surface, and meteorological parameters near the surface are typically harder to retrieve than those in the middle levels. Many of the previously-cited studies give temperature comparisons which confirm this. Much of the difficulty arises because of the strong effect of the boundary or surface temperature upon the satellite radiances. To

determine moisture the surface temperature must be either known or retrieved independently from other satellite channels. A point which must be stressed is that the synoptic surface observations of temperature and dew point were used in this study only for comparison to similar satellite-derived parameters. The surface temperatures for the moisture retrieval process were, therefore, retrieved independently by using the satellite window channels.

Moisture also tends to vary more rapidly on small space and time scales than temperature; thus, the need for high space and time resolution. Wark et al. (1974) did some of the first mesoscale moisture analysis using high-resolution satellite measurements. Smith et al. (1979a) also analyzed moisture at the mesoscale. However, most previous work has dealt with synoptic-scale retrievals and comparisons to the RAOB network, but for high-resolution satellite soundings the comparisons must be made to higher-resolution surface weather observations. In this study moisture parameters were retrieved from single satellite views at the same approximate resolution as the synoptic surface observations. The surface observations come closer to matching the high-resolution capabilities of satellite soundings even though the surface observations typically have a mean separation of at least 100 km.

#### 4.4 Background Work with HIRS-1

The scheme used to retrieve temperature and moisture parameters from HIRS-2 is based on previous work published by Hillger and Vonder Haar (1981) using HIRS-1 data from Nimbus-6. That study involved four case study days in August of 1975. Only three of the case study days were meteorologically interesting and were discussed in detail in that

publication. One of the goals of that study was the retrieval of high-resolution or high-density atmospheric parameters. The maximum resolution of HIRS-1 was about 35 km, nearly the same as HIRS-2. Satellite-conventional data comparisons were made to both NWS rawinsondes and synoptic surface observations of dew point and temperature. The comparison to surface observations gave rms differences of 2.7 K and 4.0 K for temperature and dew point, respectively. In comparison to the RAQBs the rms precipitable water difference was 5.5 mm or 14% of the mean.

Another goal of that study was to use the satellite-derived parameters to investigate the meteorological environment in pre-convective situations. Small features at a scale of approximately 100 km, below the resolution of upper air soundings, were detected by the high-resolution satellite retrievals. The 'dryline' feature typically seen over the southern Great Plains in the summer months was studied. Perturbations on the dry line were apparent in the satellite data, whereas only the general dry line position was picked up by the synoptic surface observations. Local maxima of moisture and instability also correlated well with convective development which started from 2 to 2.5 hours after the local-noon Nimbus-6 measurements. The later convection, therefore, provided verification of the highest resolution satellite-derived details which otherwise remain unconfirmed by synoptic surface observations.

The fact that moisture parameters were retrievable from satellite measurements is in itself an accomplishment considering the inherent physical limitations in remote satellite soundings. Another desirable goal is to be able to observe these moisture fields to see how they

change in time. When combined with surface winds the moisture analyses can give moisture advection patterns at a very high resolution.

Inversely, low-level flow information could possibly be obtained from movements of surface moisture, without direct wind measurements. Such time-spaced measurements will become more common when the VAS (VISSR Atmospheric Sounder) provides operational soundings from geosynchronous orbit as often as every half hour over the United States. As of this time these operational products are not yet available to us. So, by using the time-spaced polar-orbiting sounding data available in this study, an indication of how well changes in satellite-derived moisture can be resolvable in time is given.

## 5.0 TOVS RETRIEVAL SYSTEM

The retrieval scheme used to obtain the high-resolution TOVS (HIRS-2) soundings is based on a similar software used previously for HIRS-1 data. Some of the HIRS-1 retrieval details covered in that publication (Hillger and Vonder Haar, 1981) remain unchanged, but other details will be reexamined where changes have been made as a result of experience gained in iterative retrievals.

First, because of the new channels introduced by the change in instrument from HIRS-1 to HIRS-2 a few modifications were necessary in the retrieval scheme. The addition of both an extra window and an extra H<sub>2</sub>O channel were handled by incorporating them into the appropriate feedback mechanisms.

Another feature introduced into HIRS-2 retrievals was a single field-of-view cloud correction technique. This was used in an attempt to retrieve useful information in partly-cloudy cases (where the field-of-view is only partly obscured by clouds). The results of partly cloudy retrievals, however, were not used because of meteorological inconsistencies, so the cloud problem was reduced to detection and elimination of cloud-contaminated soundings.

After cloud elimination, the next step was to correct the shortwave infrared channels which are susceptible to reflected solar radiation. This was only necessary for the 1400 GMT pass from NOAA-6. Such reflected contamination can be very significant as will be shown.

A new problem was introduced by the existence of strong surface temperature inversions when attempting to retrieve nighttime or early morning soundings. The previous work using the local-noon orbits of Nimbus-6 avoided any problems caused by temperature inversions near the surface as were encountered especially with the local 4 a.m. TIROS-N satellite data in this study. To deal with this problem a temperature inversion had to be introduced into many of the nighttime retrieved temperature profiles to produce a meteorologically and physically reasonable solution to the radiative transfer equation.

Next, a terrain height correction was necessary because the satellite retrievals covered a large area where terrain elevations varied greatly. Surface pressures were estimated using the hydrostatic relationship and mean terrain elevation data for the area under study.

Finally, the iterative feedback mechanisms are mentioned. These mechanisms include feedback to the surface temperature, the moisture profile, and the temperature profile. The order of the moisture and temperature profile feedback is allowed to change in certain circumstances. Otherwise, the order is maintained until either a set number of iterations is exceeded or there is lack of reduction in the radiance residuals.

### 5.1 HIRS-2 Additional Channels

The moisture-temperature retrieval scheme developed to handle HIRS-2 infrared sounding data was modeled closely on the HIRS-1 retrieval scheme. The scheme is iterative and therefore requires an initial guess temperature and moisture profile. This initial guess is then changed in iterative steps according to the differences (or residuals) between the radiances observed by the satellite instrument

and radiances calculated using the radiative transfer equation and the transmittance information specific to the channels under consideration.

The iterative process incorporates feedback mechanisms which allow changes to be made to the surface temperature, the moisture profile, and the temperature profile. The order of the various feedback mechanisms is determined by the radiance residuals. The surface temperature feedback occurs before either the moisture or temperature profile feedback. The transmittances are then updated after each iteration or change in the temperature or moisture profiles. The amount of feedback is directly proportional to the differences between the observed and calculated radiances for the set of channels which are most responsive to each desired parameter. For the surface temperature, moisture profile, and temperature profile the selected feedback channels are the window, H<sub>2</sub>O, and CO<sub>2</sub> channels, respectively. Table 5.1 lists the appropriate channels which were considered in each case and a comparison of the HIRS-2 channels to the HIRS-1 channels used in previous work.

Table 5.1

A Comparison of HIRS-2 and HIRS-1 Channels

	<u>HIRS-2</u> <u>Channel</u>	<u>Wavelength</u> ( $\mu\text{m}$ )	<u>Approx.</u> <u>Peak</u> (mb)	<u>HIRS-1</u> <u>Channel</u>
Surface Temperature				
Feedback	8	11.11	surface	8
'	19	3.76	'	16
'	18	3.98	'	—
Moisture Feedback	10	8.16	900	9
'	11	7.32	700	—
'	12	6.72	500	10
Temperature Feedback	13	4.57	1000	11
'	14	4.52	950	12
'	15	4.46	700	13
'	16	4.40	400	14

The major changes from HIRS-1 to HIRS-2 occurred because of the introduction of both a new window channel and a new H<sub>2</sub>O channel. Also in HIRS-1 retrievals the window channel at 11 μm was used as an H<sub>2</sub>O feedback channel. This idea, however, was abandoned with the HIRS-2 data because of the inclusion of an additional H<sub>2</sub>O channel at 7.32 μm which is more transparent than the others. These three H<sub>2</sub>O channels can theoretically give a moisture retrieval with up to three degrees of freedom (i.e., in up to three vertical layers). Additionally, the multiple window channels were needed for both the reflected radiation correction and for the surface temperature inversion problem which will be discussed further in the following sections.

## 5.2 Cloud Detection

Satellite soundings in the infrared are severely limited by clouds. For this reason the cloud detection and elimination process is very important. By eliminating cloud-contaminated radiances before a retrieval is performed computer time can be saved which would be wasted by later rejection of meteorologically inconsistent soundings. These would be soundings which were performed under a clear atmosphere assumption, but which actually contained clouds. Meteorological data from such cloud-contaminated soundings may be inconsistent with neighboring or adjacent clear soundings. An attempt at partly-cloudy retrievals was made, but the process was not used because of the lack of a unique solution in single field-of-view situations. The procedure is outlined for reference in Appendix B.

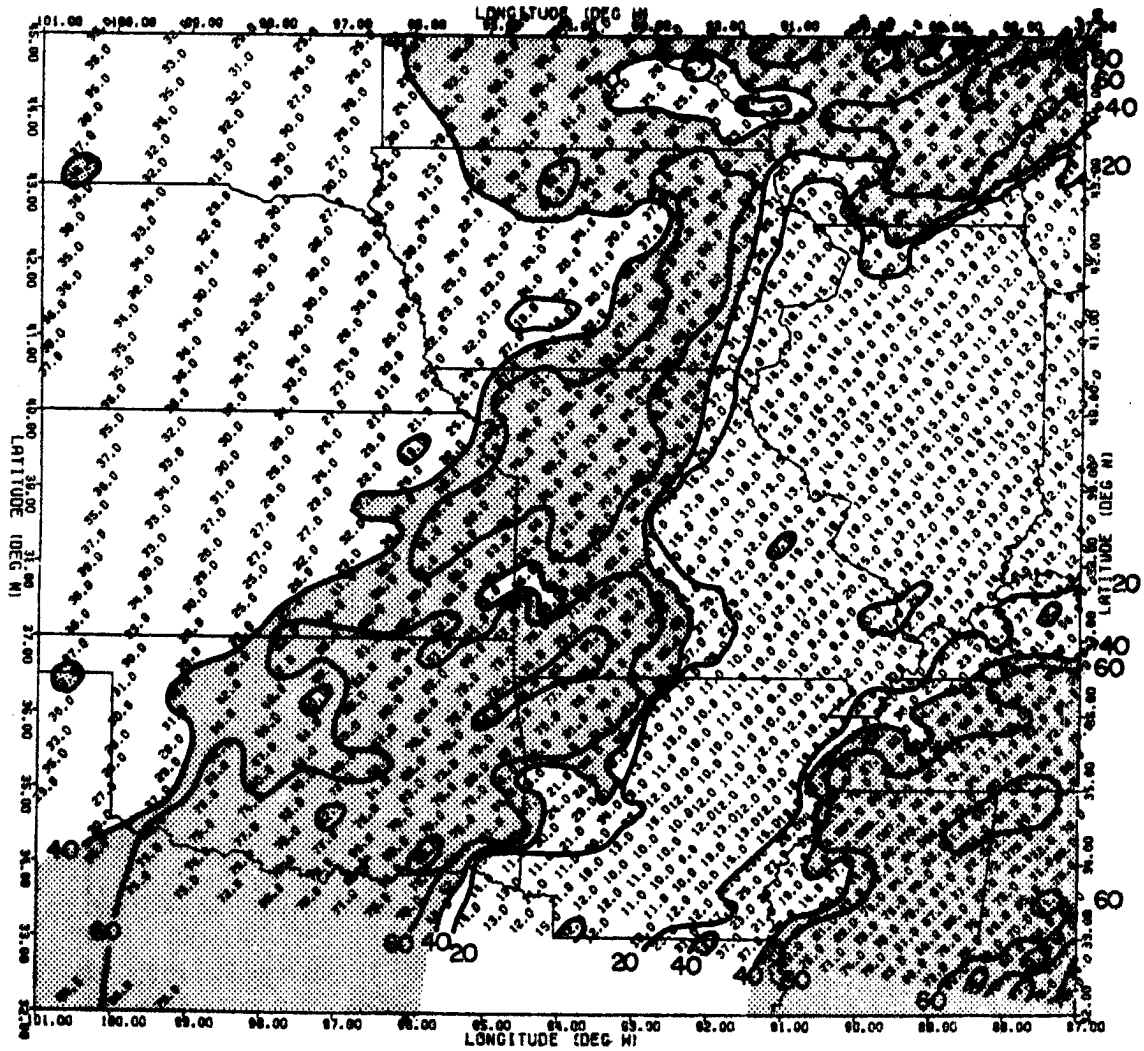
Because retrievals were not used in cloudy situations, the cloud problem was reduced to detection and elimination of cloud-contaminated radiances. The means for cloud detection depended on the time period

under study. The two satellite passes at 1000 and 1400 GMT occurred before and after sunrise, respectively.

For the 1400 GMT satellite data the cloud detection was simplified by a visible window channel at  $0.69 \mu\text{m}$ . The visible reflected radiance is not given directly, but as a fraction of its maximum possible value (assuming reflectance = 1.0). This was called the bi-directional reflectance (in percent) and is parameter 29 in Table 2.3. A value of 40% was used as the cloud-no cloud threshold, with larger values of reflectance being cloudy. A plot of the bi-directional reflectance for the area of consideration is given in Figure 5.1a. The shaded regions with values greater than 40% coincide well with the cloudy areas as were seen in the GOES visible image in Figure 2.3a.

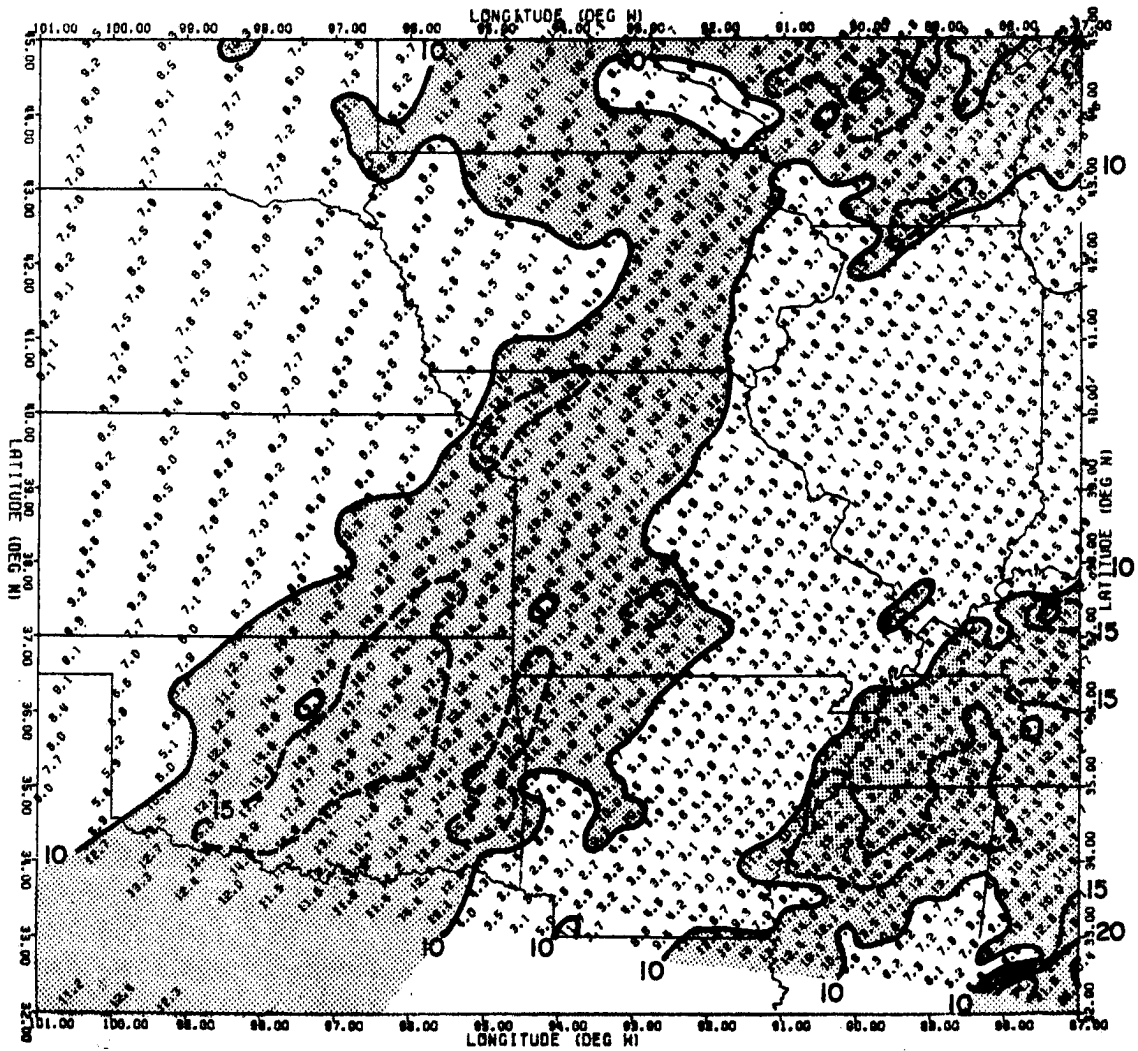
A second means of cloud detection utilized the window brightness temperature difference (WBTD) between the  $3.7$  and  $11 \mu\text{m}$  window channels. This value is plotted and contoured in Figure 5.1b. Shading is used to designate values greater than 10 K. This is approximately the same cloudy area that was designated by the values greater than 40% in Figure 5.1a. Smaller brightness temperature differences occur in the clear areas.

The reason for the large WBTD values is both related to the reflected visible radiation at  $3.7 \mu\text{m}$  (none at  $11 \mu\text{m}$ ) and because of different amounts of atmospheric absorption of these two wavelengths. (Typically the  $3.7 \mu\text{m}$  channel has a larger brightness temperature than the  $11 \mu\text{m}$  channel because of lower atmospheric absorption.) The reflected radiation effect is dominant during the day, so large brightness temperature differences can be used to detect clouds. A plot of the WBTD values versus the bi-directional reflectance is given in



30 Sept 1980  
 1400 GMT  
 Bi-directional Reflectance (%)

Figure 5.1a Bi-directional reflectance (%) at 1400 GMT on 30 September 1980 derived from TOVS window channel radiance at  $0.69 \mu\text{m}$  divided by its maximum possible value.



30 Sept 1980  
 1400 GMT  
 $\Delta T_B$  (K) (3.7-11  $\mu\text{m}$ )

Figure 5.1b Window brightness temperature difference (K) (3.7-11 $\mu\text{m}$ ) at 1400 GMT on 30 September 1980.

Figure 5.2 and shows a strong relationship. Soundings with both values below their respective thresholds of 10 K and 40% are most likely clear. Those above both thresholds are most likely cloudy. Others are possibly either partly cloudy (WBTD > 10 K but bi-directional reflectance below 40%) or possibly completely cloudy with a uniform cloud top (bi-directional reflectance > 40% but WBTD < 10 K).

At night the cloud detection is hindered by the lack of reflected visible radiation. However, the WBTD values can still be used. Since the visible radiation component at 3.7  $\mu\text{m}$  is gone, the WBTD values are reduced and may even be negative. By comparing the nighttime WBTD values in Figure 5.3a to the nighttime infrared cloud image in Figure 2.3c it appears that values greater than approximately 4 K are cloudy and are shaded accordingly.

As an additional cloud detection means at night, the infrared-microwave brightness temperature difference is used. This value is the 3.7  $\mu\text{m}$  brightness temperature minus the microwave window brightness temperature at 50 GHz (parameter 24 in Table 2.3). Caution must be used because the microwave measurements were obtained over a larger area than the infrared measurements (over 100 km resolution compared to about 35 km for the infrared). So, differences may arise due to the spatial coverage as well as the emission characteristics.

A plot of the infrared-microwave differences in Figure 5.3b shows that the cloudy areas have the most negative values. A threshold of -4 K may be used and values less than this threshold are shaded. However this would also include values covering most of Nebraska. This region of large negative values may be caused by dry surface conditions. Microwave brightness temperatures are affected strongly by the surface

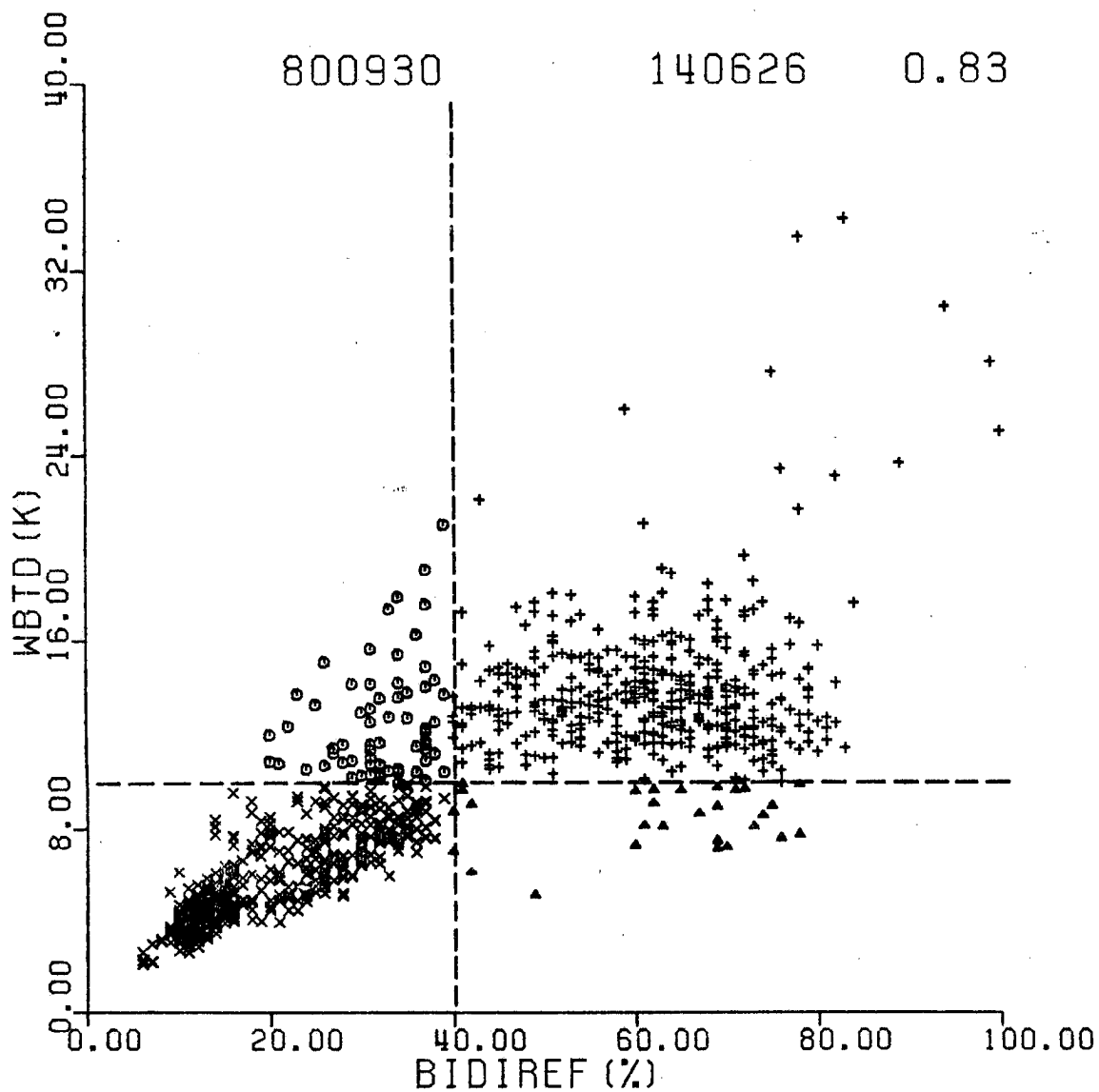
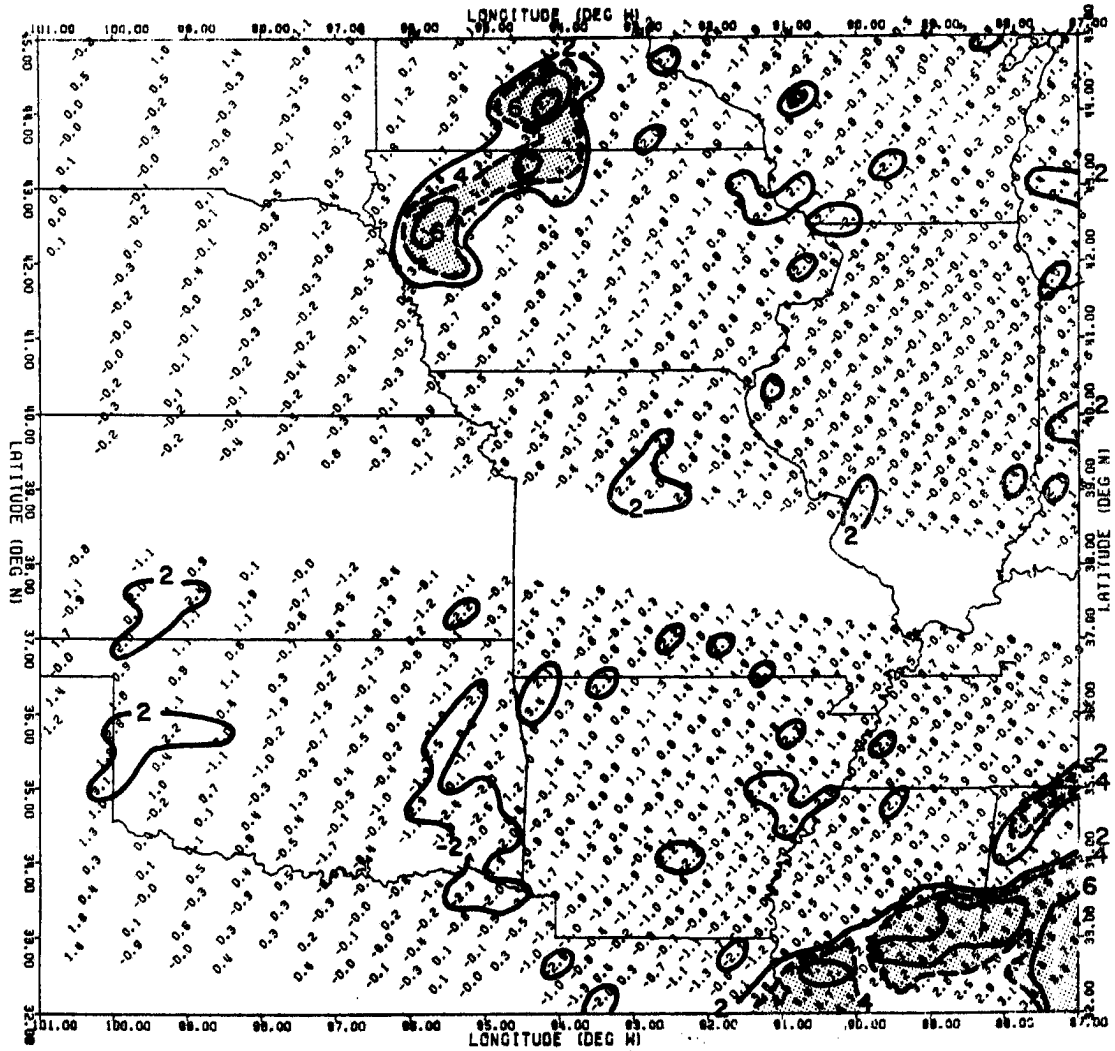
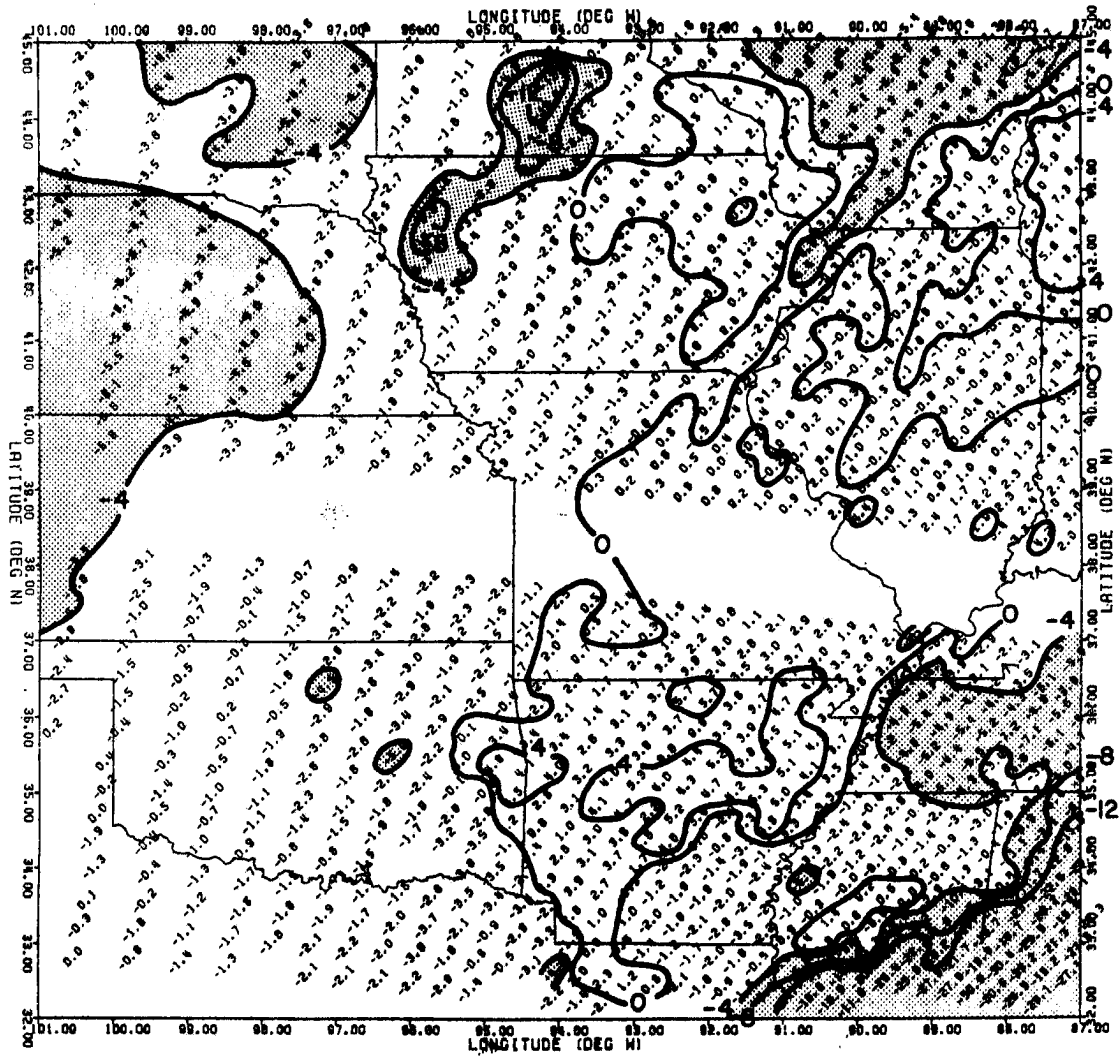


Figure 5.2 Scatter plot of window brightness temperature difference (3.7-11 $\mu$ m) versus bi-directional reflectance for the area from 32-45 $^{\circ}$ N and 87-101 $^{\circ}$ W for the 1400 GMT satellite pass on 30 September 1980. A correlation coefficient of 0.83 is given.



30 Sept 1980  
 1000 GMT  
 $\Delta T_B$  (K) (3.7-11 $\mu$ m)

Figure 5.3a Window brightness temperature difference (K) (3.7-11 $\mu$ m) at 1000 GMT on 30 September 1980.



30 Sept 1980  
 1000 GMT  
 $\Delta T_B$  (K) (3.7 $\mu$ m - 50GHz)

Figure 5.3b Infrared minus microwave brightness temperature difference (K) (3.7 $\mu$ m - 50GHz) at 1000 GMT on 30 September 1980.

emittance. A dry surface has a higher microwave emittance and therefore a higher brightness temperature. On the other hand, a wet surface would have a reduced microwave brightness and a larger infrared-microwave difference, as is seen in Arkansas. This difference should therefore be used for cloud detection only as a secondary means or with a less stringent threshold.

So, by using differences between various window channel measurements, clouds can be detected both during the day and at night. With cloudy values eliminated, temperature and moisture profiles can be retrieved by assuming clear column conditions.

### 5.3 Reflected Solar Radiation Correction

One very important correction to the HIRS-2 shorter wavelength channels is necessitated by the contamination of the radiances by solar radiation reflected from the earth's surface. The solar spectrum emitted at a brightness temperature of about 5800 K contains significant energy in the shorter wavelength window channels near 4  $\mu\text{m}$  and in the  $\text{CO}_2$  channels around 4.3  $\mu\text{m}$ . The relative amount of contamination can be found by calculating the energy as seen by the satellite from both the earth and the sun.

The solar spectral radiance  $L(k, T_{\text{sun}})$  due to a 5800 K blackbody is found by the Planck function of wavenumber  $k$  and temperature  $T$ . (Note that a uniform set of terms and symbols (Raschke, 1978) based on the International System of Units (SI) is used throughout and is listed in Appendix A.)

$$L(k, T_{\text{sun}}) = \frac{C_1 k^3}{\exp\left[\frac{C_2 k}{T_{\text{sun}}}\right] - 1} \text{ [mW (cm}^{-1}\text{)}^{-1} \text{ m}^{-2} \text{ sr}^{-1}\text{]} \quad (5.1)$$

where

$$C_1 = 1.1909\text{E-}5 \text{ mW cm}^4 \text{ m}^{-2} \text{ sr}^{-1}$$

$$C_2 = 1.438 \text{ cm K}$$

and

$$T_{\text{sun}} = 5800 \text{ K}$$

This radiance can be converted into a downward solar spectral irradiance  $E_{k, \text{sun}}$  at the top of the atmosphere by multiplying by the solid angle of the sun  $\Omega_{\text{sun}}$ .

$$E_{k, \text{sun}} = L(k, T_{\text{sun}}) \cdot \Omega_{\text{sun}} \quad (5.2)$$

where

$$\begin{aligned} \Omega_{\text{sun}} &= \frac{\text{cross-section of sun}}{(\text{earth-sun distance})^2} = \frac{\pi r_{\text{sun}}^2}{d_{\text{es}}^2} \\ &= 6.80169\text{E-}5 \text{ steradians} \end{aligned}$$

This irradiance is that impinging on a flat surface at the top of the atmosphere (i.e., the solar constant). The observed spectral irradiance  $E_{k, \text{sfc}}$  at the surface of the earth is then found by accounting for the absorption due to the downward atmospheric path having non-unity transmittance and taking into account the non-perpendicular reflecting surface. Figure 5.4 gives an illustration of the solar and satellite angles and resulting transmittances. The solar zenith angle  $\phi_{\text{sun}}$  is the important variable in determining the downward irradiance.

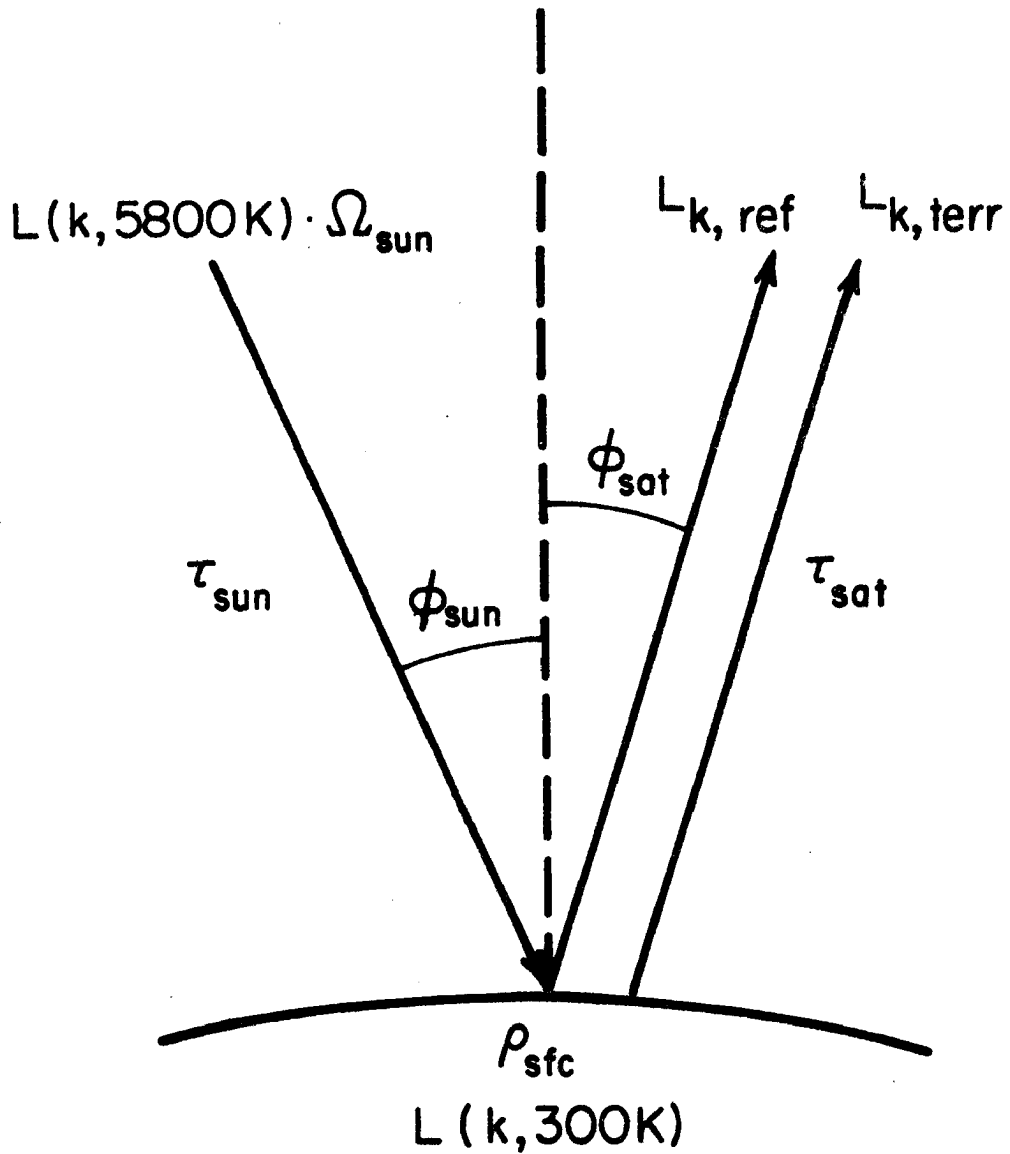


Figure 5.4 An illustration of the solar and satellite zenith angles which must be taken into account in the reflected radiation correction to the shortwave infrared channels.

$$E_{k, \text{sfc}} = E_{k, \text{sun}} \cdot \tau_{k, \text{sun}} \cdot \cos(\phi_{\text{sun}}) \quad (5.3)$$

where

$$\tau_{k, \text{sun}} = (\tau_{k, \phi=0})^{\sec(\phi_{\text{sun}})}$$

and  $\tau_{k, \phi=0}$  is the spectral atmospheric transmittance at nadir. The reflected component is then simply

$$E_{k, \text{ref}} = E_{k, \text{sfc}} \cdot \rho_{\text{sfc}} \quad (5.4)$$

where  $\rho_{\text{sfc}}$  is the unknown surface reflectance. The radiance reflected from the surface  $L_{k, \text{sfc}}$  is then found by assuming an isotropic reflecting surface. In this case the reflected solar irradiance is distributed equally into a solid angle of  $2\pi$  steradians (hemisphere)

$$E_{k, \text{ref}} = \int_{2\pi}^{\theta} \int_{\pi/2}^{\phi} L_{k, \text{sfc}} \cos\phi \sin\theta \, d\phi \, d\theta \quad (5.5)$$

$$= L_{k, \text{sfc}} \cdot \pi$$

assuming  $L_{k, \text{sfc}}$  constant with  $\phi$  and  $\theta$ , or inversely

$$L_{k, \text{sfc}} = \frac{E_{k, \text{ref}}}{\pi} \quad (5.6)$$

This solar reflected spectral radiance would be the value observed by a satellite from a non-perpendicular reflecting surface with a non-unity reflectance and without considering atmospheric absorption on the return path. To take into account the non-unity atmospheric

transmittance on the upward or return path the satellite-observed reflected spectral radiance at the top of the atmosphere becomes

$$L_{k, \text{ref}} = L_{k, \text{sfc}} \cdot \tau_{k, \text{sat}} \quad (5.7)$$

where

$$\tau_{k, \text{sat}} = (\tau_{k, \phi=0})^{\sec(\phi_{\text{sat}})}$$

is the spectral atmospheric transmittance to the satellite at zenith angle  $\phi_{\text{sat}}$ .

The satellite-observed reflected radiance is then obtained directly from the known solar irradiance by combining Equations 5.3, 5.4, 5.6, and 5.7. The result is

$$L_{k, \text{ref}} = \frac{E_{k, \text{sun}} \cdot \cos(\phi_{\text{sun}}) \cdot \tau_{k, \text{sun}} \cdot \tau_{k, \text{sat}} \cdot \rho_{\text{sfc}}}{\pi} \quad (5.8)$$

To understand the amount of solar reflected spectral radiance which contaminates various shorter wavelength channels, the terrestrial and solar radiance components are given in Table 5.2. Three cases are shown; one of which represents a maximum solar contamination case. In the maximum case the surface reflectance is assumed to be unity, and the solar and satellite zenith angles are assumed to be  $0^\circ$  (i.e., both the sun and satellite are directly over a perpendicular reflecting surface). In the non-maximum cases the solar zenith angle is increased to about  $70^\circ$ , as is typical at 1400 GMT (0800 LST), and in the final case the surface reflectance is decreased to 30%, a relatively high value for a non-cloudy surface.

Table 5.2

## Satellite-Observed Terrestrial and Reflected-Solar Radiance Contributions

HIRS-2 Channel	20	19	18	13	10	8
Wavelength ( $\mu\text{m}$ )	.69	3.76	3.98	4.56	8.16	11.11
Wavenumber ( $\text{cm}^{-1}$ )	14500	2660	2515	2190	1225	900
Terrestrial $L_{k,300K}$ ( $\text{mW cm m}^{-2} \text{sr}^{-1}$ )	0.	.65	1.1	3.5	61.9	117.7
Solar $L_{k,\text{sun}}$ (5800K) ( $\text{mW cm m}^{-2} \text{sr}^{-1}$ )	22.2	5.2	4.7	3.8	1.3	.75
Atmos. Transmittance ( $\phi=0^\circ$ ) (Standard Atmosphere)	1.00	.86	.87	.30	.55	.77
$L_{k,\text{terr}}$ ( $\text{mW cm m}^{-2} \text{sr}^{-1}$ )	0.	.56	.96	1.0	34.0	90.7
$\phi_{\text{sun}}=0^\circ, \rho_{\text{sfc}}=1.:$						
$L_{k,\text{ref}}$ ( $\text{mW cm m}^{-2} \text{sr}^{-1}$ )	22.2	3.8	3.6	.34	.40	.45
Ratio: Ref. to Total (%)	100	87	79	25	1	0
$\phi_{\text{sun}}=70^\circ, \rho_{\text{sfc}}=1.:$						
$L_{k,\text{ref}}$ ( $\text{mW cm m}^{-2} \text{sr}^{-1}$ )	22.2	.98	.94	.01	.04	.09
Ratio: Ref. to Total (%)	100	64	49	1	0	0
$\phi_{\text{sun}}=70^\circ, \rho_{\text{sfc}}=.3:$						
$L_{k,\text{ref}}$ ( $\text{mW cm m}^{-2} \text{sr}^{-1}$ )	6.7	.30	.28	.00	.01	.03
Ratio: Ref. to Total (%)	100	35	23	0	0	0

As can be seen, the reflected solar contribution to the total (terrestrial plus reflected) observed radiance at the satellite in the maximum case can be as high as 87% for the window channel at 3.76  $\mu\text{m}$  and 79% at 3.98  $\mu\text{m}$ . In the next case, when the solar zenith angle is increased to 70° (which is typical for the NOAA-6 1400 GMT data being considered) the reflected solar contributions drop to 64% and 49%, respectively. These fractions represent a maximum early morning contamination situation. In the third case, when the non-unity surface reflectance is considered, the reflected solar contributions drop further, to 35% and 23% respectively. Under these non-maximum conditions the solar contributions are still very significant for these shorter wavelength window channels. For this reason the solar contribution had to be considered for all daytime cases when using the shorter wavelength window channel radiances. Only for longer wavelength channels with lower atmospheric transmittance, such as the 11.1  $\mu\text{m}$  window channel, does the solar contribution become insignificant in all cases.

The factors contributing to the reflected solar component are known for all channels except the surface reflectance. As an aid in determining the surface reflectance, the TOVS parameters included a brightness temperature at 3.98  $\mu\text{m}$  (parameter 30 in Table 2.3) which was corrected for reflected solar contamination. The reflected component at 3.98  $\mu\text{m}$  ( $k = 2515 \text{ cm}^{-1}$ ) will then be the difference between the total (solar plus terrestrial) and solar-corrected (terrestrial only) radiances

$$L_{2515, \text{ref}} = L(2515, T_{2515, \text{tot}}) - L(2515, T_{2515, \text{corr}})$$

The surface reflectance is obtained using the known solar and satellite zenith angles and assuming that the atmospheric transmittance is known. So, by inverting Equation 5.8,

$$\rho_{\text{sfc}} = \frac{L_{2515,\text{ref}} \cdot \pi}{E_{2515,\text{sun}} \cdot \cos(\phi_{\text{sun}}) \cdot \tau_{2515,\text{sun}} \cdot \tau_{2515,\text{sat}}} \quad (5.9)$$

This calculated surface reflectance at 3.98  $\mu\text{m}$  is then assumed to be constant for the shortwave infrared spectrum and is applied to correct the other shortwave channels for their solar contamination by using Equation 5.8 at the appropriate wavenumber  $k$ .

#### 5.4 Nocturnal Surface Temperature Inversion Problem

An additional difficulty was encountered in trying to retrieve temperature and moisture soundings during the nighttime or early morning hours. TIROS-N has a nighttime pass at local 4 a.m. and NOAA-6 has an early morning pass at local 8 a.m. During these times the nocturnal cooling can allow a temperature inversion to be represented near the surface. This temperature inversion can typically be very shallow and is not easily sensed by channels other than the window channels which obtain their primary contribution from the surface. Paulson and Horn (1981) recognized and warned of the nocturnal inversion problem in the retrieval of temperature profiles from Nimbus-6 HIRS radiances. This problem is especially acute with the nighttime TIROS-N measurement, but a method was devised to compensate for the nocturnal inversion when it seemed to be implied by the window channel radiances.

The first step in determining if a temperature inversion exists is to look at the surface temperature implied by the three window channels

at 3.76, 3.98, and 11  $\mu\text{m}$ . These three window channels typically give very similar brightness temperatures (unless the field-of-view [FOV] is composed of two or more sub-areas with different temperatures, i.e., a partly cloudy FOV). The maximum of these three window brightness temperatures, after correcting the shortwave windows for reflected solar radiation, is used as the initial surface or interface temperature for the initial guess temperature profile. As mentioned, the initial guess profile was a composite of 1200 GMT RAOBs from the area under consideration. Many of the individual soundings which went into the composite initial guess profile contained temperature inversions near the surface. However, this one composite profile was used as the initial guess for all retrieved soundings at both 1000 and 1400 GMT. A temperature inversion may not be present at all places where soundings are desired, especially at the latter time. Therefore, if a temperature profile to be included in the composited initial guess profile contained an inversion, it was changed to eliminate any temperature decreases near the surface. The maximum of the window channel brightness temperatures is then allowed to effectively add a temperature inversion (temperature reduction) at the surface if this maximum window brightness temperature for a particular spot is lower than the temperature at the surface given by the initial guess profile. In a similar manner, if the maximum window channel brightness temperature at another position is larger than the initial guess surface temperature, then the surface temperature is increased, thereby allowing a larger lapse rate or even possibly allowing a superadiabatic layer to be represented near the surface.

Using the maximum window channel brightness temperature as the interface temperature in the initial guess profile has the effect of

allowing the surface temperature to float free of the temperature profile. This seems appropriate in situations where the surface temperature can vary greatly in space and time. This also allows the same initial guess profile to simulate lapse rates near the surface which range from inversion to superadiabatic, especially when that layer is shallow as is true in the cases examined. As a result, vertical temperature detail can be added near the surface as required.

An example of an added surface temperature inversion is shown in Figure 5.5. The Huron SD (HON) sounding at 1200 GMT for 30 September 1980 is shown to have a strong but shallow temperature inversion. The composite initial guess temperature profile is also shown as it is originally given but with an inversion as implied by the maximum window channel brightness temperature at 1000 GMT. The large surface temperature discrepancy between the two soundings may be due to their two-hour time difference. This new surface temperature is given an appropriate pressure according to the average terrain as will be explained in the following section.

### 5.5 Terrain Height Correction

A set of standard pressure levels was used to numerically integrate the radiative transfer equation. These pressure levels were determined by the transmittance software which was obtained from the University of Wisconsin. The 40 pressure levels range from 0.1 (level 1) to 1000 mb (level 40) with level 20 at 100 mb. Many of the levels are standard or mandatory pressure levels at which conventional balloon soundings or RAOBs are required to report. The lowest atmospheric level at a pressure of 1000 mb is nearly the mean atmospheric pressure at sea level. However, in attempting to do retrievals over land surfaces, the

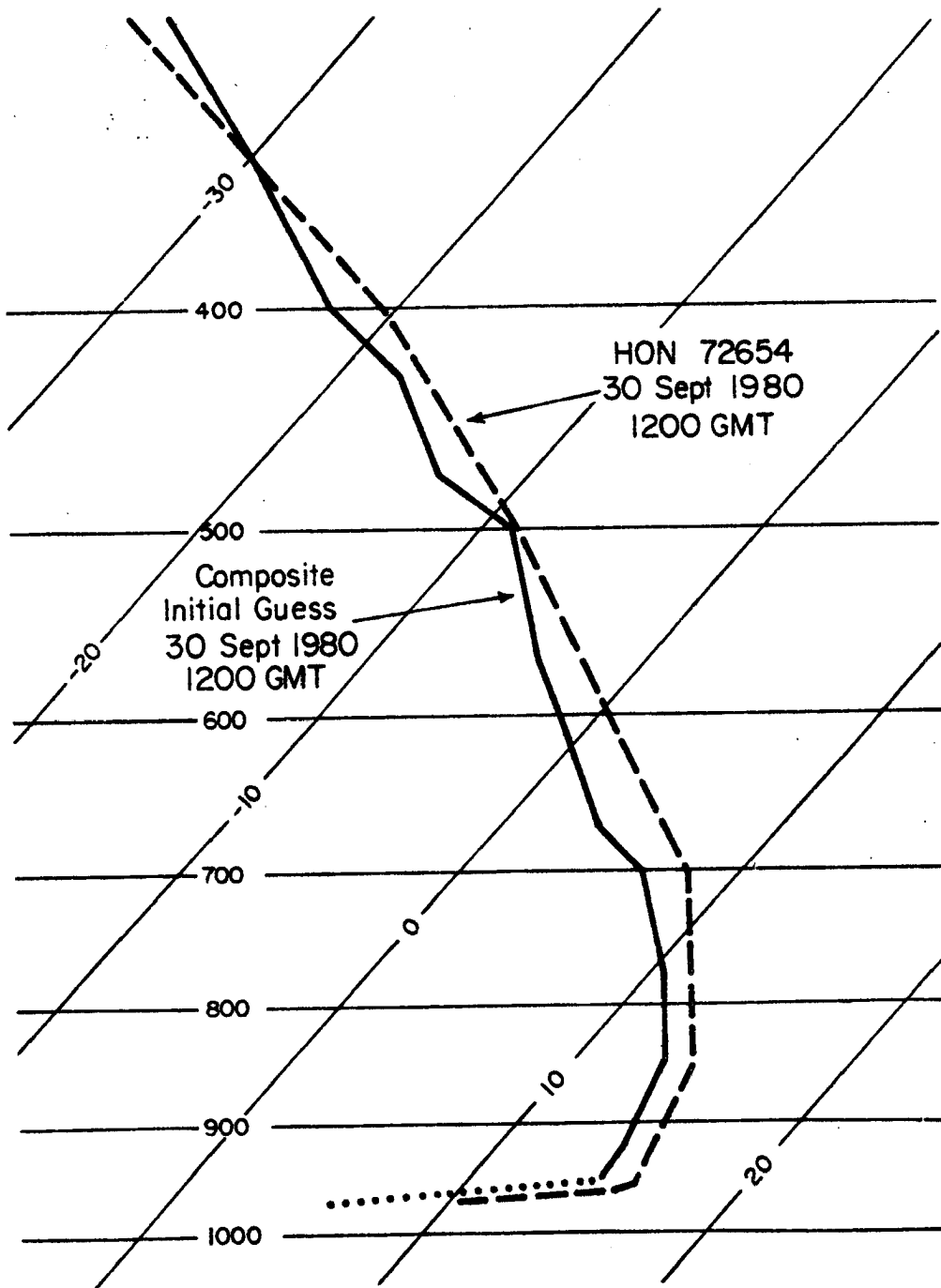


**Figure 5.5** An example of a surface temperature inversion being added to the initial guess temperature profile by using the maximum window channel brightness temperature as a floating surface or interface temperature.

elevated terrain may cause the actual surface pressure to be as low as 850 mb or less, even for non-mountainous areas of the western Great Plains. The largest effect upon the radiances integrated from a non sea-level surface would be due to the increased atmospheric transmittance to space from this elevated surface.

To alleviate this problem, so as not to require a knowledge of the exact surface pressure (to not require the input of surface data), an average surface pressure for any given area is used. This average surface pressure is obtained from knowledge of the average terrain elevation for the given area. The average terrain height is known for every one-half degree latitude by one-half degree longitude box for the United States and was obtained from the archives of the National Center for Atmospheric Research (NCAR). The hydrostatic approximation

$$\Delta p = \rho g \Delta h \quad (5.10)$$

was then used to relate the change in height  $\Delta h$  to the change in pressure  $\Delta p$  through the atmospheric density  $\rho$  (determined by the ideal gas law from pressure and temperature of a standard atmosphere) and acceleration of gravity  $g$ . So, using the terrain height and a mean sea-level pressure of 1013 mb the surface pressure for an elevated surface would be

$$p_{sfc} = 1013\text{mb} - \Delta p \quad (5.11)$$

In the case of the surface pressure being equal to 1000 mb ( $p_{sfc} = p_{40}$ ) the radiative transfer equation (RTE) in integral form is

$$L_k = L(k, T_{1000}) \cdot \tau_{k,1000} \quad (5.12)$$

$$+ \int_{p_{1000}}^0 L(k, T(p)) \cdot \frac{\delta \tau_k}{\delta p} \cdot \delta p$$

where  $L_k$  is the integrated spectral radiance. The first term is the surface or interface radiance and the integral represents the atmospheric absorption and emission.  $\tau_k$  is the spectral atmospheric transmittance at wavenumber  $k$  and is a function of the temperature, absorber amount, and pressure at any level. This dependency is not shown by this simple formulation.

In summation or quadrature form the RTE becomes

$$L_k = L(k, T_{40}) \cdot \tau_{k,40} + \sum_{m=1}^{39} \bar{L}(k, T(p_m)) \cdot \Delta \tau_{k,m} \quad (5.13)$$

where

$$\bar{L}(k, T(p_m)) = \frac{[L(k, T(p_m)) + L(k, T(p_{m+1}))]}{2}$$

and

$$\Delta \tau_{k,m} = \tau_{k,m} - \tau_{k,m+1}$$

where the integral is summed over 40 layers with  $p_1 = 0.1$  mb and  $p_{40} = 1000$  mb.

However, since the surface pressure  $p_{sfc}$  may not be equal to 1000 mb, the lowest layers are truncated from the summation until  $p_{max} > p_{sfc} > p_{max-1}$  at which point the fraction  $\alpha$  of the lowest layer below the surface pressure is determined by the pressure-weighted ratio

$$\alpha = \frac{p_{max} - p_{sfc}}{p_{max} - p_{max-1}} \quad (5.14)$$

where

$$a < 1.$$

Figure 5.6 shows an example where the surface pressure is between 920 and 950 mb, resulting in  $p_{\max} = 950$  mb. The atmospheric term is then summed to  $p_{\max}$  and the fraction of the lowest layer which is below the actual surface is subtracted.

$$L_k = L(k, T_{\text{sfc}}) \cdot \tau_{k, \text{sfc}} + \sum_{m=1}^{\max-1} \bar{L}(k, T(p_m)) \cdot \Delta\tau_{k, m} \quad (5.15)$$

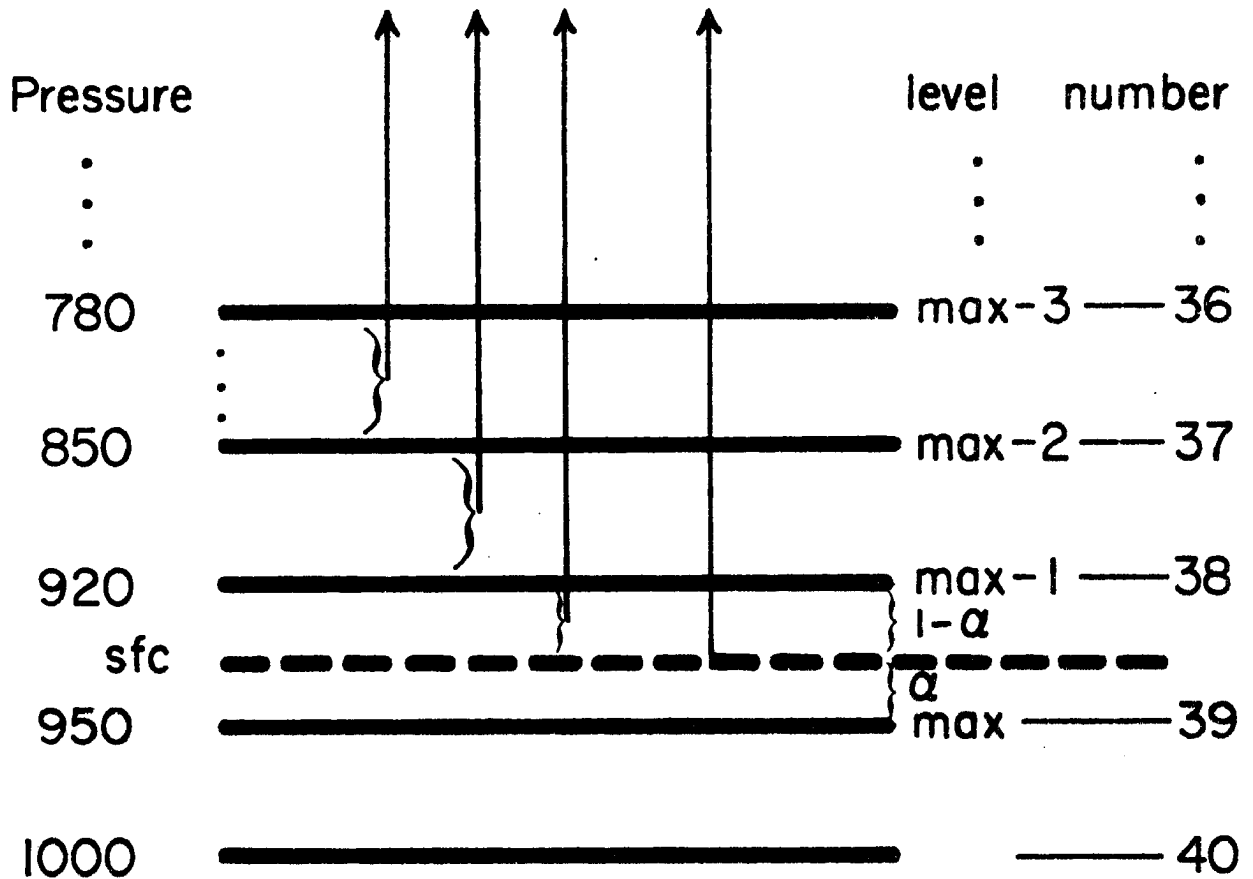
$$- a \cdot \bar{L}(k, T(p_{\max-1})) \cdot \Delta\tau_{k, \max-1}$$

where

$$\tau_{k, \text{sfc}} = a \cdot \tau_{k, \max-1} + (1-a) \cdot \tau_{k, \max}$$

This summation will also cover cases when  $p_{\text{sfc}} > p_{\max} = 1000$  mb ( $a < 0$ ). The last fractional term is then added to the other 39 atmospheric terms.

The change in elevation is very important for an accurate radiance  $L_k$  to be calculated for a given temperature and moisture profile at any location. A smooth transition in surface elevation from one scan spot to the next can then be manifested in smooth changes in retrieved parameters. Smooth horizontal transitions are important when analyzing high-density fields of satellite parameters. Because each scan spot is analyzed independently of all others, the small scale changes from one sounding to the next can be used to detect bad soundings, especially those caused by undetected cloud fields.



$$\alpha = \frac{P_{\max} - P_{\text{sfc}}}{P_{\max} - P_{\max-1}}$$

Figure 5.6 An example of numerical integration of the radiative transfer equation when an elevated surface ( $p_{\text{sfc}} < 1000\text{mb}$ ) is encountered.

### 5.6 Iterative Feedback Mechanisms

The basic iteration loop for the TOVS (HIRS-2) retrievals takes place after the previously mentioned corrections to the observed and calculated radiances. The differences between the observed radiances and the radiances calculated for the initial guess profile are used in the feedback to correct the initial guess sounding. The appropriate channels to feedback to the surface temperature, the moisture profile, and the temperature profile were listed in Table 5.1.

The surface temperature feedback is a modification of that used previously (Hillger and Vonder Haar, 1981). The modification was due to the use of 3 window channels in the surface temperature feedback. The feedback equation for iteration n becomes

$$T_{\text{sfc}}^{(n+1)} = \frac{\sum_{i=1}^3 T_{i, \text{sfc}}^{(n+1)} \cdot \tau_{i, \text{sfc}}^{(n)}}{\sum_{i=1}^3 \tau_{i, \text{sfc}}^{(n)}} \quad (5.16)$$

where

$$L(k_i, T_{i, \text{sfc}}^{(n+1)}) = L(k_i, T_{\text{sfc}}^{(n)}) + \Delta L_i^{(n)} / \tau_{i, \text{sfc}}^{(n)}$$

and

$$\Delta L_i^{(n)} = L_{i, \text{obs}} - L_{i, \text{calc}}^{(n)}$$

The new surface temperature is a weighted average of the temperatures suggested by each of the three window channels  $k_i$ , and the weights are the surface transmittances  $\tau_i$  for each channel. The surface temperature suggested by each channel is based on the radiance

difference (observed minus calculated) and is inversely proportional to the surface transmittance in that channel.

The moisture feedback is also basically similar to that used previously. The formula for the mixing ratio  $Q(p)$  at any pressure  $p$  is

$$Q^{(n+1)}(p) = Q^{(n)}(p) \cdot \left[ 1 - \frac{\sum_{i=1}^3 S_i^{(n)} \cdot \Delta L_i^{(n)} \cdot \Delta \tau_i^{(n)}(p)}{\sum_{i=1}^3 \Delta \tau_i^{(n)}(p)} \right] \quad (5.17)$$

where

$$\Delta \tau_i(p) = \tau_i(p_m) - \tau_i(p_{m+1})$$

is the weighting function for each of the  $H_2O$  channels and  $S_i^{(n)}$  is the factor to convert from radiance change to mixing ratio change. The computation of this factor is covered by Smith and Howell (1971) and Smith (1970). The physical dimension of  $S$  is percent change in mixing ratio per change in radiance  $L$  (i.e., inverse radiance units). A more complete explanation of the calculation of the  $S$  factors is given in Appendix C.

The  $S$  factors relate how the radiance in a given channel changes with the moisture profile. Typically the  $H_2O$  radiance decreases with increasing atmospheric moisture content. This is true because with increased moisture or absorber amount the transmittance of the atmosphere decreases and the resulting weighting function peaks higher in the atmosphere or at cooler temperatures. Since more of the radiance arises from cooler portions of the atmosphere, the integrated radiance is reduced. The effect, however, is reversed if a strong temperature inversion exists, especially at the surface.

The effect of the surface term on the radiance response to moisture changes is summarized in Figure 5.7. Shown are brightness temperatures calculated for the 3 H<sub>2</sub>O channels as a function of total atmospheric precipitable water. The results of the surface temperature  $T_{sfc}$  modified by adding and subtracting 10 K are shown by the dotted and dashed lines, respectively. Channel 12 at 6.7  $\mu\text{m}$  is virtually unaffected by the surface and shows, as a control, how the water vapor radiance (or brightness temperature) typically decreases with increasing moisture content. A similar effect occurs at 7.3  $\mu\text{m}$  which has only a slight surface contribution. However, the most transparent H<sub>2</sub>O channel at 8.2  $\mu\text{m}$  changes its slope as a function of the surface temperature departure. For a +10 K increase in the surface temperature (a temperature increase from the lowest level to the surface) the 'normal' effect of decreased radiance with increased moisture is more pronounced, but with a -10 K temperature inversion (decrease) at the surface the effect of changing moisture on the calculated radiance is reversed (the dashed line for Channel 10). In this case the S factor for this channel would be reversed in sign, to reflect the increase in radiance with increased moisture. The magnitude of S is initially calculated based on the guess temperature and moisture profiles and the initial surface temperature as determined previously. The S factors are then updated before each moisture iteration based on the new temperature and moisture profiles and surface temperature.

Empirical evidence of the increase in radiance with increase in moisture is given by Parmenter (1976). In nighttime infrared images moist areas appear darker (warmer) than adjacent drier areas. This effect may be caused partly by the moist atmosphere acting as a blanket

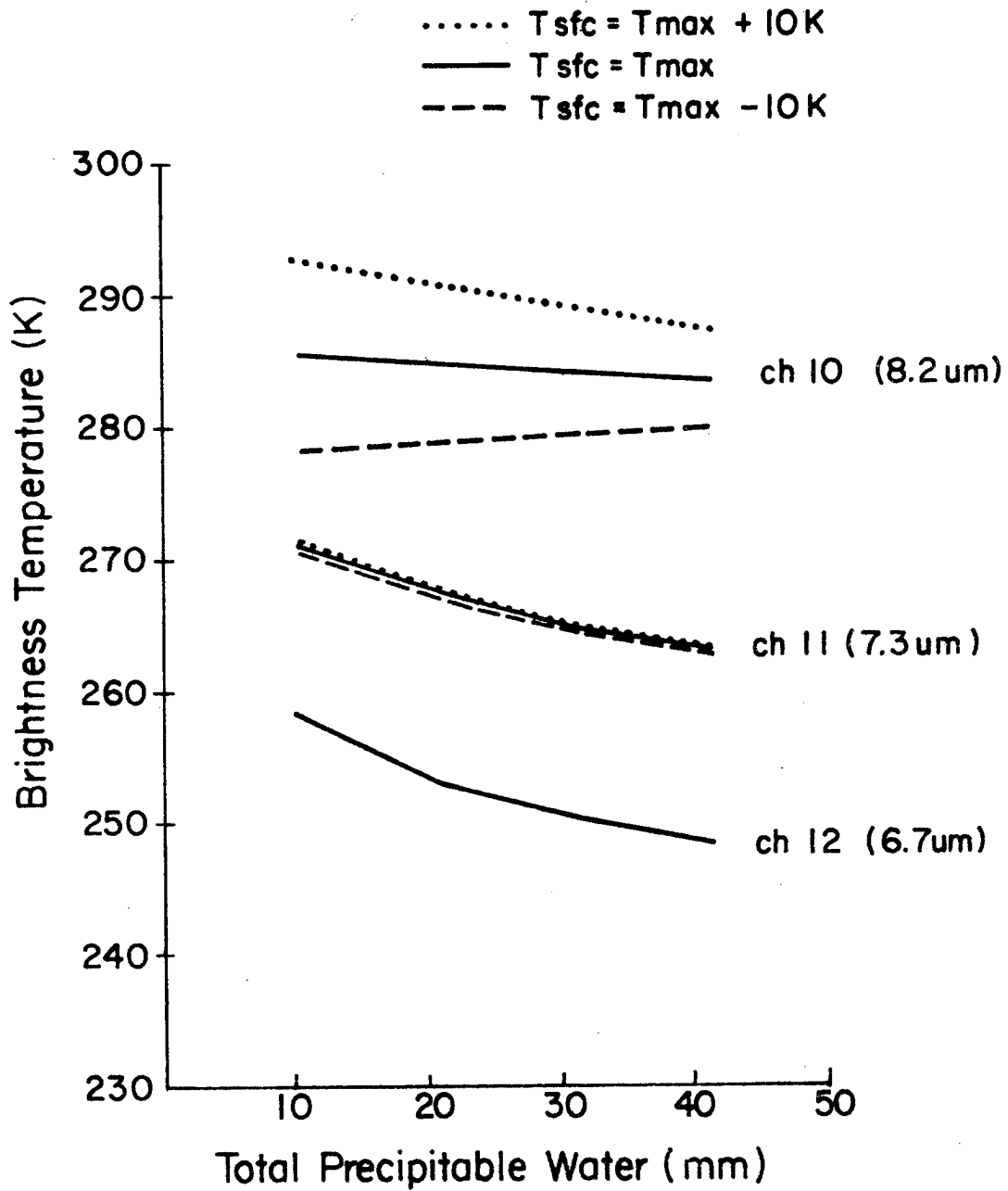


Figure 5.7 Simulated brightness temperature response as a function of the total atmospheric precipitable water and surface temperature deviation from a given temperature profile.

to keep the surface in that region warmer than in adjacent dry regions. Parmenter, however, notes that early morning surface heating quickly destroys this infrared pattern. Gurka (1976) also noted that moist areas appear warmer at night. His explanation was linked to the effect of the moist air upon the radiating surface causing changes in surface temperature, but he also said that the surface temperature measurements at the instrument shelter height do not always confirm this radiative effect. For a given line in Figure 5.7 the concern is the effect of changing atmospheric moisture upon the radiance for a constant surface temperature. It is possible that the effect noted by the above two scientists was not entirely due to a surface temperature change from moist to dry areas. In a surface temperature inversion situation the moist areas would also appear warmer because of the absorption and emission from the higher, warmer layers. In the first explanation a surface temperature change in space is required; in the second explanation a surface temperature decrease with pressure is required.

Finally, the feedback for the temperature profile is accomplished using the relaxation formula for iteration n

$$L(k_i, T^{(n+1)}(p)) = L(k_i, T^{(n)}(p)) \quad (5.18)$$

$$\cdot \left[ 1 + \frac{\sum_{i=1}^4 \Delta l_i^{(n)} \cdot \Delta \tau_i^{(n)}(p)}{\sum_{i=1}^4 \Delta \tau_i^{(n)}(p)} \right]$$

where

$$\Delta l_i^{(n)} = \frac{L_{i,obs} - L_{i,calc}^{(n)}}{L_{i,calc}^{(n)}}$$

is the normalized radiance difference. As with the moisture feedback this difference is a function of the channel  $k_i$  and causes the maximum change in the temperature profile where the weighting function  $\Delta\tau_i$  for that channel has its peak. For the temperature feedback only the 4 most transparent  $\text{CO}_2$  channels were used. These channels were listed in Table 5.1.

The order of these feedback mechanisms alternates between the moisture and temperature profiles with the surface temperature feedback occurring before each change to the moisture or temperature profile. The surface temperature feedback is computed first and more often because of its strong effect on the radiative transfer equation. In general the moisture feedback occurs before the temperature profile feedback, but the order can be reversed if the radiance residual for the lowest  $\text{CO}_2$  channels is larger than a set threshold. This is especially important when the same initial guess profile is used over an area where the actual temperature profiles differ from the initial guess by several degrees Celsius throughout large atmospheric depths. If the radiance residual for the most transparent  $\text{CO}_2$  channel (channel 13) is greater than  $.25 \text{ mW}/(\text{m}^2 \text{ sr cm}^{-1})$ , or approximately 20% of its mean value, then the temperature profile is iterated before the moisture profile. This keeps the moisture differences from being masked by large temperature differences. However, the normal situation allows the moisture feedback before the temperature profile feedback in order to allow small changes in the  $\text{H}_2\text{O}$  radiances to determine the actual direction of the moisture feedback and also because of the emphasis on moisture retrievals in this study.

Iterations are continued until either of two things happens. One is that a maximum of three iteration cycles are allowed. Experience has shown that little change occurs in the resultant profiles after three iteration cycles. Each cycle, however, includes feedback to both the moisture and temperature profiles under normal circumstances. A second reason for stopping the iteration process is if the radiance residual does not decrease. This residual is the root mean square difference between calculated and observed radiances for all channels used in the iterative process.

## 6.0 RETRIEVAL RESULTS

The retrieval system outlined in the last section was used to produce fields of high-resolution satellite soundings for the 30 September 1980 case which was introduced earlier. The two sets of HIRS-2 measurements at 1000 and 1400 GMT were analyzed independently, except for a common initial guess sounding composited from the 1200 GMT RAOBs. The satellite-derived meteorological parameters were then compared quantitatively to conventional measurements at both the RAOB and surface observation scales and were also statistically intercompared to determine inherent noise levels. The fields of satellite-derived measurements were also examined on a qualitative basis by comparison to similar fields of conventional measurements. Changes in the fields over the 4-hour time span were also examined.

### 6.1 Satellite-RAOB Comparisons

As mentioned previously, the RAOBs were only available at 1200 GMT, midway between the two satellite passes at approximately 1000 and 1400 GMT. For this reason comparison of satellite-derived values to conventional RAOB measurements includes a time separation of 2 hours. Of the 27 RAOBs in the initial guess profile, those within 150 km of a satellite measurement position were used for this comparison. However, because of limitations on the satellite data availability due to calibration gaps and clouds only 17 and 12 satellite-RAOB pairs were available at 1000 and 1400 GMT, respectively. The lower number of pairs

at 1400 GMT is due to extensive cloudiness at that time.

The results of the satellite-RAOB comparisons are shown in Table 6.1. The RAOBs provided the only set of upper-air observations for a use as 'ground truth' against which the satellite retrievals could be compared. The comparisons, therefore, included temperatures at several standard levels and various retrieved moisture parameters. Comparisons of the 1200 GMT RAOBs to the 1000 and 1400 GMT satellite-derived parameters are given separately by means of correlation coefficients, mean differences (biases) and root-mean-square (rms) differences.

Table 6.1

## Satellite-RAOB Comparisons

<u>Parameter</u>	<u>1000 vs 1200 GMT</u>			<u>1400 vs 1200 GMT</u>		
	<u>Corr.</u>	<u>Bias</u>	<u>Rms Diff.</u>	<u>Corr.</u>	<u>Bias</u>	<u>Rms Diff.</u>
<u>Temperatures</u>						
-Surface ( $^{\circ}\text{C}$ )	(.62)	.1	3.0	(.60)	6.6	7.2
-85 kPa ( $^{\circ}\text{C}$ )	(.88)	3.2	4.6	(.82)	4.0	6.5
-70 kPa ( $^{\circ}\text{C}$ )	(.71)	5.2	6.7	(.72)	5.8	7.9
-50 kPa ( $^{\circ}\text{C}$ )	(.91)	4.9	5.7	(.94)	5.6	6.8
-40 kPa ( $^{\circ}\text{C}$ )	(.84)	2.4	3.9	(.83)	3.8	5.6
-30 kPa ( $^{\circ}\text{C}$ )	(.62)	1.6	3.8	(.48)	3.7	5.8
-20 kPa ( $^{\circ}\text{C}$ )	(-.09)	-.7	7.8	(.38)	-.4	9.9
Rad. Sfc Temp ( $^{\circ}\text{C}$ )	(.57)	-4.1	4.8	(.63)	4.1	5.1
Total PW (mm)	(.66)	3.4	4.8	(.72)	4.8	6.5
<u>Dew Point Temp</u>						
-Surface ( $^{\circ}\text{C}$ )	(.55)	-3.2	4.4	(.46)	2.9	5.3
-85 kPa ( $^{\circ}\text{C}$ )	(.34)	3.6	10.1	(.33)	5.1	9.2
-70 kPa ( $^{\circ}\text{C}$ )	(.31)	7.9	10.9	(.36)	6.5	10.7
-50 kPa ( $^{\circ}\text{C}$ )	(.28)	8.2	9.9	(.05)	8.8	10.3
Sfc Rel. Hum. (%)	(.23)	-15.8	24.3	(.22)	-15.1	27.5

Nearly all the satellite-RAOB comparisons show high correlations. For the retrieval temperatures the correlations with RAOB temperatures only fall below 0.60 at and above 30 kPa (300 mb). Part of this is due to the use of only the more transparent  $\text{CO}_2$  channels in the retrieval

process. The channels which peaked at or above the tropopause were not used. The highest temperature correlations occur at 50 kPa (500 mb). Mean temperature differences (biases) are positive at all but 20 kPa (200 mb). This may be due to the assumption of the blackbody emittance (emissivity) being equal to 1.0 (blackbody), whereas an actual value may be less, causing an overestimation in the satellite-derived temperatures.

The radiative surface temperature was the value derived from the satellite window channels. This is different than the air temperature at the surface because the surface temperature was allowed to float in order to incorporate surface temperature inversions into the retrievals when necessary. The biases for the radiative surface temperature are negative and positive for 1000 and 1400 GMT, respectively. This may be reasonable, considering that the RAOB surface temperatures are measured at shelter temperature height and not at the actual surface. Also, the radiative surface temperature would be lower before sunrise (1000 GMT) and would be greater after sunrise (1400 GMT), creating the negative and positive biases.

The moisture comparisons show the highest correlations for the total precipitable water. The positive biases are probably linked to the positive temperature biases. The overestimation of temperatures would require more atmospheric moisture in the retrieved profiles to produce lower radiances equivalent to those observed by the satellite. Root-mean-square precipitable water differences are 4.8 and 6.5 mm at 1000 and 1400 GMT, respectively. For a mean total water of 25 mm these rms values represent 19 and 26% of the mean, respectively.

Although the dew point temperature comparisons showed lower

correlations than those for temperatures, the highest correlations were at the surface where more water typically resides. Biases were again positive except for the surface dew points at 1000 GMT. These values were strongly linked to the surface temperatures because at 1000 GMT saturation occurred at the surface at many retrieval locations. Rms differences are 4.4 and 5.3 K, respectively, for the surface dew points in the two comparisons.

Finally, the surface relative humidities are compared. Correlations are among the lowest of the variables compared. Biases are negative, which is reasonable considering that the biases of the surface dew points are less than those for the corresponding surface temperatures.

Because of the emphasis on moisture retrievals, a qualitative comparison of the satellite-derived and RAOB precipitable water fields was made. The satellite-derived precipitable water values at 1000 and 1400 GMT are plotted in Figures 6.1a and b, respectively. In spite of some missing values, the two fields have similar gradients of moisture from the southeast to the northwest. There are differences, however. The dry tongue from Nebraska into Illinois at 1000 GMT fills or becomes more moist by 1400 GMT. Also, the moist area over Arkansas at 1000 GMT dries somewhat by 1400 GMT. In other words, the south to north moisture gradient has been weakened.

The satellite-derived precipitable water field at 1200 GMT is plotted in Figure 6.1c. This field is composed mostly of time-interpolated values from 1000 and 1400 GMT. Because 1200 GMT is halfway in-between the two satellite times, the values plotted are equally weighted averages of the two satellite measurements when available; but







where an average is not possible, because one of the two satellite-derived values is missing, the value plotted is the available measurement regardless of whether the measurement is from 1000 or 1400 GMT. These non-interpolated values are plotted in parentheses.

Contours in Figure 6.1c are similar to the RAOB total water contours shown previously in Figure 3.4b. Generally, a moisture gradient exists from the southeast towards the northwest. The tendency towards a dry region extending from Nebraska into Indiana, however, is not quite as strong as in the RAOB analysis. The precipitable water difference field is shown in Figure 6.1d. The region of differences greater than 8 mm is the dry region in the RAOB total water plot. This is also where the RAOB surface dew points were low. So, although the satellite-derived values are also lower here, they still overestimate the total precipitable water.

## 6.2 Satellite-Surface Observation Comparisons

The conventional synoptic surface observations, as mentioned before, were used only for verification of the satellite-derived surface parameters. The typical synoptic surface observation spacing is approximately 100 km, except for a limited number of closer observing stations (refer back to Figure 3.3). The satellite-derived surface parameters, on the other hand, can be separated by as little as approximately 30 km. These spacings suggest roughly a potential 9 to 1 ratio of satellite-derived to synoptic surface observations in an extreme case. In reality the ratio is approximately 5 to 1 for the special high-density surface observations which were used in this study. However, for comparison purposes the satellite soundings were retrieved at the same approximate density as the surface observations.



In order to compare the non-synoptic satellite-derived values with the surface observations taken at synoptic times, some time-interpolation had to be performed. The synoptic surface observations are linearly interpolated in time to both 1000 and 1400 GMT. The 1000 GMT time-interpolated values are obtained by a 2-to-1 weighted average of the 0900 and 1200 GMT synoptic values, respectively. Likewise, the 1400 GMT time-interpolated values are a 1-to-2 weighted average of the 1200 and 1500 GMT synoptic values, respectively.

Because not all observing stations reported at each synoptic time, there are fewer interpolated values at either 1000 or 1400 GMT than measured values at the surrounding synoptic times. The number of interpolated observations is shown in Table 6.2.

Table 6.2

Time-Interpolated Surface Observations  
and Paired Satellite-Surface Observations

<u>Time</u>	<u>Number of Time-Interpolated Surface Observations</u>	<u>Number of Satellite-Surface Pairs</u>
1000 GMT	94	75
1400 GMT	112	63

For each of the time-interpolated observations the closest satellite-derived value was chosen for comparison. The only limitation was that the satellite value had to be within 60 km of the synoptic station, however most satellite locations were within 40 km of the surface observations with which they were paired. Also, for various reasons some of the satellite-derived values were unavailable. Two of the major reasons were the calibration gaps in the radiance fields and cloud contamination, which prohibited soundings at certain positions.

Therefore, the number of satellite-conventional pairs is less than the number of conventional observations, as shown in the last column of Table 6.2. Because of extensive cloudiness at 1400 GMT the number of satellite values was reduced and likewise the number of satellite-conventional pairs.

The three surface parameters which were compared are the temperature, dew point temperature, and the relative humidity. Also shown is a comparison of the satellite-derived total precipitable versus the precipitable water estimated from the surface dew point temperatures. Separate columns are used to compare the meteorological variables at both 1000 and 1400 GMT. Table 6.3 gives the satellite-versus-surface correlation coefficients, mean differences (or biases), and root-mean-square (rms) differences.

Table 6.3

## Satellite-Synoptic Surface Observation Comparisons

<u>Parameter</u>	<u>1000 GMT</u> (75 pair)			<u>1400 GMT</u> (63 pair)		
	<u>Corr.</u>	<u>Bias</u>	<u>Rms Diff.</u>	<u>Corr.</u>	<u>Bias</u>	<u>Rms Diff.</u>
Sfc Temperature ( $^{\circ}$ C)	(.53)	-4.5	5.2	(.75)	-.4	2.0
Sfc Dew Point Temp ( $^{\circ}$ C)	(.59)	-3.0	4.2	(.59)	1.8	4.4
Sfc Rel. Humidity (%)	(.19)	-8.9	21.0	(.33)	-5.8	24.7
Estimated Tot. PW (mm)	(.34)	.2	5.5	(.62)	1.8	5.2

In the retrieval process no special attempt was made to eliminate a bias in the satellite-retrieved parameters. A positive bias, for example, indicates that the satellite-derived values are larger than the conventional values and vice versa.

As in the case of the satellite-RAOB comparison the rms differences are the standard 'error' analyses which are typically shown in most satellite-conventional comparisons. This difference is not entirely an error in the satellite products but is composed of errors in both the satellite and conventional data and discrepancies due to different space and time sampling methods between the two sets of measurements. Bruce et al. (1977) found that rms temperature differences of a minimum of approximately 1 K can be attributed to the comparison of point versus area-averaged temperatures.

The correlation coefficients are fairly high for surface temperature and surface dew point comparisons. The square of the correlation coefficient represents the proportion of the variance in one set of measurements which can be explained by the other set of measurements (the explained variance). For example, the highest temperature correlation of 0.75 represents a 56% explained variance using satellite retrievals to predict surface temperatures. Correlation coefficients for the surface relative humidity values are lower, as was the case with the satellite-RAOB comparisons.

The last row in Table 6.3 shows a comparison of the satellite-derived precipitable water with the precipitable water estimated from the synoptic surface dew point values. The estimated total water values were obtained by the application of Equation 3.2 to the surface dew points. The correlation is higher at 1400 GMT than at 1000 GMT. Biases are surprisingly low and rms differences are similar to those for the satellite-RAOB comparisons. The rms values of 5.5 and 5.2 mm are 22% and 21%, respectively, of the previously-used mean precipitable water of 25 mm.

Point-to-point comparisons of the satellite-derived values versus conventional surface observations are given in Figure 6.2 (a, b, and c). These figures show the scatter involved in a one-to-one comparison. Also shown in each figure is a (solid) line which would represent a perfect 1 to 1 relationship between the satellite and surface data sets and a similar (dashed) line adjusted for the bias between the data sets.

The surface temperature comparisons in Figure 6.2a show a similar spread between the two sets of measurements at both 1000 and 1400 GMT. However, the larger bias at 1000 GMT is due to the strong temperature inversion situation at this time. The radiatively cold surface causes the satellite to underestimate the measured (synoptic) surface temperatures, which were recorded at instrument shelter height. A higher correlation and lower bias occurs at 1400 GMT.

The dew point temperature comparisons at both 1000 and 1400 GMT are shown in Figure 6.2b. A larger spread between the satellite and conventional dew point temperatures occurs at 1400 GMT where satellite values overestimate the moisture in the driest cases. In other locations the satellite underestimates surface moisture at this same time.

The comparisons between satellite-derived and surface-estimated total precipitable water at both 1000 and 1400 GMT are given in Figure 6.2c. There is a larger spread between the two sets of measurements at 1000 GMT than at 1400 GMT. This is probably due to the predominance of surface temperature inversions at that time. The differences between the satellite-derived and surface-estimated total water can be likened to the differences between the actual and surface-estimated total water discussed previously. The areas where these differences occur will be

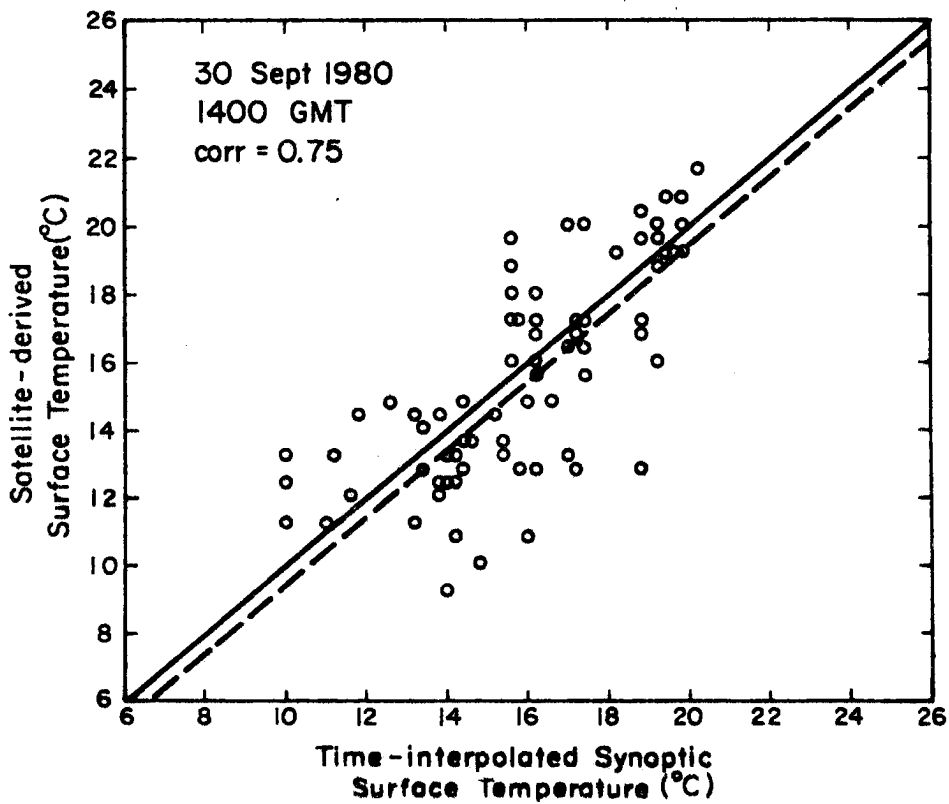
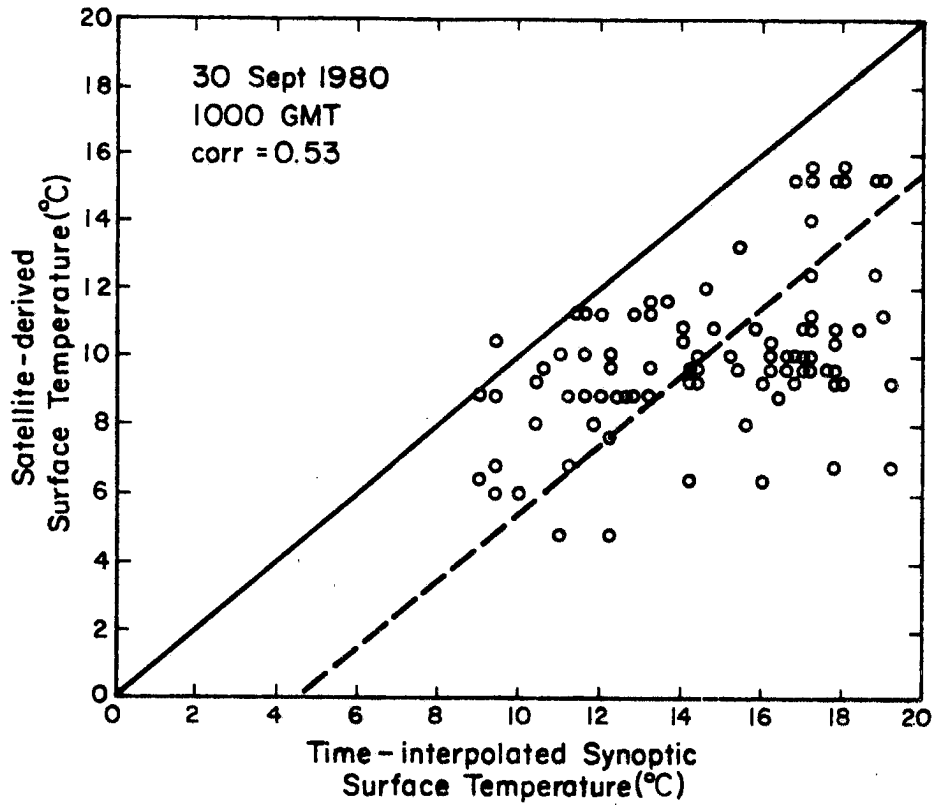


Figure 6.2a Satellite-derived versus synoptic (time-interpolated) surface temperatures at both 1000 and 1400 GMT on 30 September 1980.

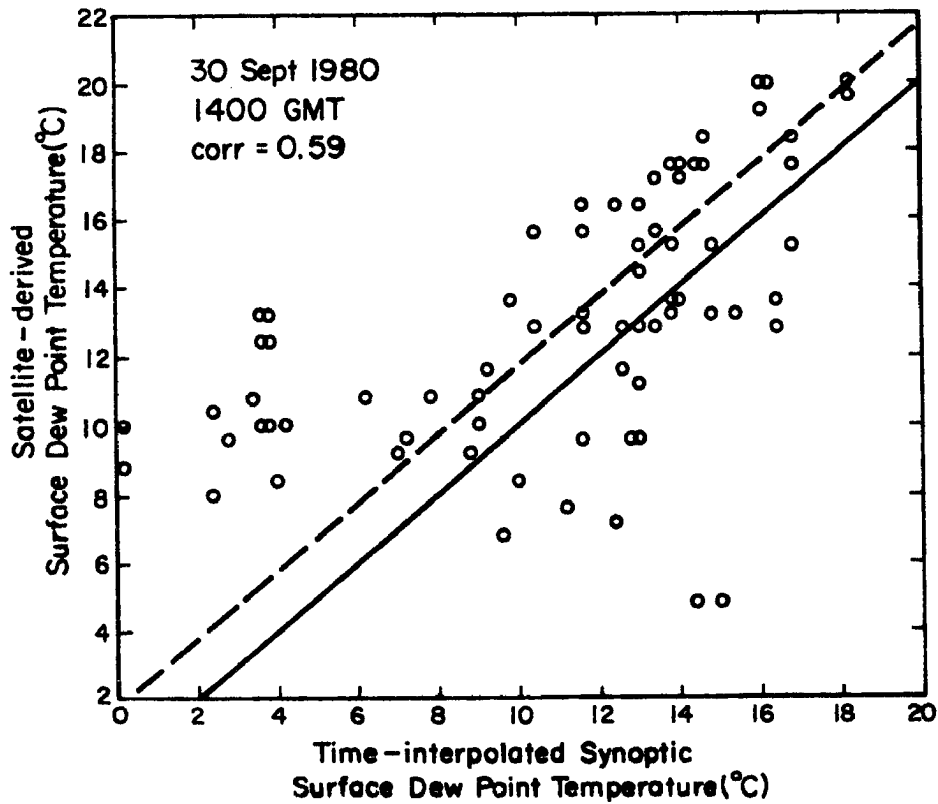
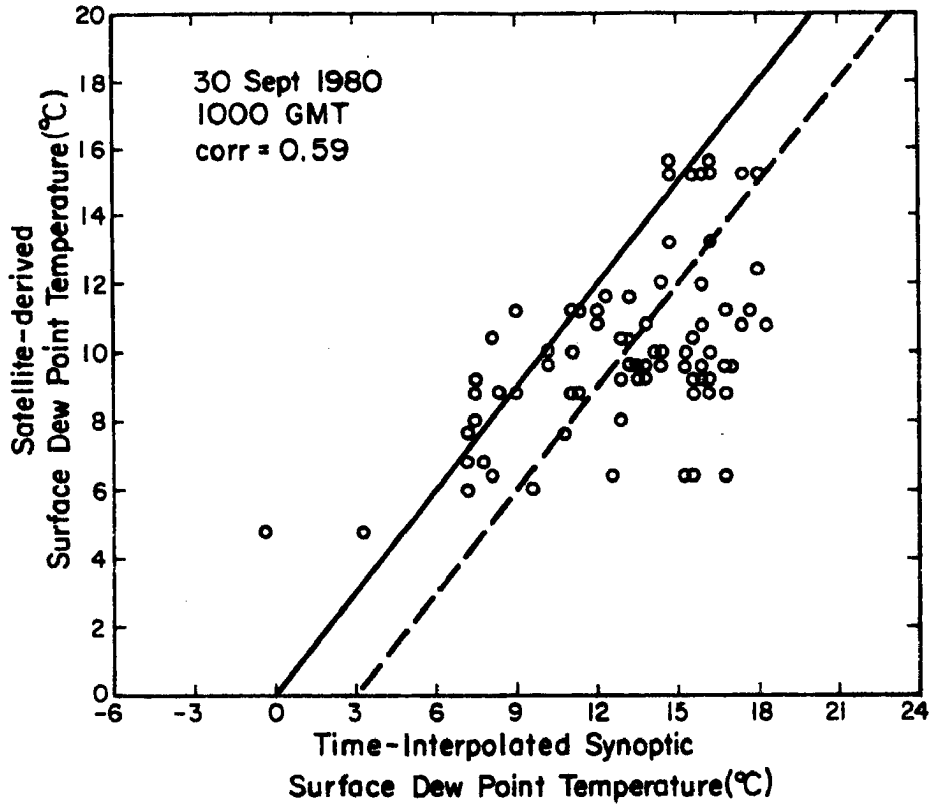


Figure 6.2b Satellite-derived versus synoptic (time-interpolated) surface dew point temperatures at both 1000 and 1400 GMT on 30 September 1980.

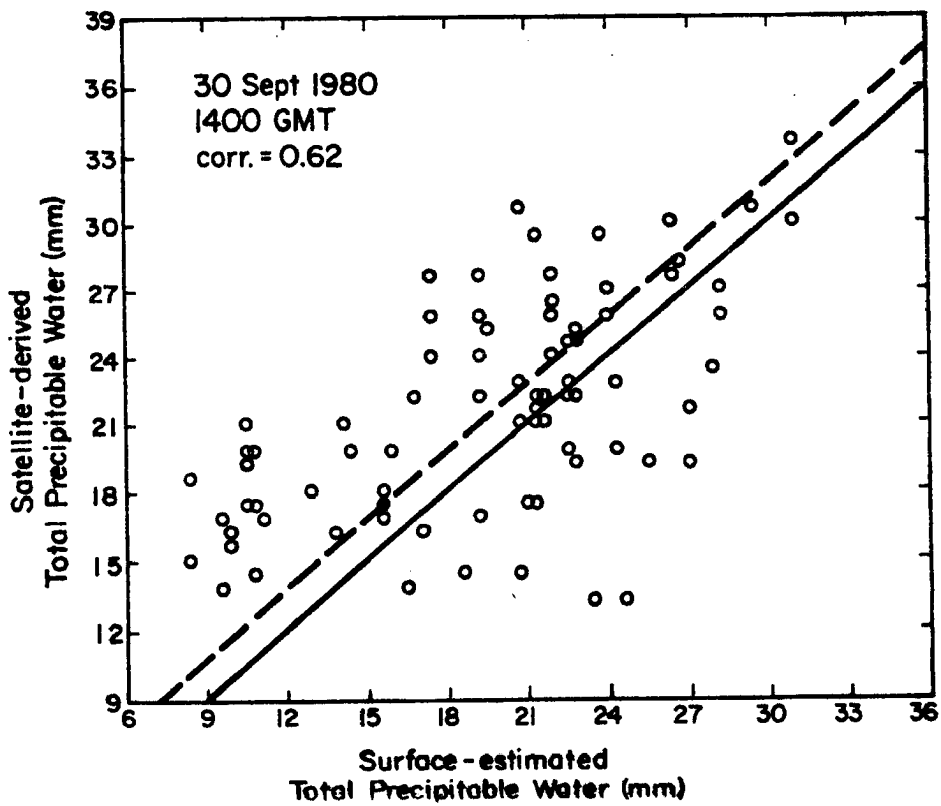
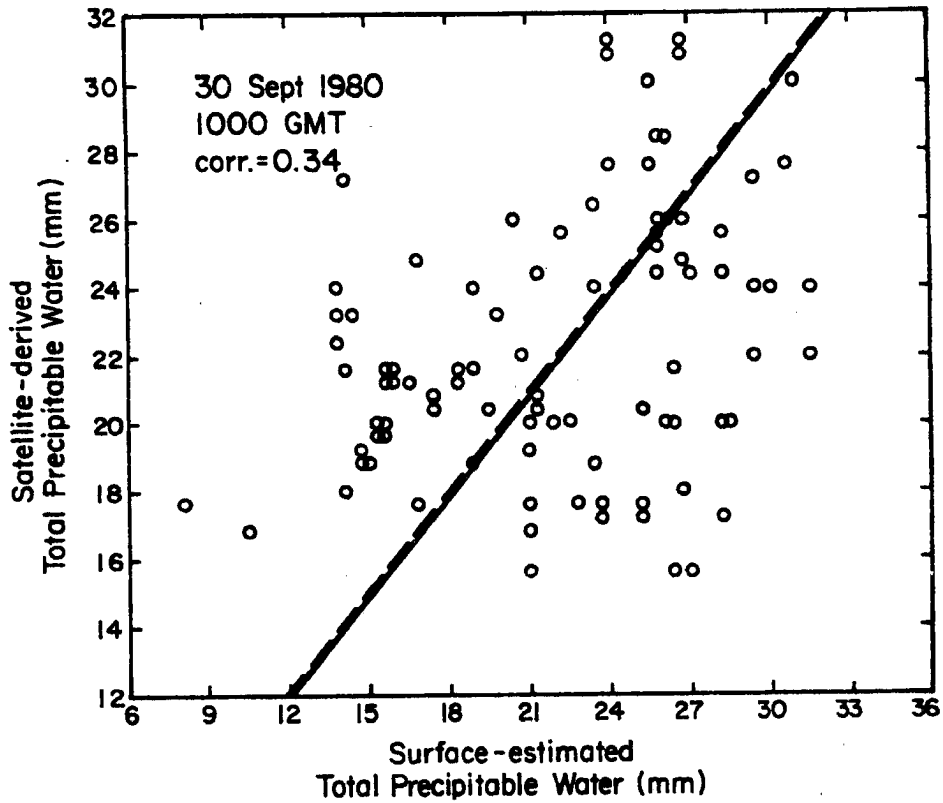


Figure 6.2c Satellite-derived versus synoptic (time-interpolated) surface-estimated total precipitable water at both 1000 and 1400 GMT on 30 September 1980.

examined thoroughly when the fields of precipitable water from each system are compared and contrasted.

The satellite-synoptic comparisons must also be examined in the light of the variability of the synoptic observations which went into each of the time-interpolations. Table 6.4 gives the correlations, mean differences (biases), and rms differences between the surface observations at various synoptic times. All of the variable correlations are high except for the 1200 versus 1500 GMT surface temperatures. This indicates a significant change in the temperature field from 1200 to 1500 GMT, probably due to horizontal variations in solar heating after sunrise.

Table 6.4

## Synoptic Surface Observation Intercomparisons

<u>Parameter</u>	<u>0900 vs 1200 GMT</u> (112 pair)			<u>1200 vs 1500 GMT</u> (94 pair)		
	<u>Corr.</u>	<u>Bias</u>	<u>Rms Diff.</u>	<u>Corr.</u>	<u>Bias</u>	<u>Rms Diff.</u>
Sfc Temperature ( $^{\circ}$ C)	(.94)	-.6	1.3	(.40)	4.0	5.3
Sfc Dew Point Temp ( $^{\circ}$ C)	(.97)	-.2	1.1	(.91)	1.6	2.6
Sfc Rel. Humidity (%)	(.90)	2.2	5.2	(.78)	-11.1	15.8
Estimated Tot. PW (mm)	(.96)	-.2	(1.6)	(.89)	2.3	3.6

The low bias and high correlation situation between 0900 and 1200 GMT gives indication of the variability or noise level of the synoptic parameters. The minimum rms values of 1.3 K and 1.1 K for surface temperatures and surface dew points are relevant to the comparison of satellite-derived values to time-interpolated synoptic values. This minimum time-difference uncertainty must be considered in addition to

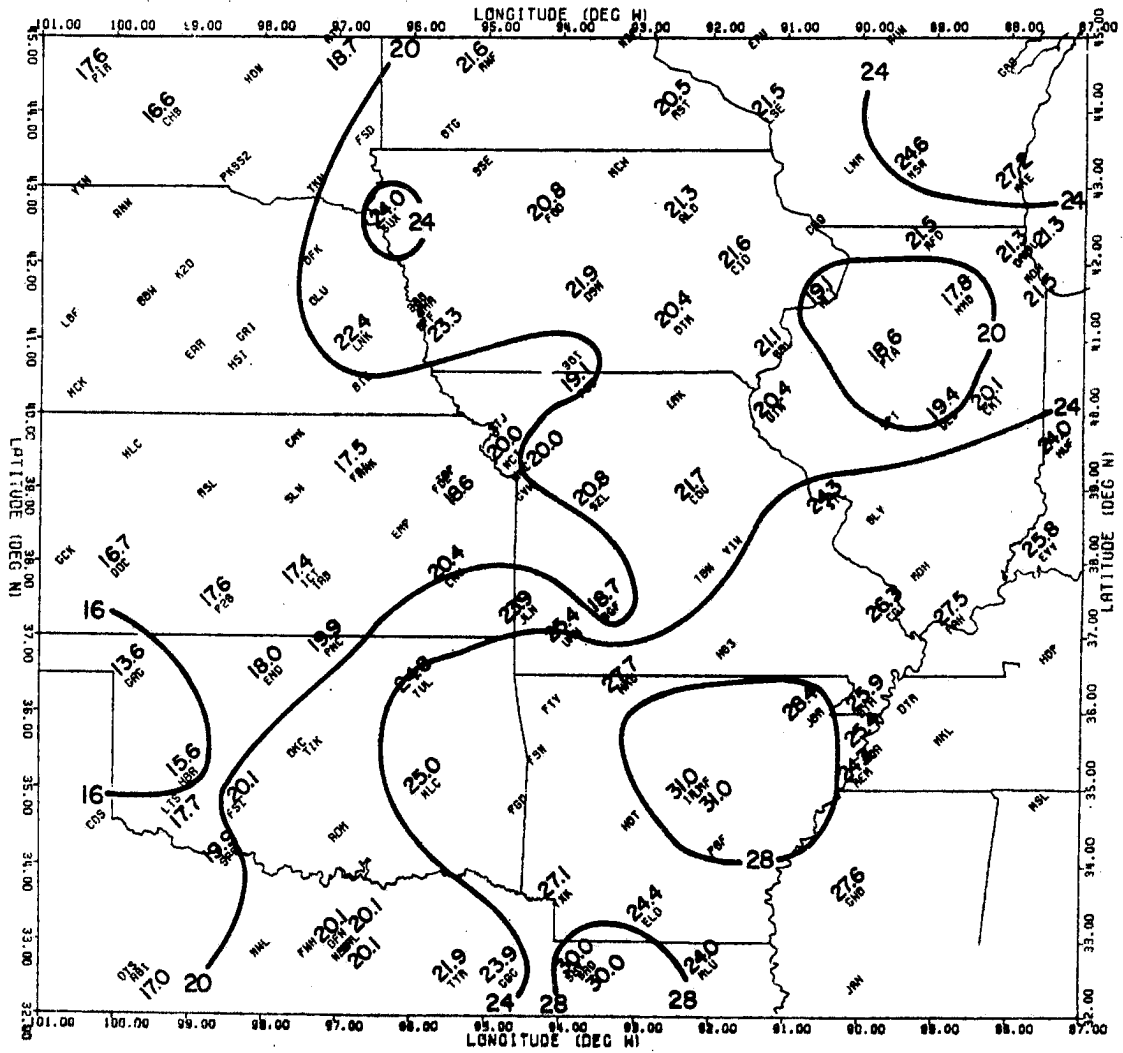
the discrepancies due to comparisons of point versus area-averaged values pointed out by Bruce et al. (1977).

In the following subsections a further qualitative comparison of the satellite-derived and conventional synoptic fields will be made. In this case fields of satellite-derived precipitable water were retrieved at the scale of the surface observations, or approximately with 100 km resolution. Satellite-derived values could be obtained at higher resolution (down to 30 km) but they were retrieved at the same approximate resolution as the surface observations for this comparison. Precipitable water fields warrant further attention, because of the emphasis on moisture retrievals in this study, and because the satellite-derived total precipitable water gave the highest correlations of the retrieved moisture parameters when compared to the RAOBs.

#### 6.2.1 A Closer Look at 1000 GMT

The satellite-derived total water field at 1000 GMT at the scale of the surface observation is plotted in Figure 6.3a. The area covered is the smaller area in Figure 3.1. More detail arises at this higher resolution than at the RAOB scale. Outstanding features include a local moisture minimum in Illinois. At this resolution this moisture minimum is separated from the dry region to the west, whereas at the RAOB scale (Figure 6.1a) the contours were drawn to indicate a dry tongue extending from Nebraska into Illinois.

Another feature is the moisture maximum in Arkansas. This same feature was shown at the RAOB scale in Figure 6.1a but here it is supported by more than one satellite-derived value. A strong moisture gradient also exists from Arkansas into Missouri.

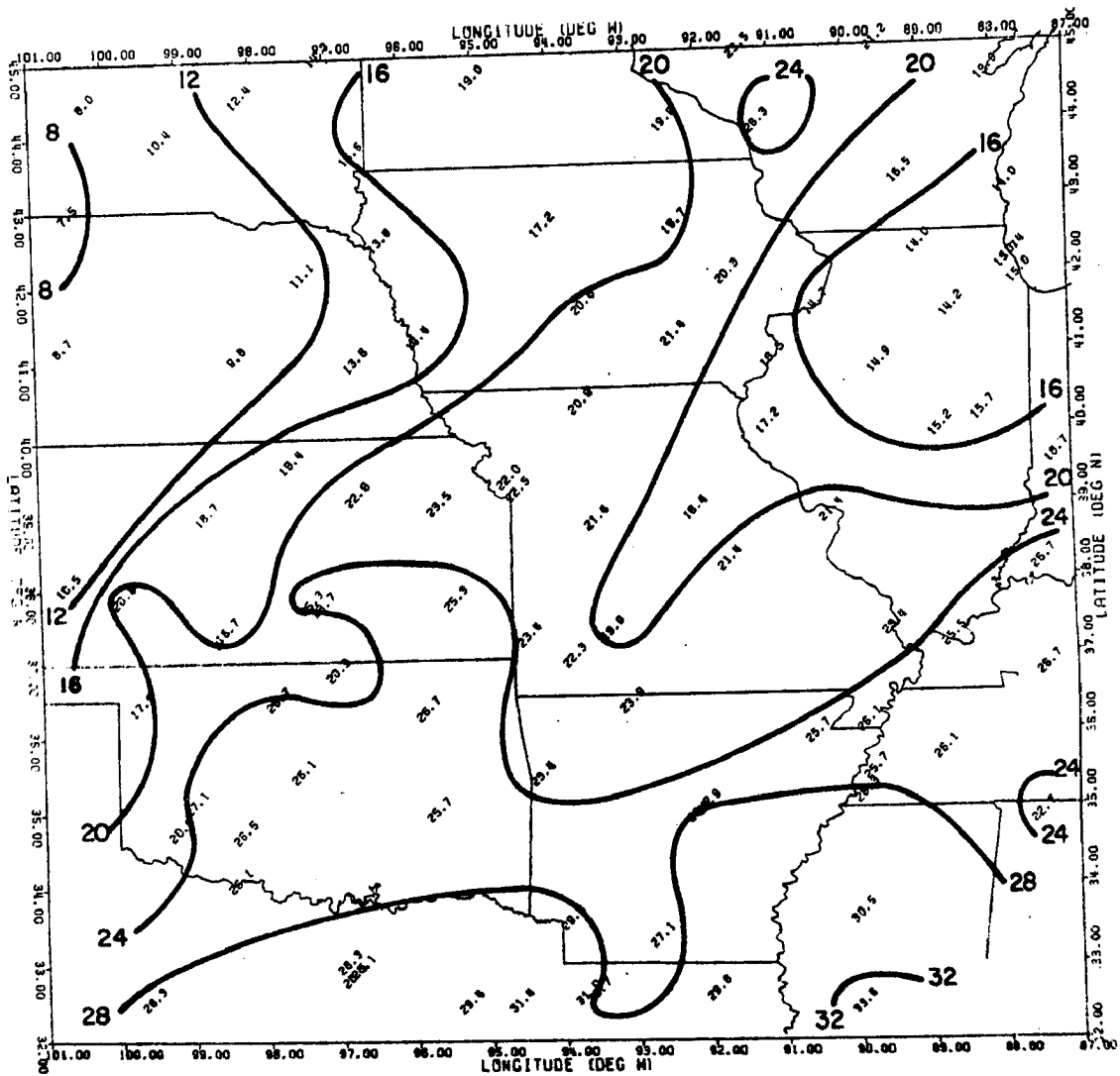


30 Sept 1980  
 1000 GMT  
 PW<sub>sat</sub> (mm)

Figure 6.3a Satellite-derived total precipitable water (mm) at surface observation resolution for 1000 GMT on 30 September 1980.

For comparison purposes, precipitable water has been estimated from the time-interpolated surface observations at 1000 GMT by using Equation 3.2. This was the surface dew point to total precipitable water relationship found for the RAOBs at 1200 GMT. The surface-estimated total water field is given in Figure 6.3b. Here the contours show a general moisture gradient from southeast to northwest. Dry regions to the west and over Illinois are separated by a thin moist region of as little as 100 km in width. This moist bridge agrees somewhat with the satellite-derived precipitable water which shows the dry tongue not linked from west to east. On the other hand, the satellite-derived moisture maximum over Arkansas is not as strong in the surface-estimated water contours. Differences will exist because of the nature of the two sets of measurements.

Figure 6.3c shows the difference field created when the surface-estimated precipitable water values are subtracted from the satellite-derived values. Because the estimated total moisture is determined by the surface dew point, it represents a certain moisture lapse rate or a given decrease in moisture with height. The satellite-derived moisture profile begins with a given initial guess moisture profile and is adjusted to try to represent the true moisture situation. If the satellite provides a better representation of the vertical moisture structure, then the satellite-minus-estimated difference shows something about the vertical extent of the moisture. This would be similar in interpretation to the actual-minus-estimated total moisture differences plotted at the RAOB locations in Figure 3.6b. Positive differences represent regions where the atmosphere is determined by the satellite to be moist aloft, i.e., more moisture is detected than is estimated from



30 Sept 1980  
 1000 GMT  
 Estimated PW' (mm)

Figure 6.3b Total precipitable water (mm) estimated from time-interpolated surface observations at 1000 GMT on 30 September 1980 by using Equation 3.2.



the surface. On the other hand, negative differences represent regions where the atmosphere is dry aloft, i.e., less moisture is detected than is estimated from the surface.

Regions of the largest positive differences in Figure 6.3c cover parts of Wisconsin and northern Illinois, parts of Nebraska and also parts of Arkansas. Here the moisture is detected by the satellite to be deeper than that suggested by a moisture profile estimated from the surface dew point. Negative values reach a maximum in Texas and Oklahoma with negative values extending up into Iowa. These negative values represent a situation where the atmosphere is detected by the satellite to be dry aloft. Not surprisingly, this is also where the fog forms which was shown in the 1400 GMT visible image in Figure 2.3a. Regions where the atmosphere is moist aloft, such as over Arkansas, are not conducive to radiation fog because of the suppressed infrared cooling to space, even though lower layers of the atmosphere may be very moist.

Examples of satellite and conventional soundings in a negative region are shown in Figure 6.4a. Here the satellite sounding at 1000 GMT is compared to the 1200 GMT RAOB at Topeka (TOP). Also shown is a power-law moisture profile generated using Equation 3.3, with the exponent determined by Equations 3.2 and 3.6. The three moisture profiles serve to compare precipitable water amounts based on three determinations; an in-situ sounding, a moisture profile estimated from a surface dew point measurement, and a satellite-derived moisture profile. Because the atmosphere is dry above a shallow moist layer, the power-law moisture profile overestimates the moisture at most levels other than near the surface. The satellite-derived profile also overestimates the

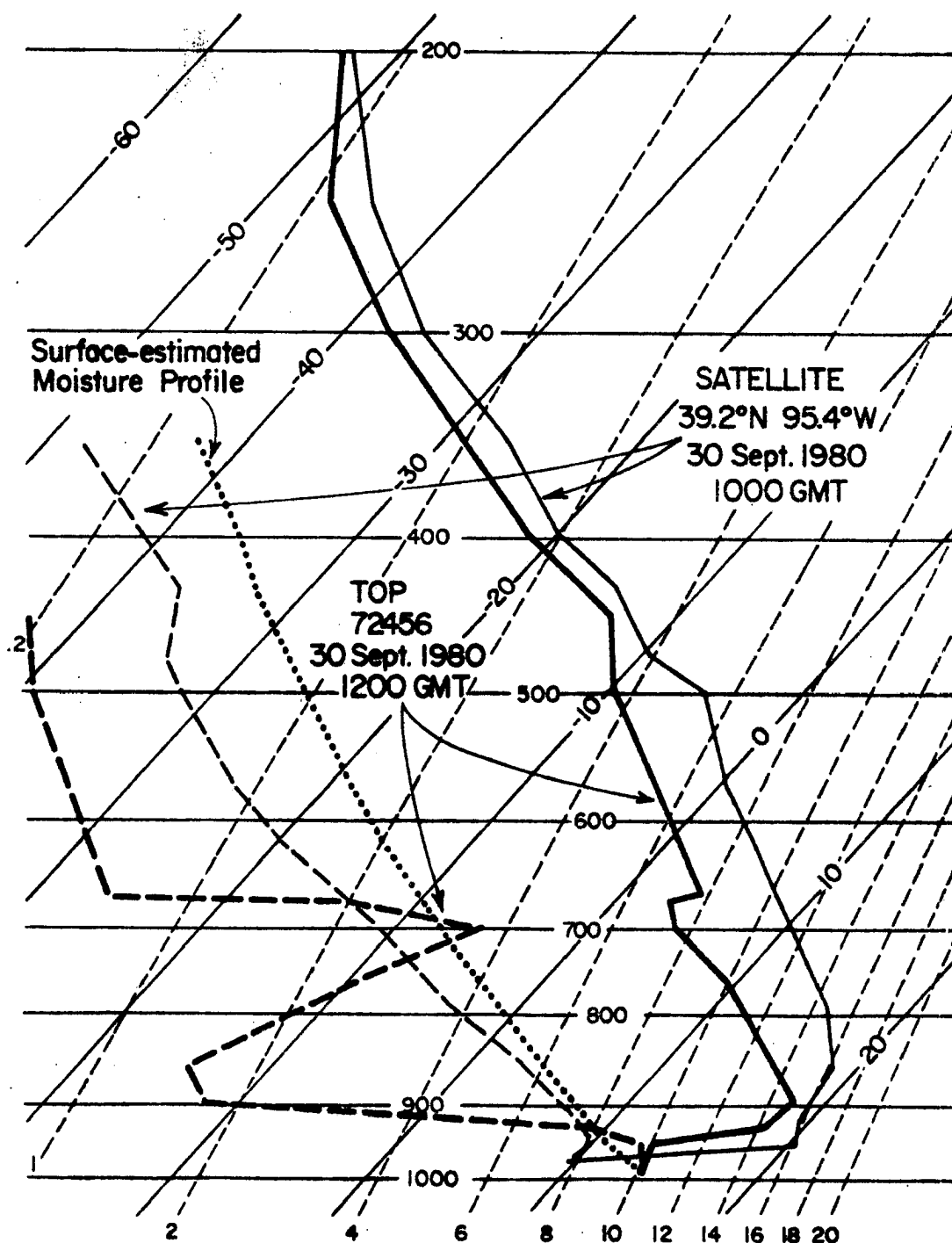


Figure 6.4a Topeka, Kansas RAOB at 1200 GMT on 30 September 1980 showing a shallow moist layer near the surface. The dotted line is a power law moisture profile based on the RAOB surface dew point temperature. (See text for more explanation). Also plotted is the nearest satellite sounding at 1000 GMT which does not contain the vertical detail of the RAOB but which better approximates the dry-over-moist situation.

moisture at most levels except near the surface, but to a lesser degree than the surface-estimated moisture profile. Thus, a negative (satellite-minus-estimated) difference is determined for this case.

Figure 6.4b shows a similar comparison of moisture profiles for a positive region in Figure 6.3c. Here surface-estimated and satellite-derived moisture profiles are compared to the 1200 GMT Peoria (PIA) RAOB. In this case the surface-estimated moisture profile underestimates the actual moisture in the deep moist layer near the surface. The satellite-derived profile, on the other hand, more closely represents this deep moisture near the surface. The positive difference for the satellite-derived minus surface-estimated total water indicates a moist aloft situation, or in this case a situation where the moisture is deeper than the previous example.

In both of these examples the satellite did provide a better moisture profile than one estimated from the surface dew point temperature. The surface-estimated moisture profiles are far from good, but they may be all that is available without an actual sounding. By comparison of satellite-derived total water to the surface-estimated moisture, which is of little value alone, there is an indication of vertical moisture structure, if only in terms of moisture depth. This is important in that only a few types of moisture profiles are meteorologically significant. Of basic importance in this case of fog formation is the vertical moisture extent. The negative values of satellite-derived minus surface-estimated moisture indicate a dry-over-moist situation for a large portion of the area where the radiation fog forms.

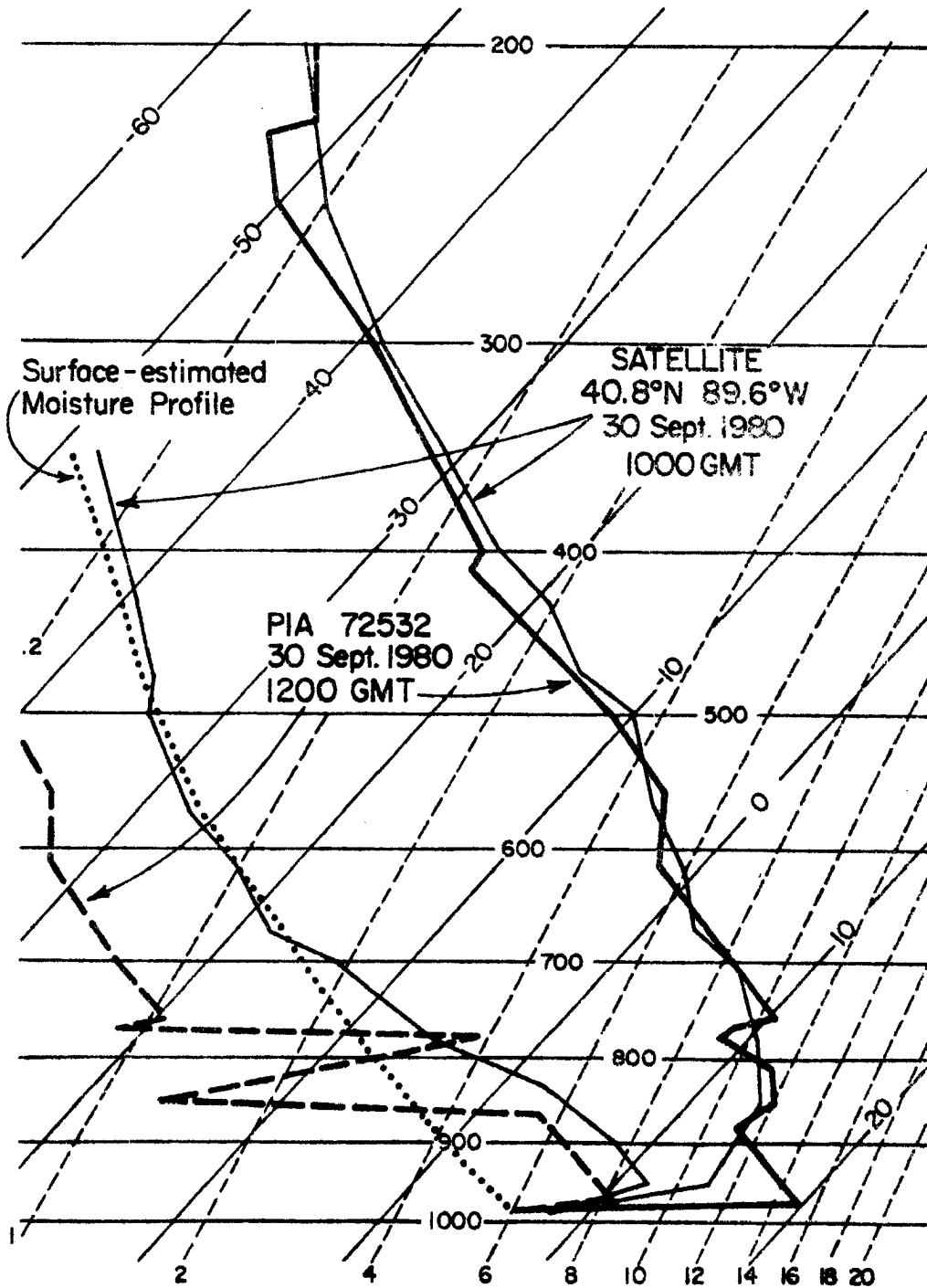


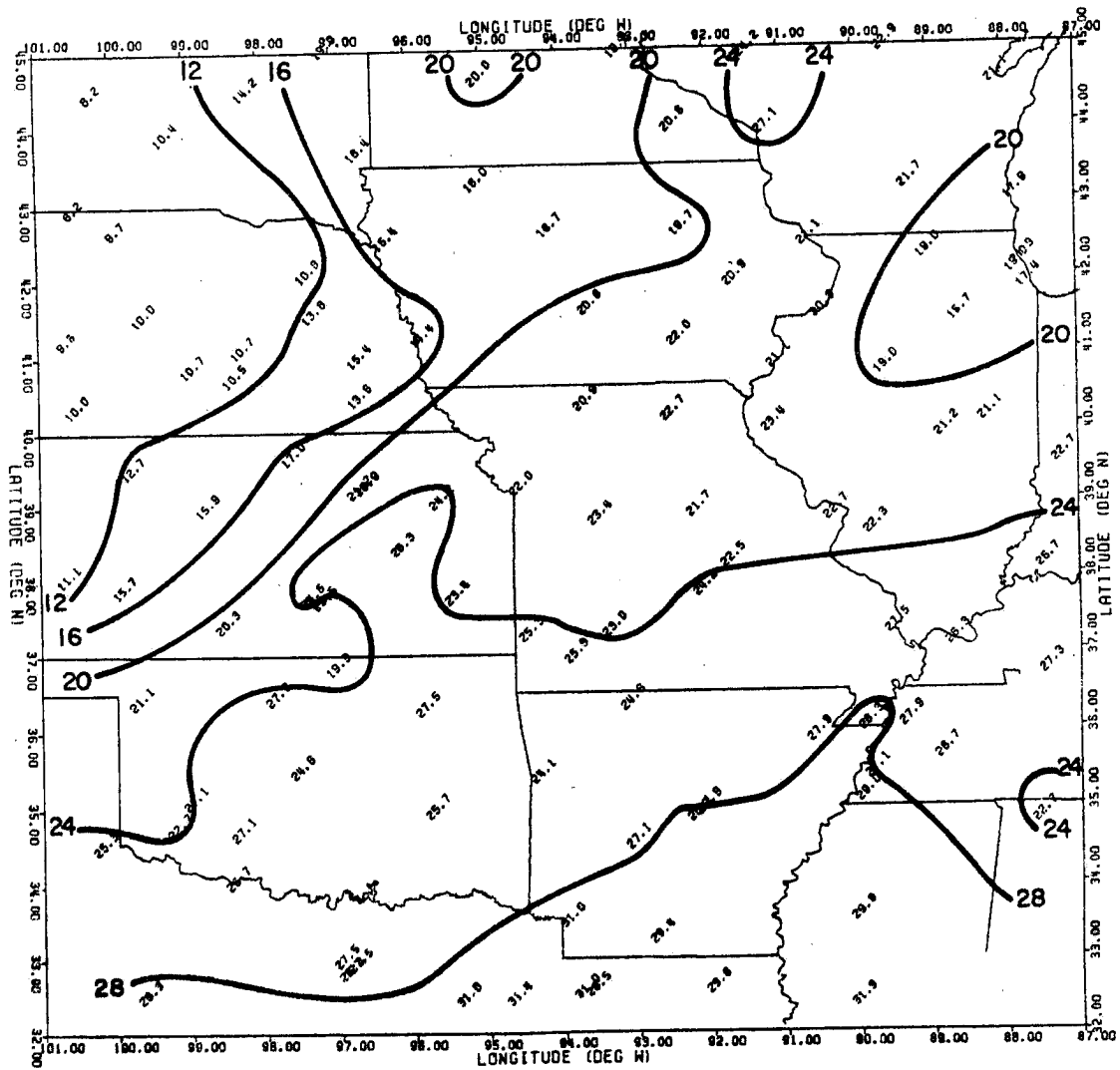
Figure 6.4b Peoria, Illinois RAOB at 1200 GMT on 30 September 1980 with a deep moist layer near the surface. The dotted line is a power law moisture profile based on the RAOB surface dew point temperature. (See text for more explanation). Also plotted is the nearest satellite sounding at 1000 GMT with its better reconstruction of the low-level moisture.

### 6.2.2 A Closer Look at 1400 GMT

A set of figures similar to those shown for 1000 GMT are given for the 1400 GMT satellite pass. Figure 6.5a shows the satellite-derived total precipitable water field. Here two major features appear which did not show up at the resolution of the RAOBs. First, a local moisture maximum on the Iowa-Illinois border occurs in a region where there are no RAOBs. The only indication in the RAOB-resolution plot in Figure 6.1b is the higher value at Peoria (PIA). The other major feature which appears at higher resolution is the dry tongue which extends from Kansas into Missouri. This feature, however, is not supported by many satellite-derived values because the fog prohibits satellite soundings over much of this area. It was also not shown at the RAOB resolution in Figure 6.1b, again because of missing values over this area. However, the few satellite-derived values which exist at the surface observation resolution indicate such a dry tongue. The visible satellite image showed this region of fog to be patchy and not as dense as fog areas to the north and south.

For comparison, Figure 6.5b is a plot of the estimated total water field from the time-interpolated surface observations at 1400 GMT. Again to obtain these values, the surface dew point to precipitable water relationship for the 1200 GMT RAOBs was used. Here, the strong local moisture maximum indicated by the satellite-derived values on the Iowa-Illinois border is not shown. The dry region in the east has also been reduced in size when compared to the similar 1000 GMT plot in Figure 6.3b.





30 Sept 1980  
 1400 GMT  
 Estimated PW' (mm)

Figure 6.5b Total precipitable water (mm) estimated from time-interpolated surface observations at 1400 GMT on 30 September 1980 by using Equation 3.2.

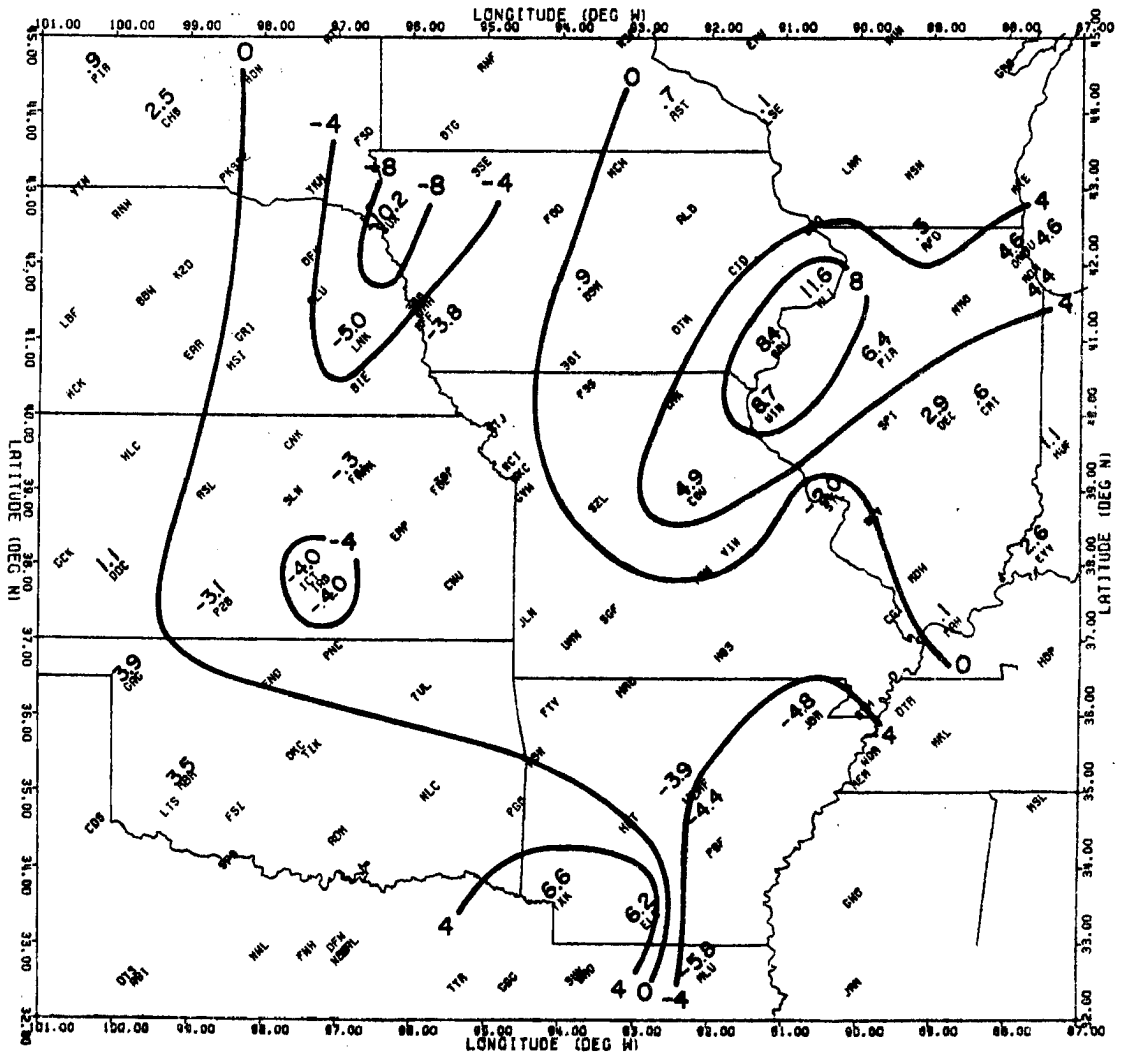
The difference field in Figure 6.5c shows areas where the atmosphere is moist (+) and dry (-) aloft. The major features are similar to those shown in the 1000 GMT difference field (Figure 6.3c). However, some shifting of the patterns has occurred, most notably the moist-aloft maximum now over the Iowa-Illinois border and the reduction in strength of the positive differences over Arkansas.

### 6.2.3 4-Hour Time Differences

One goal of this study was to examine the time change of the satellite-derived moisture values to determine if moisture changes could be detected at high space and time resolutions. For this reason, the 4-hour time change in satellite-derived total precipitable water between 1000 and 1400 GMT is plotted in Figure 6.6a. Outstanding features include a large increase in moisture along the Iowa-Illinois border and an equally strong decrease in moisture in the vicinity of northeastern Nebraska. Negative values dominated a region extending from Nebraska into Kansas and Arkansas.

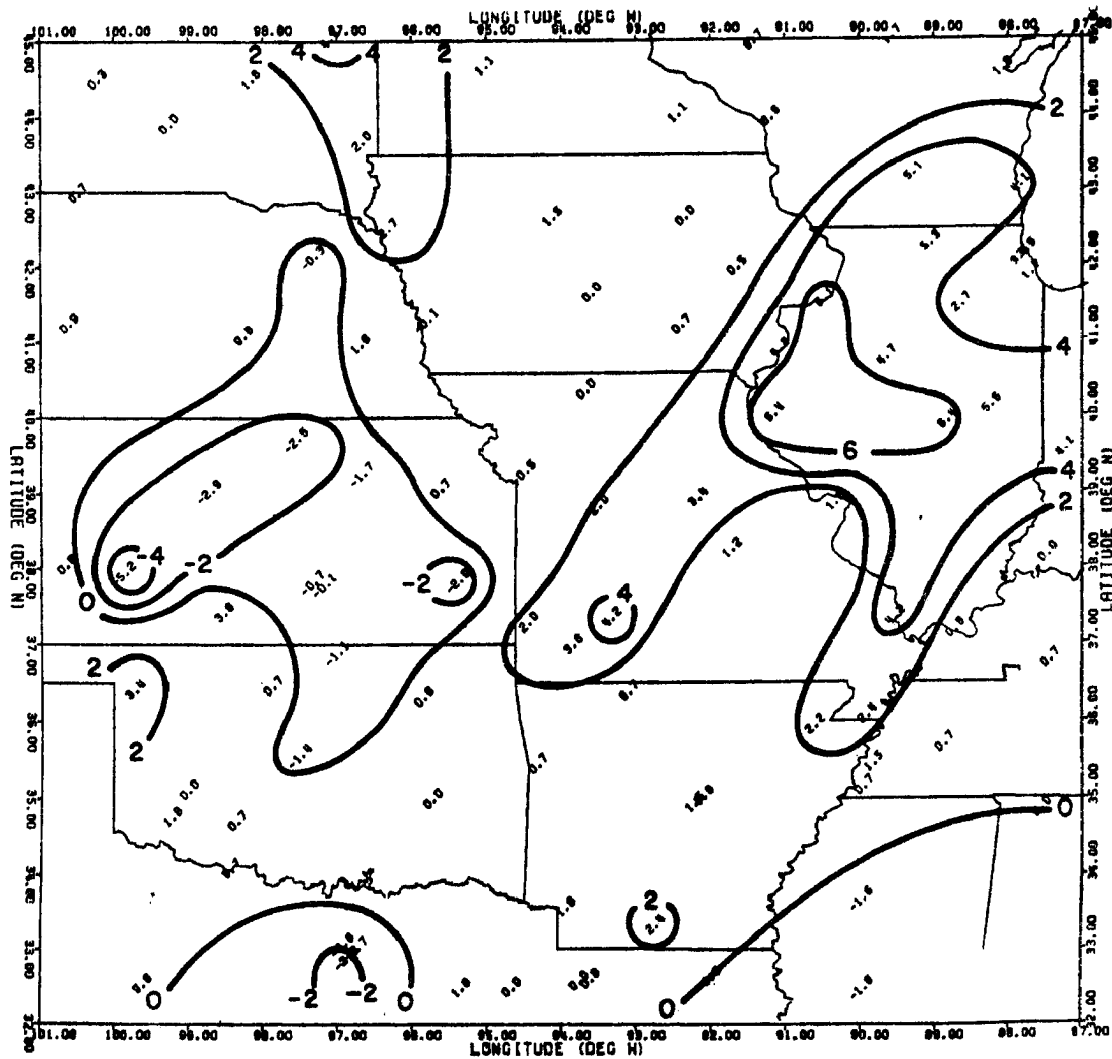
A similar time-difference analysis of the surface-estimated total precipitable water is shown in Figure 6.6b. Here, the same two features exist. The large increase in moisture, however, covers most of Illinois, approximately the region covered by weaker positive differences in the satellite-derived field in Figure 6.6a. The region of strong negative values covers most of Kansas and spreads north and south. This is approximately the same region of maximum moisture decrease shown by the satellite-derived time-difference field. However, the largest negative values in Figure 6.6b are now in Kansas and not in Nebraska. The shift of the local maxima and minima between the two fields is related to the depth over which the moisture change occurs.





30 Sept 1980  
 (1400-1000) GMT  
 $\Delta PW_{sat}$  (mm)

Figure 6.6a 4-hour time difference between satellite-derived total precipitable water (mm) at surface observation scale at 1000 and 1400 GMT on 30 September 1980.



30 Sept 1980  
 (1400 - 1000) GMT  
 $\Delta PW'$  (mm)

Figure 6.6b 4-hour time difference between surface-estimated total precipitable water (mm) at 1000 and 1400 GMT on 30 September 1980.

The surface-estimated total water values would more closely show surface moisture change and the satellite-derived values would show integrated moisture change.

The fact that the two time-change fields are similar is remarkable considering the large differences which existed between the satellite-derived and surface-estimated total precipitable water fields at both 1000 and 1400 GMT. These differences were related to the atmosphere being moist (+) and dry (-) aloft. The time-difference fields, however, show mesoscale features which are similar although dependent on depth.

A key to why these satellite-derived moisture changes are reasonable is found by looking at the 70 kPa (700 mb) winds at 1200 GMT. Benwell (1965) used 700 mb wind trajectories to compare advected moisture fields to those observed at a later time. His conclusion was that precipitable water is a fairly conservative quantity which could be advected with the 700 mb winds.

For this case the 700 mb wind and streamlines are drawn in Figure 6.7. The flow is generally from the north-northeast with a cyclonic pattern forming in the southeastern U.S. Using this flow pattern along with the RAOB total precipitable water pattern in Figure 3.4b, it is reasonable that moist air has been advected from Minnesota and Wisconsin into the previously dry slot in Iowa and Illinois. Also, the decrease in moisture in Kansas is likely associated with the advection of dry air from Colorado and western Nebraska towards the southeast.

Another possible reason for the increase in moisture in the Iowa-Illinois region may be due to low-level convergence causing moist air to be advected vertically from the surface. The surface wind analysis at 1200 GMT (not shown) indicates some low-level convergence of moisture

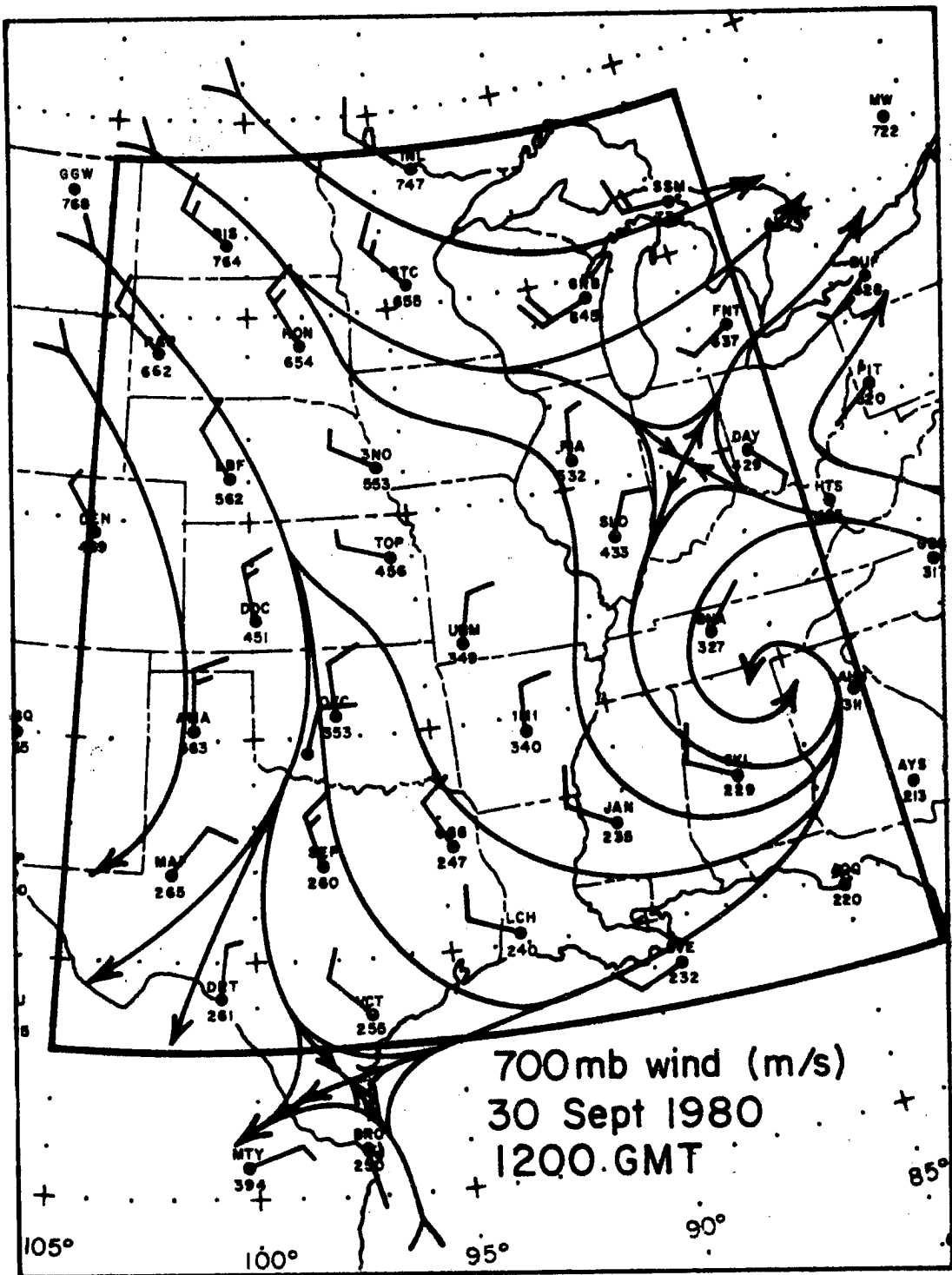


Figure 6.7 Winds (m/s) and streamlines at 70 kPa (700 mb) from 1200 GMT RAOBs on 30 September 1980.

(TROF) although the winds are weak (typically less than  $5 \text{ m sec}^{-1}$ ).

This additional explanation is plausible because of the limited ability of mid-level (700 mb) moisture advection alone, to explain the large (8 mm) satellite-derived moisture change in this region in only 4 hours.

### 6.3 Structure Analysis of Satellite-Derived Products

Another means of determining the quality of the satellite-derived products is through statistical structure analysis. For a high-resolution field of satellite-derived products a pairing of all values is performed. The pairing is done in such a way as to include all possible combinations of two values, grouped as a function of their separation distance. For various ranges of separation distances the mean-squared difference is then calculated and is plotted as in the example in Figure 6.8. This structure function (Gandin, 1963) is a statistical measure of the gradient in the field of measurements. Similar analyses of satellite measurements and satellite-derived products have been performed on other data sets (Hillger and Vonder Haar, 1979).

One feature of the structure function is the ability to estimate the noise level in an analyzed variable. This is done by compensating for the gradient in the data by extrapolating the structure to zero separation distance. For instance, in Figure 6.8 a line may be fitted to the structure values determined for various range gates. In this case the range gates are 50 km wide with structure values centered at approximately 50 km intervals. The fitting and the extrapolation process are sometimes not easy when the structure function is not well behaved. So, as an alternative, rather than extrapolating the structure to zero separation distance the value given at the smallest separation

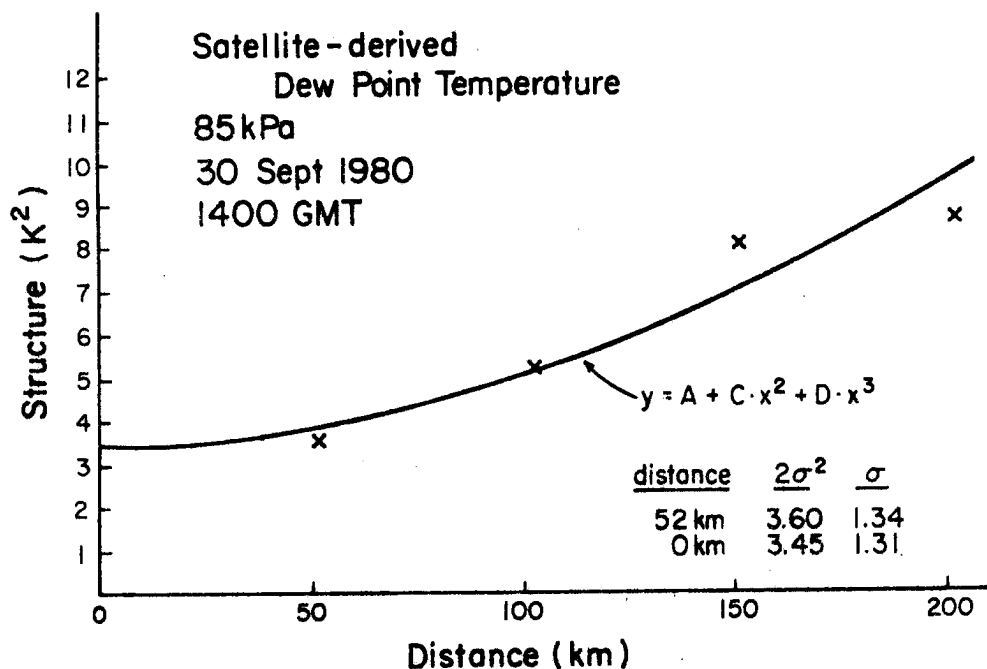


Figure 6.8 Structure as a function of separation distance for satellite-derived 85 kPa (850 mb) dew point temperatures at 1400 GMT on 30 September 1980. A third-degree polynomial with zero slope at  $x=0$  is fitted to the first four points.

can be used as a proxy noise level. For most meteorological fields only a small amount of gradient will typically exist between values separated by this small distance. As shown in Figure 6.8 for satellite-derived 85 kPa (850 mb) dew point temperatures at 1400 GMT, the structure function does not increase rapidly with separation distance. So the value at approximately 52 km (the mean separation distance for paired values in the 25 to 75 km box) can be used reliably to estimate the noise level in this parameter.

The noise level is estimated based on the assumption that each satellite-derived value contains an uncorrelated noise component. If the gradient is removed, then the structure or mean-squared difference will be reduced to  $2\sigma^2$  where  $\sigma$  is the rms noise on an individual measurement. A noise value is thereby determined for the various satellite-derived parameters. Table 6.5 gives the rms noise values estimated by the statistical analysis of the fields of satellite-derived parameters at both 1000 and 1400 GMT. Because of variations between the individual fields the results are dependent on the statistical base in each field, but similar noise levels are determined for most parameters at both 1000 and 1400 GMT.

Table 6.5

## Structure Analysis of Satellite-Derived Parameters

<u>Parameter</u>	<u>1000 GMT</u>			<u>1400 GMT</u>		
	<u>Noise</u> <sup>1</sup>	<u>Signal</u> <sup>2</sup>	<u>S/N</u> <sup>3</sup>	<u>Noise</u> <sup>1</sup>	<u>Signal</u> <sup>2</sup>	<u>S/N</u> <sup>3</sup>
Surface Temperature (°C)	1.7	3.6	(2.1)	3.1	3.7	(1.2)
Rad. Sfc Temperature (°C)	1.3	2.3	(1.8)	1.5	3.0	(2.0)
Precipitable Water (mm)	1.2	3.8	(3.2)	1.8	5.0	(2.9)
Sfc Dew Point Temp (°C)	1.3	2.3	(1.7)	1.5	3.8	(2.5)
25kPa Dew Point Temp (°C)	.8	2.1	(2.3)	1.3	2.9	(2.2)
Sfc Rel. Humidity (%)	4.6	18.8	(4.1)	8.9	24.5	(2.7)

- 1) Based on mean-squared difference between paired values at minimum separation of approximately 30 km.
- 2) Standard deviation of all values in analyzed field.
- 3) Signal-to-noise ratio.

Noise levels are estimated to be approximately 1.3 to 1.5 K for the radiative surface temperature, 1.3 to 1.5 K for the surface dew point, and 1.2 to 1.8 mm for total precipitable water. Some larger errors undoubtedly exist, but reliability should not be given to variations smaller than the estimated noise levels when analyzing the satellite-derived fields.

The noise levels for the satellite-derived parameters determined by this method are not dependent on a comparison with conventional measurements. They are merely the result of a statistical intercomparison of the individual values in a given field. For this reason the estimated errors are less than the differences determined previously by the comparison of the satellite-derived values to conventional measurements, and they, therefore, may be considered closer to the true noise levels.

Table 6.5 also contains the standard deviations of the satellite-derived values in each analyzed field. This is a measure of the data signal level. The ratio of this standard deviation to the estimated noise level gives a signal-to-noise ratio for the data set. The signal-to-noise values range from 1.2 to 4.1 for the various parameters, with a typical value of at least 2, indicating that most of the satellite-derived fields have significant structure or gradient compared to their estimated noise levels.

## 7.0 SUMMARY AND CONCLUSIONS

A physical, iterative retrieval scheme to derive meteorological parameters from satellite radiances was developed. Of major interest was the ability to derive moisture parameters and to use these parameters in a mesoscale or high-resolution situation. The satellite-derived products were then quantitatively and qualitatively compared to conventional data from both rawinsondes and surface observations. Time-differencing was also used to show the ability to obtain mesoscale moisture changes in time as well as space.

The meteorological situation under study was not of a convective nature as was the case with a previous analysis (Hillger and Vonder Haar, 1981). Instead, the situation involved the development of radiation fog. The fog formed in an area where both sufficient moisture and nocturnal cooling occurred. Surrounding regions contained either too little moisture for saturation or moisture which was too deep for sufficient radiative cooling to occur.

The availability of the satellite data at 1000 and 1400 GMT from two polar-orbiting satellites presented the challenge of doing retrievals both before and after sunrise, respectively. The main retrieval problem was caused by the existence of a surface temperature inversion over most of the area under study. The inversion lasted until solar heating destroyed it later in the morning. The after-sunrise satellite pass also presented a problem of reflected solar radiation contaminating the shortwave infrared channels. This was overcome by

appropriate corrections to the affected channels using knowledge of the known solar incident radiation and the estimated surface reflectance.

The retrieval scheme was also developed to require only a minimum input of conventional data. Basically, all that is required is an initial guess profile. In this study the initial guess profile was a composite of 1200 GMT RAOBs. No other ancilliary data was required. Some researchers use surface observations as input in order to anchor the retrieved sounding to known surface values of temperature and dew point. This, however, was not done. Satellite window channel information was used to obtain the necessary surface information. This allowed virtual freedom from conventional data sources.

Another change from earlier work of others is the use of information from only a single field-of-view for a retrieval. This allowed a single clear field-of-view to be used independently of surrounding (possibly cloudy) values. This may or may not be a direct advantage, but it allows a simplified retrieval development when cloudy situations are to be avoided.

Another problem in applying satellite soundings over land is the change in topography. This was taken into account by using the known mean terrain elevation for one-half degree latitude-longitude boxes over the area of study. This mean elevation was converted into a mean surface pressure using the hydrostatic relationship. Levels were then subtracted from (or even possibly added to) the 40 standard levels over which the radiative transfer equation was summed numerically. This smooth change in surface elevation allowed the retrieval of high-density measurements without the discontinuities which would arise from large changes due to numerical integration in large discrete vertical steps.

Such a smooth change in topography is possible only in a physical, iterative retrieval scheme such as was used in this study.

#### 7.1 Modifications Necessary for Nocturnal Inversions

The measurements from TIROS-N and NOAA-6 passes available at 1000 and 1400 GMT, respectively, over the central United States occurred at local times of approximately 4 and 8 a.m. At these times there is a high probability that a temperature inversion exists at or near the surface. The physical, iterative retrieval scheme was best able to handle this type of situation by allowing the surface or interface temperature to float free of the temperature profile above the surface. With this method, either temperature inversions or superadiabatic layers at the surface can be added to the temperature profile. This in effect adds vertical resolution to the retrieval sounding. If this were not allowed, the initial guess temperature profile would never obtain the vertical gradient necessary to reconstruct such a feature. The vertical resolution limitations of the satellite sounder would never add detail at or below a vertical scale of at least 200 or 300 mb.

The surface temperature inversion was common in the 30 September 1980 situation examined, as was confirmed by the number of RAOBs at 1200 GMT which contained such inversions. An example of a surface inversion added to the initial guess profile showed that such an addition provides a reasonable solution when compared to a nearby RAOB.

A second reason for recognizing the existence of a surface temperature inversion involves the satellite moisture retrieval capabilities. The effect of varying amounts of atmospheric moisture on the integrated radiances was simulated. In a non-inversion case the integrated radiances in a water vapor absorption band typically decrease

with increasing moisture. However, when a temperature inversion is added at the surface the integrated radiance can increase with increasing atmospheric moisture. This situation was first noticed empirically by the fact that the moisture profile was vastly overestimated when a temperature inversion was known to exist. However, by carefully calculating the moisture feedback values for the situation under study, the effect of the temperature inversion can be taken into account. For inversion cases the moisture feedback is typically reversed in sign and changed in magnitude, depending on the specific situation. So, the addition of a temperature inversion not only allowed a more correct determination of the surface temperature, but by recalculating the moisture feedback factors before each moisture iteration, it also allowed a more correct solution for the moisture profile.

## 7.2 Specific Results

The satellite-derived meteorological parameters were compared to conventional data at two scales. Comparisons were also both quantitative, in which satellite-derived parameters were compared to the equivalent conventional parameters by means of correlation coefficients and mean and rms differences; and qualitative, in which fields of total precipitable water from the two data sets were compared and contrasted.

In the initial comparison, the satellite-derived values were retrieved at the scale of the RAOBs. Direct comparisons to the 1200 GMT RAOBs were made for both the 1000 and 1400 GMT satellite-derived values. Correlation coefficients were 0.60 or greater for surface temperatures with the highest correlations at 50 kPa (500 mb). Of the moisture variables, the total precipitable water correlations were the highest,

followed by the surface dew point, with decreasing correlations for dew points at higher levels. Rms differences were typically 3 to 7 K for the satellite-derived temperatures and 3 to 10 K for the satellite-derived dew points. For the total precipitable water the rms differences were 4.8 and 6.5 mm at 1000 and 1400 GMT, respectively. These values represent about 19 and 26% of a mean value of 25 mm, respectively.

In the qualitative comparison at the RAOB scale, the satellite-derived precipitable water values were interpolated to 1200 GMT. Fields of both satellite and conventional precipitable water showed similar large scale moisture gradients. However, the largest differences occurred where the satellite-derived total water was overestimated in a relatively dry tongue shown by the RAOB values.

At the higher resolution of the surface observations similar quantitative comparisons were made between the satellite-derived and conventional data. The comparison included 75 and 63 pair at 1000 and 1400 GMT, respectively, compared to only 17 and 12 comparisons to the RAOBs at the same times, respectively. However, in this case the surface observations were time interpolated to 1000 and 1400 GMT for the comparisons.

Because the surface observations contain no vertical information, the comparisons at this higher resolution involved mainly surface values with the exception of the total water which was estimated from the surface dew point temperatures. A relationship was established between the surface dew point and the total precipitable water for the 1200 GMT RAOBs and was then used to estimate total water from all the surface observations.

Correlations were 0.53 or greater for the surface temperatures and dew point temperatures with rms differences of from 2 to 5 K for the surface temperatures and about 4 K for the surface dew points. For the total precipitable water the correlations were 0.34 and 0.62 at 1000 and 1400 GMT, respectively. Rms differences of about 5 mm were obtained at both times. Biases were much lower than for the satellite-RAOB comparisons, being less than 2 mm of water.

Scatter diagrams of the satellite-surface observation comparisons of the surface temperatures and dew points show that a few outlying points typically cause the correlation results to be degraded. These figures also show that removal of the biases would appear to greatly improve the quantitative comparisons.

An intercomparison of the synoptic surface values was used to establish a baseline variability of the fields used for comparison to the satellite-derived values. Comparisons were made between observations at 0900 and 1200 GMT and between observations at 1200 and 1500 GMT. These pairings were used to generate the time-interpolated values at 1000 and 1400 GMT. Correlations were typically high (above 0.78) for all values except surface temperatures between 1200 and 1500 GMT. During this 3-hour period solar heating probably changed the surface temperature structure drastically as witnessed by the large 4.0 K bias or average increase in temperature over this period. In contrast, between 0900 and 1200 GMT the rms values were about 1.3 K for temperatures and from 1.1 K for dew point temperatures with little if any bias present. These rms values give an indication of the minimum variability or noise in the time-interpolated synoptic values. Some of

this time-difference uncertainty will be inherent in the satellite-synoptic comparisons, since neither data set is error free.

In the qualitative comparisons at the surface observation scale, a closer look was made at the satellite-derived and surface-estimated total water fields at both 1000 and 1400 GMT as well as the time-difference fields over a 4-hour span. Three significant points were obtained from the comparisons at the higher resolution of the surface observations. First, the increased data density for the satellite-derived values showed that small scale features could remain undetected by observations at only the RAOB scale. Secondly, differences between the satellite-derived and surface-estimated total water can be used to indicate regions where the atmosphere is dry or moist aloft, or alternately an indication of vertical moisture depth. This results in a determination of moisture both in terms of total amount and vertical extent.

A third significant point arises from a comparison of the 4-hour time-difference field from the satellite with a similar field from conventional sources. The comparison shows that the satellite was able to pick up temporal moisture variations which were similar to those estimated by the surface observations, even though the individual satellite and conventional fields at 1000 and 1400 GMT contained large differences due to variations in vertical moisture extent. The time-difference fields were reasonable when both advection of moisture and moisture convergence were considered. Using the 700 mb wind the flow of moisture from both dry-to-moist and moist-to-dry regions could in part explain the major changes which occurred. Surface moisture convergence

can also be used to explain the time-increase in moisture detected by the satellite.

Finally, a statistical structure analysis of the high-density satellite-derived fields was used to estimate the noise level in each of the parameters. This technique relies on a statistical determination of the mean-squared difference in the satellite-derived parameters as a function of their spatial separation distance. The structure function so defined can be extrapolated to zero separation distance to compensate for any gradient in the data and leave only the noise. In this study the structure values at the minimum separation were used in order to avoid problems with deciding which extrapolation method best represents the fields examined.

Results of this statistical study gave estimated rms noise levels from 1 to 2 K as typical for temperatures and dew points and from 1.2 to 1.8 mm for total precipitable water. Signal-to-noise ratios from 1.2 to 4.1 were found by comparing the estimated noise to the standard deviation of the values in each field. The large signal-to-noise values for most parameters indicated that significant structure or gradient exists in the satellite-derived fields so as to be easily detected above their inherent noise levels.

These quantitative comparisons verify the quality of the satellite-derived fields at a resolution equal to the surface observation scale (<250 km). Satellite-conventional difference fields also give information on the vertical moisture structure; more information, that is, than from either system alone. However, even higher resolution fields of satellite-derived meteorological parameters could be obtained, but they would be hard to verify at the smallest

scales. Unlike a convective situation, where subsequent weather can be used as a verification, the highest resolution details may remain unverified. Only by comparison to higher resolution conventional measurements, or as input to mesoscale analysis and forecasting models, will the smallest scale features become useful and verifiable.

### 7.3 Other Possible Improvements

One possible improvement, which was considered but purposely not undertaken, was a more active role of the synoptic surface observations and RAOBs in the retrieval process. In this study the surface observations were used only for verification purposes and the RAOBs were used only to provide the initial guess profile and for a limited comparison at the larger scale. The RAOBs could provide a better initial guess field than merely the single composited sounding which was used as the initial guess for the entire field of satellite soundings. The reason for using a single initial guess profile was to allow the satellite radiances alone to reproduce the mesoscale features which appeared in the final field of soundings. In other words, as a result of using a single initial guess profile all horizontal variability in the retrieval fields was a result of the satellite radiances alone. The fact that the satellite-derived fields produced good results in comparison to the completely independent surface observations is then remarkable. This was in keeping with the original intention of providing satellite soundings which require the minimum ingest of conventional data. This feature also makes this study different from similar work of others where conventional measurements are heavily relied upon. In this case conventional data was used only in creating

the composited initial guess profile which could have easily been replaced by a climatological or forecast profile, if necessary.

The fact that the satellite soundings were able to reproduce mesoscale features in spite of the minimum ingest of conventional data implies something about the quality of the satellite data and the retrieval process. However, could the results have been improved with a successive corrections method whereby the initialize guess field already contains information from conventional sources? Such a guess field could be similar to those used to initialize numerical models and would, in the case of satellite soundings, add vertical structure to the final product. An objective analysis scheme would have to be adopted to create such an initial guess field. This would involve interpolation in space and also possibly in time, or maybe a forecast (extrapolation in time) to produce the best initial field. This route was not undertaken in this study for various reasons. The main reason was the need to know the quality of the satellite data alone. Another reason was the complexity of the required objective analysis in both space and time, especially considering the large horizontal and vertical gradients which existed among the RAOBs which went into the initial guess profile. This melding of the two data sets, however, is the next logical step which needs to be accomplished.

#### 7.4 Concluding Remarks

In retrospect, it would have been better to have had more information with which to verify the results at the smallest scales. This, however, is a problem with all types of high-resolution satellite data. In this case mesoscale details begin to appear at a resolution below that of the RAOBs. Only when such data is used at these smaller

scales, in special experimental situations, will its qualities be realized.

In this case the fog situation is to some extent predicted using the 1000 GMT satellite data alone. However, the best hints are given by differencing the satellite-derived and surface-estimated total moisture. The dry-over-moist situation found by such differences is probably best suited to radiation fog, but other dynamic effects, which are not directly measurable from the satellite, are also important.

As this study also shows, the satellite can do a respectable job with regards to its time-resolution capabilities. The limited vertical resolution of satellite soundings, however, shows a need for combining satellite data with conventional data which contains more of the vertical resolution detail necessary for true 3-dimensional analyses. In addition, the satellite sounder is capable of detecting mesoscale moisture tendencies over the relatively short time span examined in this study. This capability will be enhanced with a time resolution of up to 1/2 hour with the advent of geosynchronous sounders like VAS.

One of the applications for high space and time resolution moisture fields from the satellite is in the analysis and forecasting of severe weather. Such measurements would be especially useful in analyzing the pre-convective situation for moisture tendencies relating to later convective development. In such studies the moisture information is of great importance because of its large role in the energy processes relating to storm development.

Finally, the high-resolution moisture fields derived from satellite soundings may find applications as input to fine-scale numerical models. Such models include those giving quantitative precipitation forecasts.

Parameterization techniques for incorporating mesoscale moisture into numerical models have been under development and will continue to improve along with the satellite moisture determinations. If not already, models will some day be among the primary users of the high space and time resolution capabilities of satellite soundings.

## REFERENCES

- Benwell, G. R. R., 1965: The Estimation and Variability of Precipitable Water. Meteor. Mag., 94, 319-327.
- Bolsenga, S. J., 1965: The Relationship Between Total Atmospheric Water Vapor and Surface Dew Point on a Mean Daily and Hourly Basis. J. Appl. Meteor., 4, 430-432.
- Bruce, R. E., L. D. Duncan, and J. H. Pierluissi, 1977: Experimental Study of the Relationship Between Radiosonde Temperatures and Satellite-Derived Temperatures. Mon. Wea. Rev., 105, 493-496.
- Chesters, D., L. W. Uccellini and A. Mostek, 1982: VISSR Atmospheric Sounder (VAS) Simulation Experiment for a Severe Storm Environment. Mon. Wea. Rev., 110, 198-216.
- Dozier, J., 1980: Satellite Identification of Surface Radiant Temperature Fields of Subpixel Resolution. NOAA Technical Memorandum, NESS 113, 11 pp. [NTIS Ref: PB81-184038].
- Gandin, L. S., 1963: Objective Analysis of Meteorological Fields. Translated from Russian, Israel Program for Scientific Translations, Jerusalem, 242 pp. [NTIS Ref: TT-65-50007].
- Glahn, H. R., 1973: Comments 'On the Correlation of Total Precipitable Water in a Vertical Column and Absolute Humidity at the Surface'. J. Appl. Meteor., 12, 1411-1414.
- Gruber, A. and C. D. Watkins, 1979: Preliminary Evaluation of Initial Atmospheric Moisture from the TIROS-N Sounding System. Satellite Hydrology, American Water Resources Assoc., June, 115-123.
- Gurka, J., 1976: Using Satellite Data as an Aid to Forecasting Fog and Stratus Formation. NWS/NESS Satellite Applications Information Note 3/76-1, AWS/TN-79/003 (compiled 1979), 47-51.
- Hayden, C. M., W. L. Smith, and H. M. Woolf, 1981: Determination of Moisture from NOAA Polar Orbiting Satellite Sounding Radiances. J. Appl. Meteor., 20, 450-466.
- Hillger, D. W. and T. H. Vonder Haar, 1977: Deriving Mesoscale Temperature and Moisture Fields from Satellite Radiance Measurements over the United States. J. Appl. Meteor., 16, 715-726.

- \_\_\_\_\_ and \_\_\_\_\_, 1979: An Analysis of Satellite Infrared Soundings at the Mesoscale Using Statistical Structure and Correlation Functions. J. Atmos. Sci., 36, 287-305.
- \_\_\_\_\_ and \_\_\_\_\_, 1981: Retrieval and Use of High-Resolution Moisture and Stability Fields from Nimbus-6 HIRS Radiances in Pre-convective Situations. Mon. Wea. Rev., 109, 1788-1806.
- Kaplan, L. D., 1959: Inference of Atmospheric Structure from Remote Radiation Measurements. J. Opt. Soc. Amer., 49, 1004-1007.
- King, J. I. F., 1963: Meteorological Inferences from Satellite Radiometry, I. J. Atmos. Sci., 20, 245-250.
- Lipton, A. E. and D. W. Hillger, 1982: Objective Analysis of Discontinuous Satellite-Derived Data Fields for Grid Point Interpolation. J. Appl. Meteor., 21, 1571-1581.
- Matson, M. and J. Dozier, 1981: Identification of Subresolution High Temperature Sources Using a Thermal IR Sensor. Photogrammetric Engineering and Remote Sensing, 47, 1311-1318.
- Moyer, V., J. R. Scoggins, N. M. Chou, and G. S. Wilson, 1978: Atmospheric Structure Deduced from Routine Nimbus-6 Satellite Data. Mon. Wea. Rev., 106, 1340-1352.
- Paulson, B. A. and L. H. Horn, 1981: Nimbus-6 Temperature Soundings Obtained Using Interactive Video-Graphics Computer Techniques. Bull. Amer. Meteor. Soc., 62, 1308-1318.
- Parmenter, F. C., 1976: Low-Level Moisture Intrusion from Infrared Imagery. Mon. Wea. Rev., 104, 100-104.
- Phillips, N., L. McMillin, A. Gruber, and D. Wark, 1979: An Evaluation of Early Operational Temperature Soundings from TIROS-N. Bull. Amer. Meteor. Soc., 60, 1188-1197.
- Raschke, E. (editor), 1978: Terminology and Units of Radiation Quantities and Measurements. International Association of Meteorology and Atmospheric Physics - Radiation Commission, 17 pp.
- Reber, E. E. and J. R. Swope, 1972: On the Correlation of the Total Precipitable Water in a Vertical Column and Absolute Humidity at the Surface. J. Appl. Meteor., 11, 1322-1325.
- Reitan, C. H., 1963: Surface Dew Point and Water Vapor Aloft. J. Appl. Meteor., 2, 776-779.
- Schlatter, T. W. and G. W. Branstator, 1979: Estimation of Errors in Nimbus-6 Temperature Profiles and Their Spatial Correlation. Mon. Wea. Rev., 107, 1402-1413.

- \_\_\_\_\_, 1981: An Assessment of Operational TIROS-N Temperature Retrievals over the United States. Mon. Wea. Rev., 109, 110-119.
- Schwalb, A., 1978: The TIROS-N/NOAA A-G Satellite Series. NOAA Technical Memorandum, NESS 95, 75 pp. [NTIS Ref: PB-283859].
- Smith, W. L., 1966: Note on the Relationship Between Total Precipitable Water and Surface Dew Point. J. Appl. Meteor., 5, 726-727.
- \_\_\_\_\_, 1970: Iterative Solution of the Radiative Transfer Equation for the Temperature and Absorbing Gas Profile of an Atmosphere. Appl. Opt., 9, 1993-1999.
- \_\_\_\_\_ and H. B. Howell, 1971: Vertical Distribution of Atmospheric Water Vapor from Satellite Infrared Spectrometer Measurements. J. Appl. Meteor., 10, 1026-1034.
- \_\_\_\_\_ and P. K. Rao, 1973: The Determination of Surface Temperature from Satellite 'Window' Radiation Measurements. Temperature; Its Measurement and Control in Science and Industry, 4, Part 3, 2251-2257.
- \_\_\_\_\_, P. G. Abel, H. M. Woolf, A. W. McCulloch, and B. J. Johnson, 1975: The High Resolution Infrared Radiation Sounder (HIRS) Experiment. The Nimbus-6 User's Guide, 37-58. [NTIS Ref: N76-31256].
- \_\_\_\_\_, C. M. Hayden, H. M. Woolf, H. B. Howell, and F. W. Nagle, 1979a: Satellite Sounding Applications to Mesoscale Meteorology. Remote Sounding of the Atmosphere from Space, COSPAR, June, Innsbruck, 33-47.
- \_\_\_\_\_, H. M. Woolf, C. M. Hayden, D. Q. Wark, and L. M. McMillin, 1979b: The TIROS-N Operational Vertical Sounder. Bull. Amer. Meteor. Soc., 60, 1177-1187.
- \_\_\_\_\_, V. E. Suomi, W. P. Menzel, H. M. Woolf, L. A. Sromovsky, H. E. Revercomb, C. M. Hayden, D. N. Erickson, and F. R. Mosher, 1981: First Sounding Results from VAS-D. Bull. Amer. Meteor. Soc., 62, 232-236.
- Wark, D. Q., 1961: On Indirect Temperature Soundings of the Stratosphere from Satellites. J. Geophys. Res., 66, 77-82.
- \_\_\_\_\_, J. H. Lienesch and M. P. Weinreb, 1974: Satellite Observations of Atmospheric Water Vapor. Appl. Opt., 13, 507-511.
- Weinreb, M. P., H. E. Fleming, L. M. McMillin, and A. C. Neuendorffer, 1981: Transmittances for the TIROS Operational Vertical Sounder. NOAA Technical Report, NESS 85, 60 pp. [NTIS Ref: PB82-155920].
- Werbowetzki, A. (editor), 1981: Atmospheric Sounding User's Guide. NOAA Technical Report, NESS 83, 82 pp. [NTIS Ref: PB81-230476].

Appendix A  
TERMS AND SYMBOLS

Quality	Symbol	Unit
wavenumber	k	$\text{cm}^{-1}$
temperature	T	K or $^{\circ}\text{C}$
radiance	L	$\text{mW}(\text{cm}^{-1})^{-1}\text{m}^{-2}\text{sr}^{-1}$
irradiance	E	$\text{mW}(\text{cm}^{-1})^{-1}\text{m}^{-2}$
transmittance	$\tau$	(dimensionless)
reflectance	$\rho$	(dimensionless)
mixing ratio	Q	$\text{g kg}^{-1}$
precipitable water	U	mm
pressure	p	kPa or mb

## Appendix B

### SINGLE FIELD-OF-VIEW CLOUD DETERMINATION

The determination of temperature and moisture information from infrared sounding radiances is severely limited by clouds. An ideal case would be to gain the necessary meteorological information by working around the cloudy areas. However, this is not always possible. For this reason a simplified single-level, single field-of-view (FOV) cloud model was tested in an attempt to alleviate cloud problems and derive meteorological parameters when possible in partly-cloudy situations. (The totally cloudy situation is considered hopeless as far as determining surface parameters from infrared measurements and no attempt is made in these cases.)

The meteorological parameters derived in partly-cloudy situations are not always useful. Errors in the derived parameters may produce meteorological inconsistencies with those from surrounding clear retrievals. However, with only this simplified cloud model the derived parameters can at times be of more value than no information.

By using coincident measurements from two window channels with different spectral responses a single FOV can effectively be split into a clear sub-area, and an adjacent cloudy sub-area each with a different temperature. Various assumptions must be made about the FOV and the

window channels. The first assumption is that only two separate sub-areas comprise the total FOV (i.e. the surface and cloud sub-areas are uniform). A second assumption is that the differing measurements between channels are a result of changes in the background temperature field rather than of any atmospheric absorption differences between the two channels. The equation governing the partly-cloudy response of these window channels is then

$$L(k_i, T_{i, \text{eff}}) = (1-\beta) L(k_i, T_{\text{sfc}}) + \beta L(k_i, T_{\text{cld}}) \quad i=1,2 \quad (\text{B.1})$$

where the FOV is split into a clear (surface) and cloudy fraction with  $\beta$  equal to the cloud amount. As their name implies these window channels encounter little atmospheric absorption. Therefore, the two terms in the equation originate from the surface and cloud fractions respectively, with any atmospheric contributions being neglected.

If such a split FOV is viewed using the 3.76 and 11.1  $\mu\text{m}$  window channels of HIRS-2, then the individual spectral responses will cause each channel to give a different effective temperature,  $T_{i, \text{eff}}$ . This is due to the fact that the radiance in a given channel is a weighted average of the radiances from the two sub-areas. The non-linear response of the Planck function  $L$  with respect to temperature and wavelength causes the average radiances from the two channels to correspond to different average equivalent brightness temperatures. On the other hand, a uniform FOV would give the same effective temperature in both channels. For example, a uniform 275 K FOV will give radiances of 0.20 and 79.1  $\text{mW}/(\text{m}^2 \text{sr cm}^{-1})$  at 3.76 and 11.1  $\mu\text{m}$ , respectively. However, a FOV which is partially cloud-contaminated would give lower radiances and lower effective temperatures in both channels. The

channel affected most would be the longwave (11.1  $\mu\text{m}$ ) channel. The warm (surface) fraction of the FOV would effectively contribute more to the 3.76  $\mu\text{m}$  radiance than the 11.1  $\mu\text{m}$  radiance although both channels have the same FOV and therefore the same cloud amount.

The use of the two window channels to obtain cloud information is not without precedence. Smith and Rao (1973) used the 3.7 and 11  $\mu\text{m}$  window channels as applied to two adjacent FOVs. They solved four equations with four unknowns: the surface and cloud temperatures and the cloud amount in each FOV. To do this they assumed that the average surface and cloud temperatures are the same for the two FOVs.

Dozier (1980) and Matson and Dozier (1981), however, dealt with similar window channels using a single FOV by assuming that the surface temperature  $T_{\text{sfc}}$  is known or can be assumed. This allows a solution for the cloud temperature  $T_{\text{cld}}$  and cloud amount  $\beta$  by using only two equations. The solution is dependent on the assumed surface temperature, but the solution is unique. The noise on the radiances, however, may place the solution outside of physically reasonable limits.

By eliminating the cloud amount  $\beta$  from the two equations of the form of Equation B.1 we get

$$A \cdot L(k_1, T_{\text{cld}}) + B \cdot L(k_2, T_{\text{cld}}) + C = 0 \quad (\text{B.2})$$

where

$$A = L_{2, \text{sfc}} - L_{2, \text{eff}}$$

$$B = L_{1, \text{eff}} - L_{1, \text{sfc}}$$

$$C = L_{2, \text{eff}} \cdot L_{1, \text{sfc}} - L_{1, \text{eff}} \cdot L_{2, \text{sfc}}$$

and

$$L_{i, \text{sfc}} = L(k_i, T_{\text{sfc}})$$

$$L_{i, \text{eff}} = L(k_i, T_{i, \text{eff}}).$$

The effective temperature  $T_{i,eff}$  in each channel is a known measurement, as well as the channel wavenumber  $k_i$ . Therefore, if the surface temperature is assumed then A, B, and C are known.

Equation B.2 cannot be solved explicitly since it is nonlinear in temperature. An iterative solution is simple if a starting cloud temperature is assumed. A simple starting assumption would be

$$T_{cld} < T_{11} < T_{3.76} < T_{sfc}. \quad (B.3)$$

After the cloud temperature is found, the cloud fraction is determined by solving for  $\beta$  from the original two equations, one for each channel.

$$\beta = \frac{C}{D} \quad (B.4)$$

where

$$D = L_{2,cld} \cdot L_{1,sfc} - L_{1,cld} \cdot L_{2,sfc}$$

and

$$L_{i,cld} = L(k_i, T_{cld}).$$

In the case of the equal signs in Equation B.3 the cloud amount  $\beta$  either equals 0 or 1. These limiting cases result in no distinction between the two window channels (i.e. a FOV comprised of only a single effective temperature, either totally clear or totally cloudy).

The assumption of little or no atmospheric contribution for the window channels can be overcome by correcting the window channels for any atmospheric absorption which might occur. By using assumed atmospheric temperature and moisture profiles the atmospheric

transmittance in each channel can be estimated. This however, was not done in this study.

Using this two window channel technique a cloud temperature (or a cloud height) and a cloud amount can therefore be determined for a single partly-cloudy FOV. Uncertainty in the radiances and the corrections to the radiances will cause some non-physical solutions (i.e.  $\beta < 0$  or  $\beta > 1$ ). These, however, can be handled as the limiting cases  $\beta = 0$  or  $\beta = 1$  within the bounds of the uncertainty in the measurements and assumptions. The solution using this model will sometimes yield a reasonable single-level cloud which will effectively represent the true cloud situation. In these cases the results of using this cloud model will be to obtain meteorological parameters using the same retrieval technique as in a clear situation but with a FOV partly obscured by cloud. This involves integrating the radiative transfer equation separately for each of the cloudy and clear sub-areas of the FOV. The retrieval process then continues normally. Meteorological parameters derived which are consistent with those derived from surrounding clear FOVs can be considered useful information which could not have been obtained without the cloud correction to the infrared radiances.

## Appendix C

### NUMERICAL CALCULATION OF MOISTURE FEEDBACK CONVERSION FACTORS

In order to explicitly add the effect of a temperature inversion into the moisture feedback, it was necessary to modify the feedback equation originally developed by Smith (1970). The modifications given here are an extension of the Smith development (see also Smith and Howell, 1971) and are necessary due to numerical integration by computer.

Starting from Equation 13 in Smith (1970), the equivalent integral for  $S_k$  is

$$S_k^{-1} = \int_0^{p_{\max}} U(p) \frac{\delta \tau_k(p)}{\delta U(p)} \delta L(k, T(p)) \quad (C.1)$$

where  $U(p)$  is the precipitable water integrated to pressure level  $p$ ,  $\tau(p)$  is the transmittance to level  $p$  and  $L$  is the Planck function of wavenumber  $k$  and temperature  $T$  (Equation 5.1).

In summation form Equation C.1 becomes

$$S_k^{-1} = \sum_{m=1}^{\max-1} \bar{U}_m \cdot \Delta \tau_{k,m} \cdot \Delta L_{k,m} \cdot \Delta U_m^{-1} \quad (C.2)$$

where

$$\bar{U}_m = \frac{U(p_m) + U(p_{m+1})}{2}$$

$$\Delta\tau_{k,m} = \tau_{k,m} - \tau_{k,m+1}$$

$$\Delta L_{k,m} = L(k, T(p_{m+1})) - L(k, T(p_m))$$

and

$$\Delta U_m = U(p_{m+1}) - U(p_m).$$

The precipitable water increases with pressure by definition, since it is integrated downward.

$$U(p) = g^{-1} \int_0^p Q(p) \delta p \tag{C.3}$$

where  $Q(p)$  is the mixing ratio profile. Therefore  $\Delta U$  is positive. Likewise  $\Delta\tau$  is positive since the transmittance  $\tau$  decreases with pressure (increasing  $m$ ). The remaining term  $\Delta L$  is also positive if temperature  $T$  increases with pressure. However, this is not always the case. When a temperature inversion exists at the surface then  $T_{sfc} < T_{max}$ .

In order to account for the strong effect of a lowered surface temperature upon the integrated radiance (as shown in Figure 5.7) a term similar to the surface term in the RTE (Equation 5.12) has been added to Equation C.2. That term is

$$S_k^{-1} = S_k^{-1} + \tau_{k,max} \cdot \Delta L_{k,sfc} \tag{C.4}$$

where

$$\Delta L_{k,sfc} = L(k, T_{sfc}) - L(k, T_{max}).$$

This term will be negative for  $T_{sfc} < T_{max}$ , so it will reduce the magnitude or even cause  $S^{-1}$  to become negative. This is especially likely for the most transparent channel since the surface transmittance  $\tau_{k,sfc}$  can be large. If  $S^{-1}$  is negative then the reverse effect of increased radiance with increased precipitable water can be simulated. Empirical testing has shown that this actually happens. Unfortunately, the  $S^{-1}$  term can approach zero causing  $S$  to approach infinity. This possibility is eliminated by forcing  $S$  to zero as  $S^{-1}$  approaches zero, in such a way that the mapping is continuous. The reasoning is that as  $S^{-1}$  approaches zero, the direction of the moisture feedback becomes uncertain. By forcing  $S$  to zero in these cases the uncertainty is not carried over into large feedback but is diminished in magnitude. By empirical testing if  $S^{-1} < 4$ , then  $S = S/16$  is used. Values larger than  $S = 0.25$  (25%) cause too much moisture feedback. The units of  $S$  are inverse radiance units.